Manipulation of Mesenchymal Stem Cell Morphology and Functions through Nano- and Micro-patterned Surfaces

Manipulation of Mesenchymal Stem Cell Morphology and Functions through Nano- and Micro-patterned Surfaces

Yingjun YANG

February 2019

Manipulation of Mesenchymal Stem Cell Morphology and Functions through Nano- and Micro-patterned Surfaces

Yingjun YANG

Doctoral Program in Materials Science and Engineering

Submitted to the Graduate School of Pure and Applied Science

in Partial Fulfillment of the Requirements for the

Degree of Doctor of Philosophy in Engineering

at the

University of Tsukuba

Contents

List of abbreviations

AFM	Atomic force microscope
ALP	Alkaline phosphatase
ASCs	Adult stem cells
AzPhPVA	Azidophenyl-derivatized poly (vinyl alcohol)
BEC	Biphasic electric current
BMPs	Bone morphogenetic proteins
BSA	Bovine serum albumin
DEX	Dexamethasone
DMEM	Dulbecco's modified eagle medium
ECM	Extracellular matrix
ESCs	Embryonic stem cells
FBS	Fetal bovine serum
FGF	Fibroblast growth factor
GP	β-glycerophosphate disodium salt hydrate
HGF	Hepatocyte growth factor
IBMX	3-isobutyl-1-methylxanthine
IDO	Indoleamine-pyrrole 2,3-dioxygenase
IGF-1	Insulin-like growth factor – 1
IL-1β	Interleukin 1 beta
iPSCs	Induced multipotent stem cells
iNOS	Inducible nitric oxide synthase
MSCs	Mesenchymal stem cells
NMR	Nuclear magnetic resonance
MMP-2	Matrix metalloproteinase 2
MT1-MMP	Membrane type 1 matrix metalloproteinase 2
PBS	Phosphate buffer saline
PDMS	Poly (dimethyl siloxane)
PGE2	Prostaglandin E2
PDGF	Platelet-derived gr2owth factor

PIGF	Placental growth factor
PS	Polystyrene
PVA	Poly (vinyl alcohol)
RUNX2	Runt-related transcription factor 2
SMA	Smooth muscle actin
TCPS	Tissue culture polystyrene
TGF-β	Transforming growth factor-β
TIMP	Tissue inhibitor of metalloproteinase
TNF-α	Tumor necrosis factor alpha
VEGF-A	Vascular endothelial growth factor-A

Chapter 1

General introduction

1.1 Mesenchymal stem cells

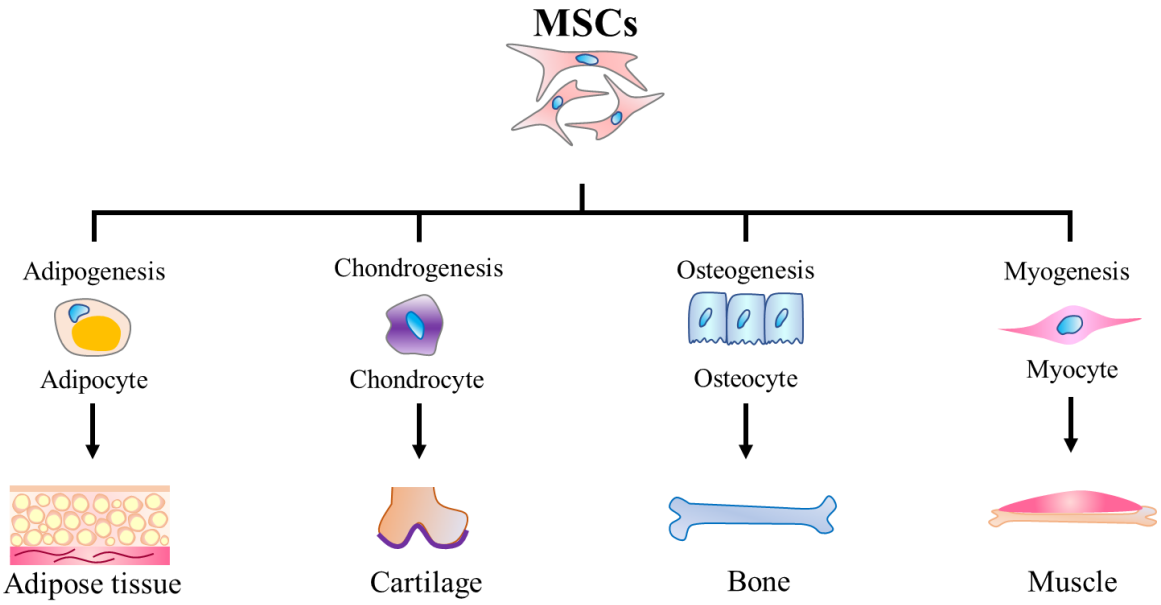

Figure 1.1 Multipotency of mesenchymal stem cells (MSCs)

Mesenchymal stem cells (MSCs) are a kind of unspecialized adult stem cells with expression of typical stem cell surface markers including CD44 (cell-surface glycoprotein), CD73 (5'-nucleotidase), CD90 (Thy1), CD105 (endoglin), CD106 (vascular cell adhesion protein 1, VCAM-1) and STRO-1 and lacking of hematopoietic markers like CD11b (integrin alpha M), CD19 (B-lymphocyte antigen), CD34 (transmembrane phosphoglycoprotein protein) and CD45 (protein tyrosine phosphatase, receptor type, C) [1]. Based on many attractive advantages, MSCs have tremendous potentials in the development of regenerative medicine and numerous diseases treatment [2]. They can be easily isolated from adipose tissue, bone marrow, and peripheral blood [3] and rapidly expanded *in vitro* with the maintenance of multipotency [4]. They are demonstrated to be able to differentiate into osteoblast [5], myocytes [6], chondrocytes [7] and adipocytes [8]. Additionally, MSCs also possess the ability to migrate into injured, inflammation or tumor site without suffering from the immune rejections [9]. Beneficial from these properties, MSCs are widely applied in tissue engineering and cell-based gene therapy. Therefore, it is extreme valuable for investigation of MSC functions regulation.

1.1.1 MSCs in tissue engineering

Tissue engineering is a field that focuses on repairing or regeneration of physically or disease injured tissues through integrated application of cells, materials and biological factors [10]. As one of the essential components in tissue engineering, cells are the source for the new tissues or organs formation [11]. Various kinds of cells could be applied as the cell source for tissue engineering [12]. All of them are summarized to somatic cells and stem cells. At the primary stage of tissue engineering development, the somatic cells are commonly applied for the recreation of injured tissues. For example, the autologous chondrocytes are successfully been applied to repair the damaged cartilage [13] while the fibroblasts and their extracellular matrix (ECM) are the attractive cell source and induction factor for skin repairment [14]. However, the autologous somatic cells from injured sites are always insufficient to be harvested and the diseased somatic cells are unable to be expanded *in vitro.* In another words, the autologous somatic cells limite the further development of damaged or pathological tissues repairment [15].

Therefore, the stem cells including embryonic stem cells (ESCs), adult stem cells (ASCs) and induced multipotent stem cells (iPSCs) are applied to substitute the autologous somatic cells for tissue engineering [16]. The stem cell is an umbrella term for series cells with the ability of differentiation [17]. Due to the limited source and ethics argument of ESCs [18] and limited production efficiency of iPSCs [19], ASCs are most widely applied in the recreation of tissues or organs. As one of the ASCs, MSCs are famous for their multipotency to develop into various cell lineages under different biochemical or biophysical stimuli [3] (Figure 1.1). Benefitted from the multipotency, they are subsequently been applied in repairment of adipose tissue [8], bone [20], cartilage [21], vascular [22] and muscle [6]. Among them, the adipogenic, osteogenic and myogenic differentiation of MSCs are most widely analyzed and applied in the tissue engineering. The MSCs proceed the osteogenesis with the occurrence of dexamethasone (DEX) and β-glycerophosphate (GP) [23]. The activity of alkaline phosphatase (ALP) and calcium deposition are commonly determined to indicate the osteogenesis level of MSCs [24]. The adipogenesis of MSCs is stimulated by insulin [25], DEX [26] and 3-isobutyl-1-methylxanthine (IBMX) [27]. The occurrence of lipid vacuoles in cytoplasm is demonstrated as the striking evidence for MSCs directed into adipocyte lineage [8]. The myogenesis of MSCs is related to generation of skeletal muscle cells [28] and cardiomyocytes [29]. It is stimulated by TGF-β1 (transforming growth factor beta 1) [30] and monitored by the level of the smooth muscle actin (SMA) and calponin expression [28]. Under stimuli of β-mercaptoethanol, MSCs are able to change to neuronal phenotype with expressing neuron-specific marker [31]. Additionally, MSCs also have some other advantages that they can be easily isolated from various sources and rapidly expanded *in vitro*.

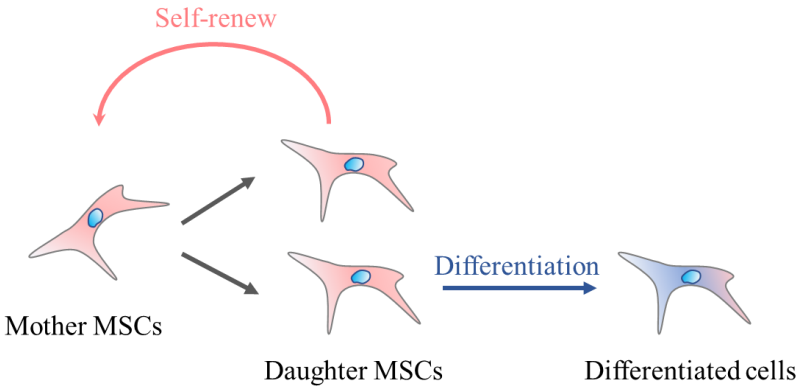

Figure 1.2 Self-renewability and multipotency of MSCs.

MSCs attract tremendous attention in tissue engineering based on their multipotency and self-renewability. However, there are still many urgent issues of applications in tissue engineering need to be settled. The primary task

for development of new tissues or organs from MSCs is how to induce and manipulate them into a specific cell lineage and further develop to functional mature tissues or organs. Although some biochemical and biophysical factors are revealed to be efficient in regulation of MSCs commitment, the influence of some certain factors are still necessary to be clarified. Additionally, the differentiation of MSCs is well-recognized as a reversible process [32-34]. Therefore, after the *in vitro* differentiated MSCs transplant into patient's body for tissue repairment, their ability of differentiated phenotype maintenance is limited by the insufficient chemical induction factors [35]. Additionally, the critical role of cell morphology in regulation of MSCs differentiations have been demonstrated [36, 37]. However, the influence of some kinds of cell morphology in regulation of MSCs differentiations is still confusing with each other.

1.1.2 MSCs in cell-based gene therapy

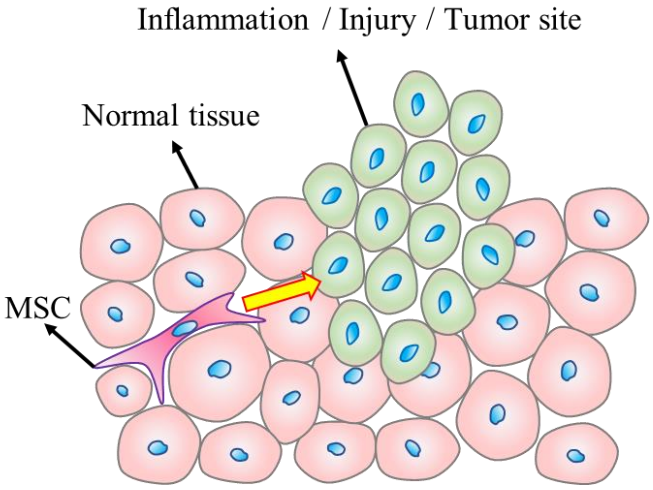

Figure 1.3 Directional migration of mesenchymal stem cells.

In contrast to the traditional therapeutic interventions such as physical surgery or chemical medicine, gene therapy is a novel technique that delivers the exogeneous functional gene into human cells for diseases treatment [38]. Nowadays, human healthy are threatened by a variety of diseases and tissue defects. Gene therapy has been widely applied for treatment of gene defects related diseases including cystic fibrosis [39], hemophilia [40], muscular dystrophy [41] and sickle cell anemia [42]. In particular, the genetically modified MSCs also provide a promising approach for the treatment of diabetes [43], obesity [44] or inflammatory diseases [45].

During recent years, MSCs become an attractive cell vector for gene therapy since they are able to initially migrate into some specific regions in the human body. For instance, MSCs are showing the significant potential in wound healing and able to migrate into injury and inflammation sites [46]. In addition, after activated by liver cancer cells secreted epithelial cell adhesion cell molecular, MSCs are also able to migrate to liver tumor site [47]. Additionally, with the occurrence of breast cancer cells secreted monocyte chemotactic protein-1, MSCs are able to migrate into breast tumor sites [48].

Furthermore, based on numerous secreted functional biomolecules MSCs have wide immunoregulatory properties that make them able to avoid the immune rejection during gene therapy [49]. Firstly, MSCs are hypoimmunogenic with lack of expression of major histocompatibility complex (MHC) class II proteins [50]. Additionally, MSCs are efficient in preventing T cells activation through regulation of dendritic cells functions [51]. Simultaneously, MSCs are able to secrete some soluble factors including TGF-β [52], hepatocyte growth factor (HGF) [53], prostaglandin E2 (PGE2) [54], indoleamine-pyrrole 2,3-dioxygenase (IDO) [55] and inducible nitric oxide synthase (iNOS) [56] for immunosuppression.

Furthermore, the genetically modified MSCs have board applications in diseases treatment. The superoxide dismutase-2 (SOD-2) overexpressed MSCs are efficient in the treatment of type 2 diabetes [44]. Interferon beta (INF-β) [57], TNF-related apoptosis-inducing ligand (TRAIL) [58] or pigment epithelium-derived factor (PEDF) [59] upregulated MSCs are effective in inhibition of tumor growth. The neurodegenerative diseases could be treated by transgenic MSCs with modification of insulin-like growth factor -1 (IGF-1) [60]. The placental growth factor (PIGF) gene-modified MSCs are beneficial for the treatment of cerebral ischemia [61].

Additionally, since the MSCs differentiation can be enhanced by some specific kind of exogenous gene, the MSCs based gene therapy is also applied in tissue regeneration. The osteogenesis of MSCs is promoted by overexpressed runt-related transcription factor 2 (RUNX2) [62], bone morphogenetic protein 2 (BMP-2) [63]. The overexpressed TGF-β is beneficial for chondrogenic differentiation of MSCs [64].

Even the MSCs owning many advantages to be the cell vector in gene therapy, there are still many obstacles limit their board applications. The major problem is the challenges in genetic modification of MSCs. Since they are a kind of typical difficult-to-transfect cells [65] with the low viability and transfection efficiency after transfection [66, 67], MSCs are very difficult to be transfected. Nowadays, many advanced techniques are developed to improve the transfection efficiency of MSCs, but all of them still have their own disadvantages. A novel method in regulation of MSCs transfection is necessary for the application of MSCs based gene therapy.

1.2 Factors in regulation of MSC functions

To broaden the applications of MSCs in tissue engineering and gene therapy, some obstacles including determination of differentiation direction, maintaining differentiated phenotype and improving MSCs transfection efficiency should be overcome. Therefore, the regulation of MSC functions and behavior is necessary for development of tissue engineering and gene therapy techniques. *In vivo* microenvironment, MSCs are affected by various functional factors including biochemical factors and biophysical factors from extracellular matrix (ECM) or adjacent cells (Figure 1.4). Furthermore, the cell morphology is demonstrated as another critical factor in the regulation of MSC functions and behavior recently.

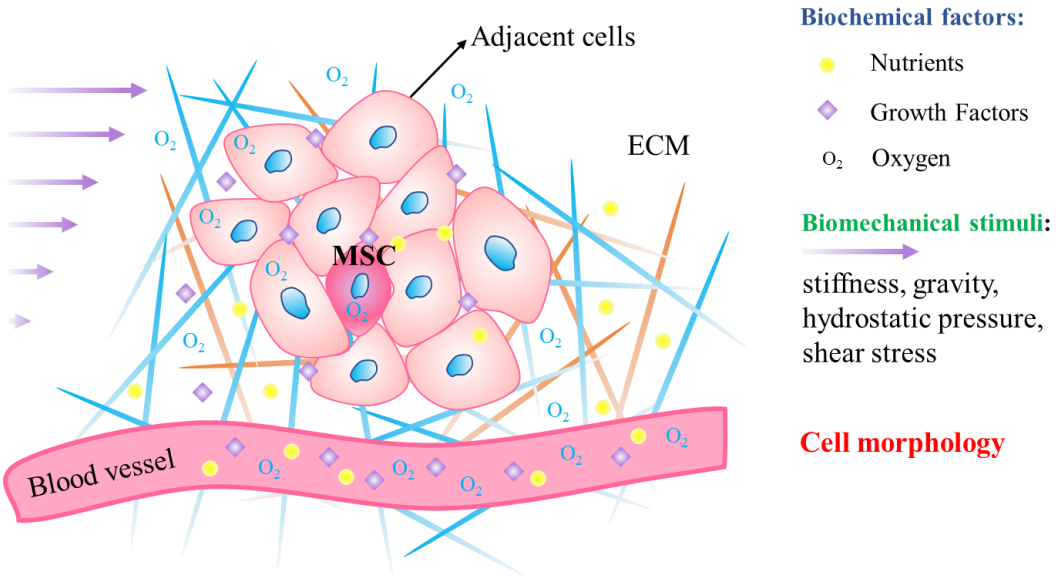

Figure 1.4 In vivo microenvironment of MSCs.

1.2.1 Biochemical factors

The biochemical factors including various kinds of cytokines and growth factors, different concentration of oxygen or nutrients and other functional proteins or molecules *in vivo* microenvironment are effective in the regulation of MSC functions and behavior.

Previous researches demonstrated bone morphogenetic proteins (BMPs) are effective in the promotion of MSCs osteogenesis [68] and inhibition of MSCs proliferation [69]. For the generation of brown adipose tissues from MSCs, BMP-7 is necessary [70]. Epidermal growth factor (EGF) accelerates the proliferation of MSCs [71, 72]. The fibroblast growth factor-2 (FGF-2) could enhance the chondrogenesis [73] and osteogenesis [74] of MSCs. Hepatocyte growth factor (HGF) and IGF-1 are also critical in the regulation of MSCs myogenesis [75]. IGF-1 can also enhance the migration of MSCs [76]. Platelet-derived growth factor (PDGF) is efficient in the regulation of vascular generation through enhancement of MSCs different into endothelial cells or vascular smooth muscle cells [77]. TGF-β1 can not only induce myogenic differentiation of MSCs [30] but also stimulate the MSCs proliferation [78]. TGF-β3 [7] can be applied to induce chondrogenic differentiation of MSCs. Vascular endothelial growth factor-A (VEGF-A) is able to induce MSC differentiation into endothelial cells [79].

Some kinds of cytokines have also been applied to manipulate MSC functions and behavior. Stromal-cell derived factor 1 (SDF-1) is essential for MSCs migration [80]. Inflammatory cytokines including interleukin 1 beta (IL-1β) and tumor necrosis factor alpha (TNF-α) are effective to improve MSCs migration ability through up-regulation of matrix metalloproteinase 2 (MMP-2), membrane type 1 MMP (MT1-MMP), tissue inhibitor of metalloproteinase 1 (TIMP-1), and tissue inhibitor of metalloproteinase 2 (TIMP-2) [81]. Interferons c (IFN-c) [82] and interleukin 17 receptor A (IL17RA) [83] are necessary for the immunosuppressive capacity of MSCs.

Additionally, the other chemical molecules are also playing a critical role in regulation of MSC functions and behavior. The low concentration ascorbic acid is effective in the promotion of MSCs proliferation, while the high concentration of ascorbic acid leads to the MSCs differentiation into osteoblast [84]. The different concentration of glucose is critical in the different stage of MSCs chondrogenesis [85] and the low glucose concentration is beneficial for MSCs proliferation [86]. The insulin, DEX, and IBMX are essential in stimulation of MSCs adipogenesis [27]. The DEX, ascorbic acid, and GP are efficient in the regulation of MSCs osteogenesis [23]. Oxygen is another kind of important biochemical molecular for regulation of MSC functions and behavior. The low concentration of oxygen is benefited for the maintenance of genetic stability [87] and proliferation [88]. The ideal concentration of oxygen for chondrogenic differentiation of MSCs is 10 – 11% [89].

1.2.2 Biophysical factors

1.2.2.1 Biomechanical factors

Besides the biochemical factors, the functions and behavior of MSCs are highly relevant with many different kinds of biomechanical factors including stiffness of ECM, gravity, hydrostatic pressure and shear stress *in vivo* microenvironment.

Many researchers have investigated the influence of substrate stiffness on MSC functions and behavior by using stiffness tunable hydrogels. The low stiffness (soft) of the substrate is beneficial for chondrogenesis and adipogenesis of MSCs. On the other hand, the higher stiffness (hard) substrate promotes the osteogenesis and myogenesis of MSCs [90-92]. In addition, the mechanical stretch has a marked impact on MSCs proliferation [93]. The hypergravity having the positive functions on the myogenesis and osteogenesis of MSCs [94] while showing inhibitory functions on MSCs proliferation [95]. The unidirectional and isotropic directional gravity showing

significant influence in the regulation of MSCs actin stress fiber structure [96]. By using a bioprocessor, the hydrostatic pressure is demonstrated to be functional in the stimulation of MSCs proliferation and osteogenesis [97, 98]. The shear stress is useful to induce the MSCs developed into osteoblast [99] and smooth muscle cells [100]. The cyclic strain promotes the myogenesis of MSCs [101]. Pulsatile biphasic electric current (BEC) contributes to the osteogenesis of MSCs [102]. Electrical stimuli can enhance the neurogenesis of MSCs [103]. The mechanical stimuli from structured substrate are efficient in the regulation of focal adhesion and cytoskeleton structure of MSCs [104] and favorable for enhancement of MSCs osteogenesis [105] and neurogenesis [106].

1.2.2.2 Cell morphology

MSCs in vivo microenvironment are surrounded and constrained by ECM and adjacent cells. Subsequently, their morphology is determined by the different structure of the surrounding environment. In recent years, the importance of cell morphology in the regulation of MSC functions and behavior has been revealed through various structured substrates. By seeding cells on micro- or nano-structured surfaces, the morphology of cells is easily manipulated and the influence of cell morphology on MSC functions and behavior is also investigated. The larger spreading area or size of MSCs is beneficial for stimulation of osteogenesis [107, 108] and cellular uptake capacity for gold nanoparticles (AuNPs) of MSCs [109]. On the contrast, the smaller spreading area or cell size will facilitate the adipogenesis [108], chondrogenesis [110] and maintenance of stemness [111]. The highly elongated MSCs have the positive effects on the stimulation of osteogenesis and inhibition of adipogenesis of MSCs [112, 113]. The different curvature of MSCs with the same spreading area is also effective in regulation of osteogenic and adipogenic differentiation of MSCs [36, 112]. The highly alignment of MSCs is critical in the promotion of osteogenesis [114] and myogenesis [75]. After MSCs morphology is controlled by the grid-structured graphene oxide surfaces, the neurogenesis can be facilitated under electronic stimulation [103, 115].

1.3 Nano- and micro-patterning techniques

As mentioned above, the biomechanical stimuli and cell morphology have been demonstrated as the critical factors in the regulation of MSC functions and behavior. Additionally, the cell morphology is manipulated by the ECM and adjacent cells *in vivo* microenvironment. Therefore, mimicking the different structure of ECM and adjacent cell by using nano- or micro-patterning techniques is necessary for manipulation of MSC functions and behavior.

1.3.1 Micro-patterning techniques

Micropatterning techniques including photolithography, micro-contact printing, plasma/laser ablation and stencil associated micropatterning are applied to prepare micropatterned surfaces to precisely control cell morphology (Figure 1. **5**). Benefitted from the stability of prepared surfaces and simplicity of preparing process, photolithography has been well applied on the preparation of micropatterned surfaces. The photo-reactive cell adhesion repellent materials are firstly coated on a cell adhesive substrate and selectively been photo-irradiated through a micropatterned photomask. The photo-reactive materials below transparent regions of the photomask are activated and grafted on the cell adhesive substrate. On the contrast, the photo-reactive materials under opaque areas of the photomask are easily removed after washing process to expose cell adhesive substrate. After cell culture, cells adhere only to the exposed regions of substrate and cell morphology is easily confined by the different shape of micropatterned surfaces [20, 116]. The microcontact printing is also widely applied to prepare biomolecular printed

micropatterned surfaces. For instance, a micro-structured PDMS stamp is prepared through curving on a microfabricated silicon wafer. Then, the pre-prepared micro-structured stamp is coated by a thin layer of cell adhesive biomolecules through self-assembling and gently pressed on the substrate. After removal of stamp, the micropatterned biomolecular could be printed on the surface of substrate. The cells trend to adhere on the cell adhesive biomolecular coated parts on the substrate [117, 118]. Recently, an advanced micropatterning technique by using plasma or laser ablation has been developed to prepare complex structured micropatterned surfaces. A well-controlled laser beam or plasma through precise instruments is applied to selectively ablate the antifouling materials on the substrate. After incubated with cell adhesive molecules, they can deposit only on the exposed regions of the substrate for cell adhesion [119]. After repeating this process, several different kinds of proteins are coated at a different position in sequence [120]. The stencil associate micropatterning technique was also applied to prepare micropatterned surfaces. The micro-structured stencil is pre-prepared and attached on a rigid substrate. Then, the substrate and micro-structured stencil are immersed in the cell adhesive molecular solution or simply sprayed by the cell adhesive molecules. The micropatterned cell adhesive molecules on the substrate are harvested after the micro-structured stencil is peeled off from the substrate [121]. The micropatterning techniques are commonly applied to control cell morphology [122] through confinement of cell adhesion and spreading region. Furthermore, micropatterned surfaces are also applied to generate the different size of cell spheroids [123].

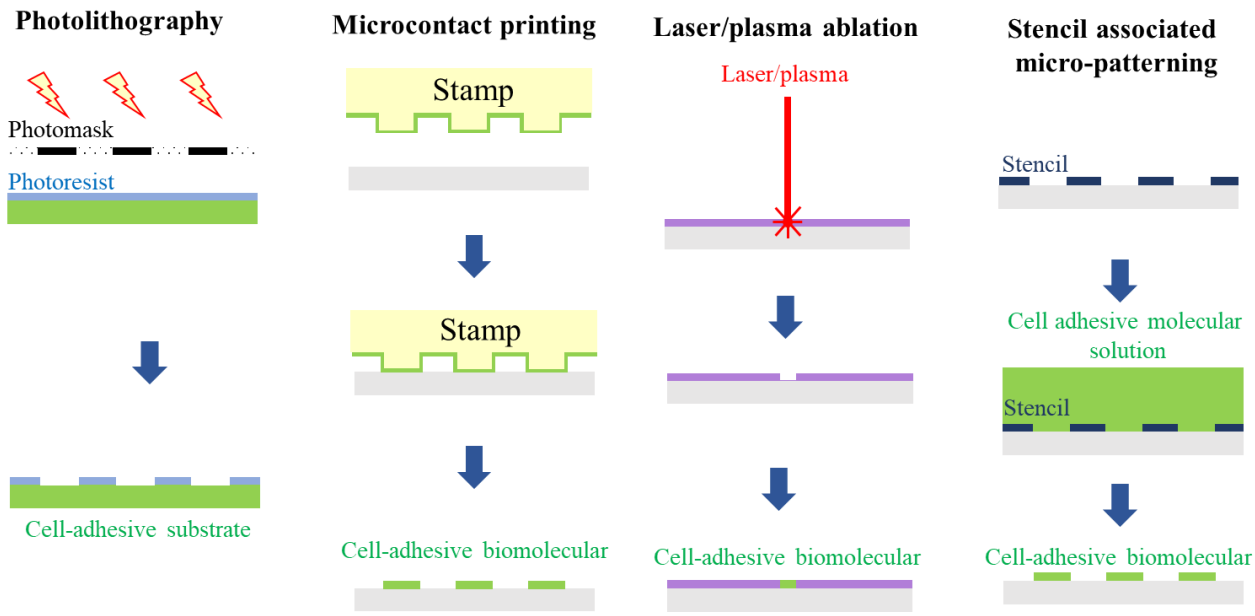

Figure 1. 5 Micropatterning techniques

1.3.2 Nano-patterning techniques

In vivo microenvironment includes both micro- and nano-structured components. Recently, researchers have developed some nanopatterning techniques to mimic the nanostructured components *in vivo* microenvironment and further manipulating the cell morphology or functions (Figure 1. **6**). The simple and low-cost nanoimprinting method including thermoplastic nanoimprinting, photo nanoimprinting, and resist-free nanoimprinting are widely applied to prepare nanostructured surfaces. Briefly, a nanostructured mold is pre-prepared and impressed on a layer of polymer solution. After curing of the polymer through temperature changing, photoirradiation or drying, the mold will be peeled off to harvest the nanostructured surfaces [124]. The nanolithography is also developed to prepare nanopatterned surfaces. It is always consisting with photo-reactive photoresist. The photoresist is firstly coated on

the substrate and UV irradiated through a nanopatterned photomask. The unreacted photoresist is removed before etching process. After incubated with etching reagent, the exposed substrate is etched to generate the nanostructured substrate [125]. The electrospinning method is also applied to prepare nanofibers structured surfaces. When a high voltage is applied to a polymer solution on the needle of syringe, the polymer solution droplet tends to be elongated to generate nanofibers. A collector is set to recover the resulting polymer nanofibers. The structure and orientation of nanofibers can be adjusted by changing the voltage, a distance between needle and collector and the different shape of the collector [126-128]. The nanopatterned surfaces are always applied to inducing the unification of cell orientation, cell elongation and cell spreading through manipulation of focal adhesion (FA) and plasma membrane structures [126, 129, 130]. Besides controlling cell morphology, nano-structured surfaces containing nanowires and nanopillars are also applied to regulating cell migration and direct delivery [131] of exogeneous for improvement transfection [132] through stretching on the cytoplasm membrane.

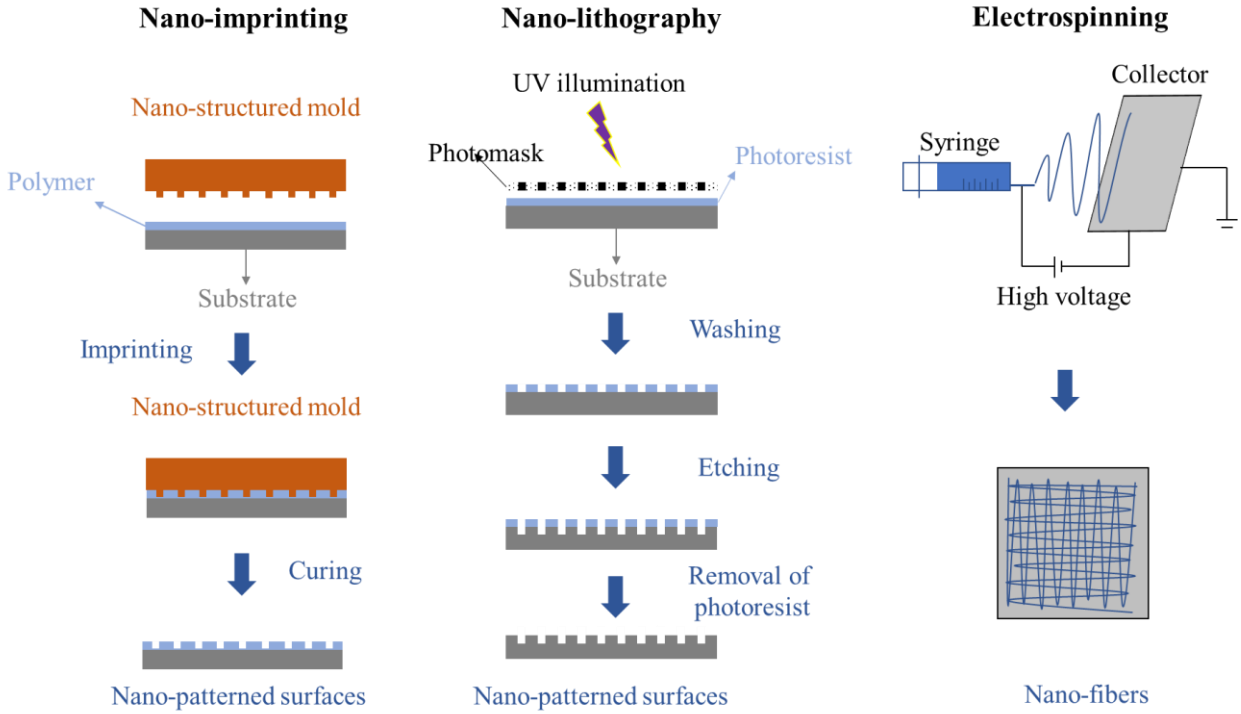

Figure 1. 6 Nano-patterning techniques

1.4 Issues and objectives

As mentioned above, MSCs have many advantages in the development of tissue engineering, regenerative medicine, and cell-based gene therapy. Thus, manipulation of MSC functions and behavior is necessary for further broader their applications. The present research focuses on the influence of biophysical cues, especially for the cell morphology, in the regulation of MSC functions and behavior. In recent years, many researches have revealed the importance of various cell morphology in the regulation of MSC functions. However, some elusive issues in the relationship between cell morphology and MSCs are still not clear and need to be clarified.

1.4.1 Issues of MSCs morphology in differentiation

It is demonstrated that the differentiated MSCs could return to unspecialized state or transdifferentiate into

another cell linage after withdrawing or changing induction factors [33, 34, 89, 133]. The differentiation of MSCs is regarded as a strongly reversible process [133]. As a result, the differentiated MSCs are very difficult to maintain their differentiated phenotypes without sufficient biochemical stimuli [134]. It is a challenge to keep the differentiated MSCs developing into the matured functional tissues or organs after transplantation. The significant influence of biochemical stimuli in the induction of MSCs differentiation and maintenance of differentiation phenotype has already been revealed over decades. The conventional solutions in maintaining differentiated phenotype *in vivo* are based on the sustained release systems or materials [135-137]. However, the functions of cell morphology are still not clear. The clear role of cell morphology in the maintenance of MSCs differentiated phenotype will provide a new sight in the design and development of biomaterials for tissue regeneration.

Based on previous researches, the effective functions of cell alignment and elongation in the regulation of MSCs differentiation have already been demonstrated [6, 22, 114]. The cell orientation and elongation are controlled by the manipulation of FA structure through nano-patterned surfaces and confinement of cell adhesion area through micropatterned surfaces. However, by using nano- or micro-patterned surfaces separately, the unified cell orientation is accompanied by a high cell elongation. Therefore, the different functions of cell alignment and aspect ratio in regulation of MSCs differentiation are still not clear.

1.4.2 Issues of MSCs morphology in transfection

Because of their migratory capacity, immunosuppression ability, and potential in diseases treatment, MSCs are an attractive carrier for gene therapy. However, MSCs are very difficult to be genetically modified. Nowadays, many transfection techniques including various materials-based transfection, physical-based transfection, and virus-based transfection have been developed to improve gene transfection efficiency into MSCs. However, all of them have their own disadvantages. The cationic materials-based transfection related with low transfection efficiency [65]. The physical-based transfection through direct delivery of plasmid into mammalian cells are often resulted in low cell viability [138]. Although virus-based transfection could get high transfection efficiency, the risk of oncogenesis limits their board applications in clinical treatments [139]. All of these techniques are focus on the exogenous gene delivery method and a little attention has been paid to the effects of cell functions or behavior on transfection efficiency. In addition, the role of cell morphology in MSCs transfection is still not clear.

1.4.3 Objectives and outline

In this study, the role of MSCs morphology in the regulation of their differentiated phenotype maintenance, differentiation and transfection was investigated by using nano- and micro-patterned surfaces prepared through nano-imprinting and photolithography. The azidophenyl-derivatized poly (vinyl alcohol) (AzPhPVA) was synthesized through Steglich esterification between hydroxy groups of poly (vinyl alcohol) (PVA) and carboxy groups of azidobenzoic acid to prepare micropatterned surface. The polystyrene (PS) nano-grooved surfaces were prepared through nano-imprinting method and applied to prepare nano-micro hybrid surfaces with using of photo-reactive AzPhPVA. MSCs were cultured on the different kinds of the surfaces to investigate the effects of cell morphology on MSC functions and behavior. The detailed outline is shown as below.

Chapter 2 describes the role of cell size in MSCs osteogenic commitment and differentiated phenotype maintenance. MSCs were cultured on micropatterned surfaces with micro-dots containing different diameter to control the size of MSCs. The synthesis process and characterization of photo-reactive AzPhPVA were introduced in this chapter. The micropatterned MSCs were cultured in osteogenic induction media for different periods to clarify the role of cell size in osteogenic commitment. Then, the induction medium was replaced and the differentiated

micropatterned MSCs were further cultured in basal medium to check the function of cell size in MSCs osteogenic differentiated phenotype maintenance without biochemical stimuli. The stemness marker CD105, early osteogenesis marker ALP, and late osteogenesis marker calcium deposition were analyzed to characterize MSCs phenotype at different time points.

Chapter 3 introduces the influence of cell morphology on gene transfection efficiency in MSCs. MSCs were cultured on micropatterned surfaces containing micro-dots with different diameter to control cell size and micro-ellipses with different aspect ratio and same area to control cell elongation. The micropatterned MSCs were transfected with plasmid DNA encoding green fluorescence protein (GFP) to check the influence of cell morphology on gene transfection efficiency. The relationship between cell morphology and cellular uptake capacity, DNA synthesis activity and cytoskeleton organization were also investigated to clarify the possible mechanism.

Chapter 4 introduces a new method for preparation of nano-micro hybrid pattern surfaces through nano-imprinting and photolithography. The different orientation of PS nanogrooves and different spacing of PVA microstripes were prepared to control MSCs alignment and elongation simultaneously. The cell alignment, aspect ratio and structure of focal adhesion were controlled to investigate the different role of cell alignment and elongation in the regulation of MSCs myogenesis, osteogenesis and adipogenesis.

Finally, Chapter 5 provides the concluding remarks and future prospects of this study.

1.5 References

[1] R. Hass, C. Kasper, S. Bohm, R. Jacobs, Different populations and sources of human mesenchymal stem cells (MSC): A comparison of adult and neonatal tissue-derived MSC, Cell Commun Signal 9 (2011) 12.

[2] H.J. Kim, J.S. Park, Usage of Human Mesenchymal Stem Cells in Cell-based Therapy: Advantages and Disadvantages, Dev Reprod 21(1) (2017) 1-10.

[3] H. Klingemann, D. Matzilevich, J. Marchand, Mesenchymal Stem Cells - Sources and Clinical Applications, Transfus Med Hemother 35(4) (2008) 272-277.

[4] D.C. Colter, R. Class, C.M. DiGirolamo, D.J. Prockop, Rapid expansion of recycling stem cells in cultures of plastic-adherent cells from human bone marrow, Proceedings of the National Academy of Sciences 97(7) (2000) 3213-3218.

[5] R.M. Salasznyk, R.F. Klees, W.A. Williams, A. Boskey, G.E. Plopper, Focal adhesion kinase signaling pathways regulate the osteogenic differentiation of human mesenchymal stem cells, Experimental cell research 313(1) (2007) 22-37.

[6] P.Y. Wang, W.T. Li, J. Yu, W.B. Tsai, Modulation of osteogenic, adipogenic and myogenic differentiation of mesenchymal stem cells by submicron grooved topography, Journal of materials science. Materials in medicine 23(12) (2012) 3015-28.

[7] L. Bian, D.Y. Zhai, E. Tous, R. Rai, R.L. Mauck, J.A. Burdick, Enhanced MSC chondrogenesis following delivery of TGF-beta3 from alginate microspheres within hyaluronic acid hydrogels in vitro and in vivo, Biomaterials 32(27) (2011) 6425-34.

[8] T. Fink, V. Zachar, Adipogenic differentiation of human mesenchymal stem cells, Methods in molecular biology 698 (2011) 243-51.

[9] G.S. Oggu, S. Sasikumar, N. Reddy, K.K.R. Ella, C.M. Rao, K.K. Bokara, Gene Delivery Approaches for Mesenchymal Stem Cell Therapy: Strategies to Increase Efficiency and Specificity, Stem Cell Rev 13(6) (2017) 725-740.

[10] S. Yang, K.-F. Leong, Z. Du, C.-K. Chua, The Design of Scaffolds for Use in Tissue Engineering. Part I. Traditional Factors, 7(6) (2001) 679-689.

[11] D. Howard, L.D. Buttery, K.M. Shakesheff, S.J. Roberts, Tissue engineering: strategies, stem cells and scaffolds, J Anat 213(1) (2008) 66-72.
[12] C.A. Heath, Cells for tissue engineering, Trends in Biotechnology 18(1) (2000) 17-19.
[13] M. Brittberg, T. Tallheden, E. Sjögren-Jansson, A. Lindahl, L. Peterson, Autologous Chondrocytes Used for Articular Cartilage Repair: An Update, 391 (2001) S337-S348.
[14] H.-J. Wang, J. Pieper, R. Schotel, C.A.V. Blitterswijk, E.N. Lamme, Stimulation of Skin Repair Is Dependent on Fibroblast Source and Presence of Extracellular Matrix, 10(7-8) (2004) 1054-1064.
[15] P. T. Brown, A. M. Handorf, W. Bae Jeon, W.-J. Li, Stem Cell-based Tissue Engineering Approaches for Musculoskeletal Regeneration, Current Pharmaceutical Design 19(19) (2013) 3429-3445.
[16] P. Bianco, P.G. Robey, Stem cells in tissue engineering, Nature 414(6859) (2001) 118-21.
[17] I.L. Weissman, Stem Cells, Cell 100(1) (2000) 157-168.
[18] B.E. Strauer, R. Kornowski, Stem Cell Therapy in Perspective, Circulation 107(7) (2003) 929-934.
[19] S.P. Medvedev, A.I. Shevchenko, S.M. Zakian, Induced Pluripotent Stem Cells: Problems and Advantages when Applying them in Regenerative Medicine, Acta naturae 2(2) (2010) 18-28.
[20] B. Chang, C. Ma, X. Liu, Nanofibers Regulate Single Bone Marrow Stem Cell Osteogenesis via FAK/RhoA/YAP1 Pathway, ACS applied materials & interfaces 10(39) (2018) 33022-33031.
[21] J.P. Garcia-Ruiz, A. Diaz Lantada, 3D Printed Structures Filled with Carbon Fibers and Functionalized with Mesenchymal Stem Cell Conditioned Media as In Vitro Cell Niches for Promoting Chondrogenesis, Materials (Basel) 11(1) (2017).
[22] T. Nakamoto, X. Wang, N. Kawazoe, G. Chen, Influence of micropattern width on differentiation of human mesenchymal stem cells to vascular smooth muscle cells, Colloids and surfaces. B, Biointerfaces 122 (2014) 316-323.
[23] F. Langenbach, J. Handschel, Effects of dexamethasone, ascorbic acid and beta-glycerophosphate on the osteogenic differentiation of stem cells in vitro, Stem Cell Res Ther 4(5) (2013) 117.
[24] E. Birmingham, G.L. Niebur, P.E. McHugh, G. Shaw, F.P. Barry, L.M. McNamara, Osteogenic differentiation of mesenchymal stem cells is regulated by osteocyte and osteoblast cells in a simplified bone niche, European Cells and Materials 23 (2012) 13-27.
[25] D.J. Klemm, J.W. Leitner, P. Watson, A. Nesterova, J.E. Reusch, M.L. Goalstone, B. Draznin, Insulin-induced adipocyte differentiation. Activation of CREB rescues adipogenesis from the arrest caused by inhibition of prenylation, The Journal of biological chemistry 276(30) (2001) 28430-5.
[26] V. Zilberfarb, K. Siquier, A.D. Strosberg, T. Issad, Effect of dexamethasone on adipocyte differentiation markers and tumour necrosis factor-α expression in human PAZ6 cells, Diabetologia 44(3) (2001) 377-386.
[27] M.A. Scott, V.T. Nguyen, B. Levi, A.W. James, Current methods of adipogenic differentiation of mesenchymal stem cells, Stem Cells Dev 20(10) (2011) 1793-804.
[28] E.J. Gang, J.A. Jeong, S.H. Hong, S.H. Hwang, S.W. Kim, I.H. Yang, C. Ahn, H. Han, H. Kim, Skeletal myogenic differentiation of mesenchymal stem cells isolated from human umbilical cord blood, Stem Cells 22(4) (2004) 617-24.
[29] X. Guo, Y. Bai, L. Zhang, B. Zhang, N. Zagidullin, K. Carvalho, Z. Du, B. Cai, Cardiomyocyte differentiation of mesenchymal stem cells from bone marrow: new regulators and its implications, Stem Cell Res Ther 9(1) (2018) 44.
[30] M.S. Liang, S.T. Andreadis, Engineering fibrin-binding TGF-beta1 for sustained signaling and contractile function of MSC based vascular constructs, Biomaterials 32(33) (2011) 8684-93.
[31] D. Woodbury, E.J. Schwarz, D.J. Prockop, I.B. Black, Adult rat and human bone marrow stromal cells differentiate into neurons, Journal of Neuroscience Research 61(4) (2000) 364-370.
[32] Y. Rui, L. Xu, R. Chen, T. Zhang, S. Lin, Y. Hou, Y. Liu, F. Meng, Z. Liu, M. Ni, K.S. Tsang, F. Yang, C. Wang,

H.C. Chan, X. Jiang, G. Li, Epigenetic memory gained by priming with osteogenic induction medium improves osteogenesis and other properties of mesenchymal stem cells, Scientific reports 5 (2015) 11056.
[33] L. SONG, R.S. TUAN, Transdifferentiation potential of human mesenchymal stem cells derived from bone marrow, 18(9) (2004) 980-982.
[34] M. Ullah, S. Stich, M. Notter, J. Eucker, M. Sittinger, J. Ringe, Transdifferentiation of mesenchymal stem cells-derived adipogenic-differentiated cells into osteogenic- or chondrogenic-differentiated cells proceeds via dedifferentiation and have a correlation with cell cycle arresting and driving genes, Differentiation 85(3) (2013) 78-90.
[35] Y. Liu, X. Jiang, X. Zhang, R. Chen, T. Sun, K.L. Fok, J. Dong, L.L. Tsang, S. Yi, Y. Ruan, J. Guo, M.K. Yu, Y. Tian, Y.W. Chung, M. Yang, W. Xu, C.M. Chung, T. Li, H.C. Chan, Dedifferentiation-reprogrammed mesenchymal stem cells with improved therapeutic potential, Stem Cells 29(12) (2011) 2077-89.
[36] K.A. Kilian, B. Bugarija, B.T. Lahn, M. Mrksich, Geometric cues for directing the differentiation of mesenchymal stem cells, Proceedings of the National Academy of Sciences of the United States of America 107(11) (2010) 4872-7.
[37] J. Lee, A.A. Abdeen, T.H. Huang, K.A. Kilian, Controlling cell geometry on substrates of variable stiffness can tune the degree of osteogenesis in human mesenchymal stem cells, Journal of the mechanical behavior of biomedical materials 38 (2014) 209-18.
[38] T. Niidome, L. Huang, Gene therapy progress and prospects: nonviral vectors, Gene therapy 9(24) (2002) 1647-52.
[39] Riordan, J. Rommens, B. Kerem, N. Alon, R. Rozmahel, Z. Grzelczak, J. Zielenski, S. Lok, N. Plavsic, J. Chou, a. et, Identification of the cystic fibrosis gene: cloning and characterization of complementary DNA, Science 245(4922) (1989) 1066-1073.
[40] C.S. Manno, G.F. Pierce, V.R. Arruda, B. Glader, M. Ragni, J.J.E. Rasko, M.C. Ozelo, K. Hoots, P. Blatt, B. Konkle, M. Dake, R. Kaye, M. Razavi, A. Zajko, J. Zehnder, P. Rustagi, H. Nakai, A. Chew, D. Leonard, J.F. Wright, R.R. Lessard, J.M. Sommer, M. Tigges, D. Sabatino, A. Luk, H. Jiang, F. Mingozzi, L. Couto, H.C. Ertl, K.A. High, M.A. Kay, Successful transduction of liver in hemophilia by AAV-Factor IX and limitations imposed by the host immune response, Nature Medicine 12 (2006) 342.
[41] M. Koenig, E.P. Hoffman, C.J. Bertelson, A.P. Monaco, C. Feener, L.M. Kunkel, Complete cloning of the duchenne muscular dystrophy (DMD) cDNA and preliminary genomic organization of the DMD gene in normal and affected individuals, Cell 50(3) (1987) 509-517.
[42] R. Saiki, S. Scharf, F. Faloona, K. Mullis, G. Horn, H. Erlich, N. Arnheim, Enzymatic amplification of beta-globin genomic sequences and restriction site analysis for diagnosis of sickle cell anemia, Science 230(4732) (1985) 1350-1354.
[43] M.S. Wong, W.J. Hawthorne, N. Manolios, Gene therapy in diabetes, Self Nonself 1(3) (2010) 165-175.
[44] C.C. Domingues, N. Kundu, F.J. Dore, S. Sen, Genetic Modification of Stem Cells in Diabetes and Obesity, Genetic Engineering - An Insight into the Strategies and Applications2016.
[45] S.H. Kim, N.R. Bianco, W.J. Shufesky, A.E. Morelli, P.D. Robbins, Effective Treatment of Inflammatory Disease Models with Exosomes Derived from Dendritic Cells Genetically Modified to Express IL-4, The Journal of Immunology 179(4) (2007) 2242-2249.
[46] K.C. Rustad, G.C. Gurtner, Mesenchymal Stem Cells Home to Sites of Injury and Inflammation, Adv Wound Care (New Rochelle) 1(4) (2012) 147-152.
[47] B. Endaya, S.P. Guan, J.P. Newman, H. Huynh, K.C. Sia, S.T. Chong, C.Y.L. Kok, A.Y.F. Chung, B.B. Liu, K.M. Hui, P.Y.P. Lam, Human mesenchymal stem cells preferentially migrate toward highly oncogenic human hepatocellular carcinoma cells with activated EpCAM signaling, Oncotarget 8(33) (2017) 54629-54639.
[48] R.M. Dwyer, S.M. Potter-Beirne, K.A. Harrington, A.J. Lowery, E. Hennessy, J.M. Murphy, F.P. Barry, T.

O'Brien, M.J. Kerin, Monocyte chemotactic protein-1 secreted by primary breast tumors stimulates migration of mesenchymal stem cells, Clin Cancer Res 13(17) (2007) 5020-7.
[49] M. Wang, Q. Yuan, L. Xie, Mesenchymal Stem Cell-Based Immunomodulation: Properties and Clinical Application, Stem Cells Int 2018 (2018) 3057624.
[50] R. Romieu-Mourez, M. Francois, M.N. Boivin, J. Stagg, J. Galipeau, Regulation of MHC Class II Expression and Antigen Processing in Murine and Human Mesenchymal Stromal Cells by IFN- , TGF- , and Cell Density, The Journal of Immunology 179(3) (2007) 1549-1558.
[51] J.M. Ryan, F.P. Barry, J.M. Murphy, B.P. Mahon, Mesenchymal stem cells avoid allogeneic rejection, J Inflamm (Lond) 2 (2005) 8.
[52] S.W. Yoo, D.Y. Chang, H.S. Lee, G.H. Kim, J.S. Park, B.Y. Ryu, E.H. Joe, Y.D. Lee, S.S. Kim, H. Suh-Kim, Immune following suppression mesenchymal stem cell transplantation in the ischemic brain is mediated by TGF-beta, Neurobiol Dis 58 (2013) 249-57.
[53] L. Bian, Z.-K. Guo, H.-X. Wang, J.-S. Wang, H. Wang, Q.-F. Li, Y.-F. Yang, F.-J. Xiao, C.-T. Wu, L.-S. Wang, In vitro and in vivo immunosuppressive characteristics of hepatocyte growth factor-modified murine mesenchymal stem cells, In Vivo 23(1) (2009) 21-27.
[54] M. Zafranskaya, D. Nizheharodava, M. Yurkevich, G. Ivanchik, Y. Demidchik, H. Kozhukh, A. Fedulov, PGE2 contributes to in vitro MSC-mediated inhibition of non-specific and antigen-specific T cell proliferation in MS patients, Scand J Immunol 78(5) (2013) 455-62.
[55] W. Ling, J. Zhang, Z. Yuan, G. Ren, L. Zhang, X. Chen, A.B. Rabson, A.I. Roberts, Y. Wang, Y. Shi, Mesenchymal stem cells use IDO to regulate immunity in tumor microenvironment, Cancer Res 74(5) (2014) 1576-87.
[56] W. Li, G. Ren, Y. Huang, J. Su, Y. Han, J. Li, X. Chen, K. Cao, Q. Chen, P. Shou, L. Zhang, Z.R. Yuan, A.I. Roberts, S. Shi, A.D. Le, Y. Shi, Mesenchymal stem cells: a double-edged sword in regulating immune responses, Cell Death Differ 19(9) (2012) 1505-13.
[57] M. Studeny, F.C. Marini, J.L. Dembinski, C. Zompetta, M. Cabreira-Hansen, B.N. Bekele, R.E. Champlin, M. Andreeff, Mesenchymal stem cells: potential precursors for tumor stroma and targeted-delivery vehicles for anticancer agents, J Natl Cancer Inst 96(21) (2004) 1593-603.
[58] L.S. Sasportas, R. Kasmieh, H. Wakimoto, S. Hingtgen, J.A. van de Water, G. Mohapatra, J.L. Figueiredo, R.L. Martuza, R. Weissleder, K. Shah, Assessment of therapeutic efficacy and fate of engineered human mesenchymal stem cells for cancer therapy, Proceedings of the National Academy of Sciences of the United States of America 106(12) (2009) 4822-7.
[59] Q. Chen, P. Cheng, T. Yin, H. He, L. Yang, Y. Wei, X. Chen, Therapeutic potential of bone marrow-derived mesenchymal stem cells producing pigment epithelium-derived factor in lung carcinoma, Int J Mol Med 30(3) (2012) 527-34.
[60] N. Joyce, G. Annett, L. Wirthlin, S. Olson, G. Bauer, J.A. Nolta, Mesenchymal stem cells for the treatment of neurodegenerative disease, 5(6) (2010) 933-946.
[61] H. Liu, O. Honmou, K. Harada, K. Nakamura, K. Houkin, H. Hamada, J.D. Kocsis, Neuroprotection by PlGF gene-modified human mesenchymal stem cells after cerebral ischaemia, Brain 129(Pt 10) (2006) 2734-45.
[62] K. Yanagihara, S. Uchida, S. Ohba, K. Kataoka, K. Itaka, Treatment of Bone Defects by Transplantation of Genetically Modified Mesenchymal Stem Cell Spheroids, Mol Ther Methods Clin Dev 9 (2018) 358-366.
[63] K. Tai, G. Pelled, D. Sheyn, A. Bershteyn, L. Han, I. Kallai, Y. Zilberman, C. Ortiz, D. Gazit, Nanobiomechanics of repair bone regenerated by genetically modified mesenchymal stem cells, Tissue Eng Part A 14(10) (2008) 1709-20.
[64] F. Janina, V.J. Kumar, R.-R. Ana, S. Gertrud, M. Henning, C. Magali, Determination of the Chondrogenic Differentiation Processes in Human Bone Marrow-Derived Mesenchymal Stem Cells Genetically Modified to

Overexpress Transforming Growth Factor-β via Recombinant Adeno-Associated Viral Vectors, 25(12) (2014) 1050-1060.
[65] C. Madeira, R.D. Mendes, S.C. Ribeiro, J.S. Boura, M.R. Aires-Barros, C.L. da Silva, J.M. Cabral, Nonviral gene delivery to mesenchymal stem cells using cationic liposomes for gene and cell therapy, Journal of biomedicine & biotechnology 2010 (2010) 735349.
[66] N.S. Abdul Halim, K.S. Fakiruddin, S.A. Ali, B.H. Yahaya, A comparative study of non-viral gene delivery techniques to human adipose-derived mesenchymal stem cell, Int J Mol Sci 15(9) (2014) 15044-60.
[67] T.G. de Carvalho, F.M. Pellenz, A. Laureano, L.M. da Rocha Silla, R. Giugliani, G. Baldo, U. Matte, A simple protocol for transfecting human mesenchymal stem cells, Biotechnol Lett 40(3) (2018) 617-622.
[68] M. Beederman, J.D. Lamplot, G. Nan, J. Wang, X. Liu, L. Yin, R. Li, W. Shui, H. Zhang, S.H. Kim, W. Zhang, J. Zhang, Y. Kong, S. Denduluri, M.R. Rogers, A. Pratt, R.C. Haydon, H.H. Luu, J. Angeles, L.L. Shi, T.C. He, BMP signaling in mesenchymal stem cell differentiation and bone formation, J Biomed Sci Eng 6(8A) (2013) 32-52.
[69] Z. Liu, Y. Tang, T. Qiu, X. Cao, T.L. Clemens, A dishevelled-1/Smad1 interaction couples WNT and bone morphogenetic protein signaling pathways in uncommitted bone marrow stromal cells, The Journal of biological chemistry 281(25) (2006) 17156-63.
[70] Y.H. Tseng, E. Kokkotou, T.J. Schulz, T.L. Huang, J.N. Winnay, C.M. Taniguchi, T.T. Tran, R. Suzuki, D.O. Espinoza, Y. Yamamoto, M.J. Ahrens, A.T. Dudley, A.W. Norris, R.N. Kulkarni, C.R. Kahn, New role of bone morphogenetic protein 7 in brown adipogenesis and energy expenditure, Nature 454(7207) (2008) 1000-4.
[71] C. Knight, S. James, D. Kuntin, J. Fox, K. Newling, S. Hollings, R. Pennock, P. Genever, Epidermal growth factor can signal via beta-catenin to control proliferation of mesenchymal stem cells independently of canonical Wnt signalling, Cell Signal 53 (2019) 256-268.
[72] X. Zhang, Y. Wang, Y. Gao, X. Liu, T. Bai, M. Li, L. Li, G. Chi, H. Xu, F. Liu, J.Y. Liu, Y. Li, Maintenance of high proliferation and multipotent potential of human hair follicle-derived mesenchymal stem cells by growth factors, Int J Mol Med 31(4) (2013) 913-21.
[73] L.A. Solchaga, K. Penick, J.D. Porter, V.M. Goldberg, A.I. Caplan, J.F. Welter, FGF-2 enhances the mitotic and chondrogenic potentials of human adult bone marrow-derived mesenchymal stem cells, 203(2) (2005) 398-409.
[74] T. Ito, R. Sawada, Y. Fujiwara, T. Tsuchiya, FGF-2 increases osteogenic and chondrogenic differentiation potentials of human mesenchymal stem cells by inactivation of TGF-beta signaling, Cytotechnology 56(1) (2008) 1-7.
[75] R. Witt, A. Weigand, A.M. Boos, A. Cai, D. Dippold, A.R. Boccaccini, D.W. Schubert, M. Hardt, C. Lange, A. Arkudas, R.E. Horch, J.P. Beier, Mesenchymal stem cells and myoblast differentiation under HGF and IGF-1 stimulation for 3D skeletal muscle tissue engineering, BMC Cell Biol 18(1) (2017) 15.
[76] Y. Li, X. Yu, S. Lin, X. Li, S. Zhang, Y.-H. Song, Insulin-like growth factor 1 enhances the migratory capacity of mesenchymal stem cells, Biochemical and Biophysical Research Communications 356(3) (2007) 780-784.
[77] C.A. Shuttleworth, C.M. Kielty, Platelet-derived growth factor receptors regulate mesenchymal stem cell fate: implications for neovascularization AU - Ball, Stephen G, Expert Opinion on Biological Therapy 10(1) (2010) 57-71.
[78] H. Jian, X. Shen, I. Liu, M. Semenov, X. He, X.F. Wang, Smad3-dependent nuclear translocation of beta-catenin is required for TGF-beta1-induced proliferation of bone marrow-derived adult human mesenchymal stem cells, Genes Dev 20(6) (2006) 666-74.
[79] M. Khaki, A.H. Salmanian, H. Abtahi, A. Ganji, G. Mosayebi, Mesenchymal Stem Cells Differentiate to Endothelial Cells Using Recombinant Vascular Endothelial Growth Factor –A %J Reports of Biochemistry and Molecular Biology, 6(2) (2018) 144-150.
[80] A.E. Karnoub, A.B. Dash, A.P. Vo, A. Sullivan, M.W. Brooks, G.W. Bell, A.L. Richardson, K. Polyak, R. Tubo, R.A. Weinberg, Mesenchymal stem cells within tumour stroma promote breast cancer metastasis, Nature 449 (2007)

557.
[81] C. Ries, V. Egea, M. Karow, H. Kolb, M. Jochum, P. Neth, MMP-2, MT1-MMP, and TIMP-2 are essential for the invasive capacity of human mesenchymal stem cells: differential regulation by inflammatory cytokines, Blood 109(9) (2007) 4055-63.
[82] H. Ren, Y. Cao, Q. Zhao, J. Li, C. Zhou, L. Liao, M. Jia, Q. Zhao, H. Cai, Z.C. Han, R. Yang, G. Chen, R.C. Zhao, Proliferation and differentiation of bone marrow stromal cells under hypoxic conditions, Biochemical and Biophysical Research Communications 347(1) (2006) 12-21.
[83] M.n. Kurte, P. Luz-Crawford, A.M. Vega-Letter, C. Fern?ndez, M. Gauthier, I.n. Moya, C. D?az, D. Ruiz-Higgs, F. Djouad, F. Carri?n, IL17RA knockout mesenchymal stem cells lose their immunosuppressive capacity and exerts deleterious effects on EAE mice.
[84] K.-M. Choi, Y.-K. Seo, H.-H. Yoon, K.-Y. Song, S.-Y. Kwon, H.-S. Lee, J.-K. Park, Effect of ascorbic acid on bone marrow-derived mesenchymal stem cell proliferation and differentiation, Journal of Bioscience and Bioengineering 105(6) (2008) 586-594.
[85] T.L. Tsai, P.A. Manner, W.J. Li, Regulation of mesenchymal stem cell chondrogenesis by glucose through protein kinase C/transforming growth factor signaling, Osteoarthritis and cartilage 21(2) (2013) 368-76.
[86] A. Stolzing, N. Coleman, A. Scutt, Glucose-Induced Replicative Senescence in Mesenchymal Stem Cells, 9(1) (2006) 31-35.
[87] J.C. Estrada, C. Albo, A. Benguria, A. Dopazo, P. Lopez-Romero, L. Carrera-Quintanar, E. Roche, E.P. Clemente, J.A. Enriquez, A. Bernad, E. Samper, Culture of human mesenchymal stem cells at low oxygen tension improves growth and genetic stability by activating glycolysis, Cell Death Differ 19(5) (2012) 743-55.
[88] M. Ejtehadifar, K. Shamsasenjan, A. Movassaghpour, P. Akbarzadehlaleh, N. Dehdilani, P. Abbasi, Z. Molaeipour, M. Saleh, The Effect of Hypoxia on Mesenchymal Stem Cell Biology, Adv Pharm Bull 5(2) (2015) 141-9.
[89] A. Krinner, M. Zscharnack, A. Bader, D. Drasdo, J. Galle, Impact of oxygen environment on mesenchymal stem cell expansion and chondrogenic differentiation, Cell Prolif 42(4) (2009) 471-84.
[90] J.S. Park, J.S. Chu, A.D. Tsou, R. Diop, Z. Tang, A. Wang, S. Li, The effect of matrix stiffness on the differentiation of mesenchymal stem cells in response to TGF-beta, Biomaterials 32(16) (2011) 3921-30.
[91] A.S. Mao, J.W. Shin, D.J. Mooney, Effects of substrate stiffness and cell-cell contact on mesenchymal stem cell differentiation, Biomaterials 98 (2016) 184-91.
[92] Y.R. Shih, K.F. Tseng, H.Y. Lai, C.H. Lin, O.K. Lee, Matrix stiffness regulation of integrin-mediated mechanotransduction during osteogenic differentiation of human mesenchymal stem cells, Journal of bone and mineral research : the official journal of the American Society for Bone and Mineral Research 26(4) (2011) 730-8.
[93] G. Song, Y. Ju, H. Soyama, T. Ohashi, M. Sato, Regulation of cyclic longitudinal mechanical stretch on proliferation of human bone marrow mesenchymal stem cells, Mol Cell Biomech 4(4) (2007) 201-210.
[94] Y. Huang, Z.Q. Dai, S.K. Ling, H.Y. Zhang, Y.M. Wan, Y.H. Li, Gravity, a regulation factor in the differentiation of rat bone marrow mesenchymal stem cells, J Biomed Sci 16 (2009) 87.
[95] R. Meng, H.Y. Xu, S.M. Di, D.Y. Shi, A.R. Qian, J.F. Wang, P. Shang, Human mesenchymal stem cells are sensitive to abnormal gravity and exhibit classic apoptotic features, Acta Biochim Biophys Sin (Shanghai) 43(2) (2011) 133-42.
[96] C. Koaykul, M. Kim, Y. Kawahara, L. Yuge, M. Kino-oka, Influence of isotropic gravity culture on cytoskeleton structure and formation of focal adhesions in human mesenchymal stem cells, Cytotherapy 20(5) (2018) S43.
[97] C. Huang, R. Ogawa, Effect of Hydrostatic Pressure on Bone Regeneration Using Human Mesenchymal Stem Cells, 18(19-20) (2012) 2106-2113.
[98] Y. Reinwald, A.J. El Haj, Hydrostatic pressure in combination with topographical cues affects the fate of bone marrow-derived human mesenchymal stem cells for bone tissue regeneration, Journal of biomedical materials

research. Part A 106(3) (2018) 629-640.
[99] G. Yourek, S.M. McCormick, J.J. Mao, G.C. Reilly, Shear stress induces osteogenic differentiation of human mesenchymal stem cells, Regen Med 5(5) (2010) 713-24.
[100] J.D. Dong, Y.Q. Gu, C.M. Li, C.R. Wang, Z.G. Feng, R.X. Qiu, B. Chen, J.X. Li, S.W. Zhang, Z.G. Wang, J. Zhang, Response of mesenchymal stem cells to shear stress in tissue-engineered vascular grafts, Acta Pharmacol Sin 30(5) (2009) 530-6.
[101] S.W. Liao, K. Hida, J.S. Park, S. Li, Mechanical regulation of matrix reorganization and phenotype of smooth muscle cells and mesenchymal stem cells in 3D matrix, The 26th Annual International Conference of the IEEE Engineering in Medicine and Biology Society, 2004, pp. 5024-5027.
[102] I.S. Kim, J.K. Song, Y.M. Song, T.H. Cho, T.H. Lee, S.S. Lim, S.J. Kim, S.J. Hwang, Novel Effect of Biphasic Electric Current on In Vitro Osteogenesis and Cytokine Production in Human Mesenchymal Stromal Cells, 15(9) (2009) 2411-2422.
[103] W. Guo, X. Zhang, X. Yu, S. Wang, J. Qiu, W. Tang, L. Li, H. Liu, Z.L. Wang, Self-Powered Electrical Stimulation for Enhancing Neural Differentiation of Mesenchymal Stem Cells on Graphene–Poly(3,4-ethylenedioxythiophene) Hybrid Microfibers, ACS nano 10(5) (2016) 5086-5095.
[104] E.K.F. Yim, E.M. Darling, K. Kulangara, F. Guilak, K.W. Leong, Nanotopography-induced changes in focal adhesions, cytoskeletal organization, and mechanical properties of human mesenchymal stem cells, Biomaterials 31(6) (2010) 1299-1306.
[105] M.J. Dalby, N. Gadegaard, R. Tare, A. Andar, M.O. Riehle, P. Herzyk, C.D. Wilkinson, R.O. Oreffo, The control of human mesenchymal cell differentiation using nanoscale symmetry and disorder, Nature materials 6(12) (2007) 997-1003.
[106] E.K. Yim, S.W. Pang, K.W. Leong, Synthetic nanostructures inducing differentiation of human mesenchymal stem cells into neuronal lineage, Experimental cell research 313(9) (2007) 1820-9.
[107] W. Song, N. Kawazoe, G. Chen, Dependence of Spreading and Differentiation of Mesenchymal Stem Cells on Micropatterned Surface Area, Journal of Nanomaterials 2011 (2011) 1-9.
[108] R. McBeath, D.M. Pirone, C.M. Nelson, K. Bhadriraju, C.S. Chen, Cell Shape, Cytoskeletal Tension, and RhoA Regulate Stem Cell Lineage Commitment, Developmental Cell 6(4) (2004) 483-495.
[109] X. Wang, X. Hu, J. Li, A.C. Russe, N. Kawazoe, Y. Yang, G. Chen, Influence of cell size on cellular uptake of gold nanoparticles, Biomaterials science 4(6) (2016) 970-8.
[110] J. Eyckmans, G.L. Lin, C.S. Chen, Adhesive and mechanical regulation of mesenchymal stem cell differentiation in human bone marrow and periosteum-derived progenitor cells, Biol Open 1(11) (2012) 1058-68.
[111] X. Wang, T. Nakamoto, I. Dulińska-Molak, N. Kawazoe, G. Chen, Regulating the stemness of mesenchymal stem cells by tuning micropattern features, J. Mater. Chem. B 4(1) (2016) 37-45.
[112] R. Peng, X. Yao, J. Ding, Effect of cell anisotropy on differentiation of stem cells on micropatterned surfaces through the controlled single cell adhesion, Biomaterials 32(32) (2011) 8048-57.
[113] X. Yao, R. Peng, J. Ding, Effects of aspect ratios of stem cells on lineage commitments with and without induction media, Biomaterials 34(4) (2013) 930-9.
[114] I.A. Janson, Y.P. Kong, A.J. Putnam, Nanotopographic substrates of poly (methyl methacrylate) do not strongly influence the osteogenic phenotype of mesenchymal stem cells in vitro, PloS one 9(3) (2014) e90719.
[115] T.H. Kim, S. Shah, L. Yang, P.T. Yin, M.K. Hossain, B. Conley, J.W. Choi, K.B. Lee, Controlling differentiation of adipose-derived stem cells using combinatorial graphene hybrid-pattern arrays, ACS nano 9(4) (2015) 3780-90.
[116] X. Wang, X. Hu, N. Kawazoe, Y. Yang, G. Chen, Manipulating Cell Nanomechanics Using Micropatterns, Advanced Functional Materials 26(42) (2016) 7634-7643.
[117] K.J. Min, T.H. Kim, J.W. Choi, Magnetic Force-Driven Graphene Patterns to Direct Synaptogenesis of Human

Neuronal Cells, Materials (Basel) 10(10) (2017).
[118] I. Elloumi Hannachi, K. Itoga, Y. Kumashiro, J. Kobayashi, M. Yamato, T. Okano, Fabrication of transferable micropatterned-co-cultured cell sheets with microcontact printing, Biomaterials 30(29) (2009) 5427-32.
[119] A. Higuchi, Q.D. Ling, S.T. Hsu, A. Umezawa, Biomimetic cell culture proteins as extracellular matrices for stem cell differentiation, Chemical reviews 112(8) (2012) 4507-40.
[120] P.O. Strale, A. Azioune, G. Bugnicourt, Y. Lecomte, M. Chahid, V. Studer, Multiprotein Printing by Light-Induced Molecular Adsorption, Advanced materials 28(10) (2016) 2024-9.
[121] J. Yuan, G. Sahni, Y.C. Toh, Stencil Micropatterning for Spatial Control of Human Pluripotent Stem Cell Fate Heterogeneity, Methods in molecular biology 1516 (2016) 171-181.
[122] M. Thery, Micropatterning as a tool to decipher cell morphogenesis and functions, Journal of cell science 123(Pt 24) (2010) 4201-13.
[123] Y.B. Lee, E.M. Kim, H. Byun, H.K. Chang, K. Jeong, Z.M. Aman, Y.S. Choi, J. Park, H. Shin, Engineering spheroids potentiating cell-cell and cell-ECM interactions by self-assembly of stem cell microlayer, Biomaterials 165 (2018) 105-120.
[124] M.S. Kim, A.Y. Kim, K.J. Jang, J.H. Kim, J.B. Kim, K.Y. Suh, Effect of nanogroove geometry on adipogenic differentiation, Nanotechnology 22(49) (2011) 494017.
[125] Y.Y. Amin, K. Runager, F. Simoes, A. Celiz, V. Taresco, R. Rossi, J.J. Enghild, L.A. Abildtrup, D.C. Kraft, D.S. Sutherland, M.R. Alexander, M. Foss, R. Ogaki, Combinatorial Biomolecular Nanopatterning for High-Throughput Screening of Stem-Cell Behavior, Advanced materials 28(7) (2016) 1472-6.
[126] J.M. Dang, K.W. Leong, Myogenic Induction of Aligned Mesenchymal Stem Cell Sheets by Culture on Thermally Responsive Electrospun Nanofibers, Advanced materials 19(19) (2007) 2775-2779.
[127] Y. Li, X. Jiang, H. Zhong, W. Dai, J. Zhou, H. Wu, Hierarchical Patterning of Cells with a Microeraser and Electrospun Nanofibers, Small 12(9) (2016) 1230-9.
[128] X. Wang, F. Lv, T. Li, Y. Han, Z. Yi, M. Liu, J. Chang, C. Wu, Electrospun Micropatterned Nanocomposites Incorporated with Cu2S Nanoflowers for Skin Tumor Therapy and Wound Healing, ACS nano 11(11) (2017) 11337-11349.
[129] C.Y. Xu, R. Inai, M. Kotaki, S. Ramakrishna, Aligned biodegradable nanofibrous structure: a potential scaffold for blood vessel engineering, Biomaterials 25(5) (2004) 877-86.
[130] S.H. Lim, X.Y. Liu, H. Song, K.J. Yarema, H.Q. Mao, The effect of nanofiber-guided cell alignment on the preferential differentiation of neural stem cells, Biomaterials 31(34) (2010) 9031-9.
[131] D.-J. Kim, J.-K. Seol, G. Lee, G.-S. Kim, S.-K. Lee, Cell adhesion and migration on nanopatterned substrates and their effects on cell-capture yield, Nanotechnology 23(39) (2012) 395102.
[132] B.G. Nair, K. Hagiwara, M. Ueda, H.-h. Yu, H.-R. Tseng, Y. Ito, High Density of Aligned Nanowire Treated with Polydopamine for Efficient Gene Silencing by siRNA According to Cell Membrane Perturbation, ACS applied materials & interfaces 8(29) (2016) 18693-18700.
[133] M. Tagami, S. Ichinose, K. Yamagata, H. Fujino, S. Shoji, M. Hiraoka, S. Kawano, Genetic and ultrastructural demonstration of strong reversibility in human mesenchymal stem cell, Cell Tissue Res 312(1) (2003) 31-40.
[134] A.M. Leferink, D. Santos, M. Karperien, R.K. Truckenmuller, C.A. van Blitterswijk, L. Moroni, Differentiation capacity and maintenance of differentiated phenotypes of human mesenchymal stromal cells cultured on two distinct types of 3D polymeric scaffolds, Integr Biol (Camb) 7(12) (2015) 1574-86.
[135] G. Fernandes, C. Wang, X. Yuan, Z. Liu, R. Dziak, S. Yang, Combination of Controlled Release Platelet-Rich Plasma Alginate Beads and Bone Morphogenetic Protein-2 Genetically Modified Mesenchymal Stem Cells for Bone Regeneration, J Periodontol 87(4) (2016) 470-80.
[136] Y. Gan, S. Li, P. Li, Y. Xu, L. Wang, C. Zhao, B. Ouyang, B. Tu, C. Zhang, L. Luo, X. Luo, X. Mo, Q. Zhou, A Controlled Release Codelivery System of MSCs Encapsulated in Dextran/Gelatin Hydrogel with TGF-beta3-

Loaded Nanoparticles for Nucleus Pulposus Regeneration, Stem Cells Int 2016 (2016) 9042019.
[137] T.N. Vo, F.K. Kasper, A.G. Mikos, Strategies for controlled delivery of growth factors and cells for bone regeneration, Adv Drug Deliv Rev 64(12) (2012) 1292-309.
[138] Y.M. Shen, R.R. Hirschhorn, W.E. Mercer, E. Surmacz, Y. Tsutsui, K.J. Soprano, R. Baserga, Gene transfer: DNA microinjection compared with DNA transfection with a very high efficiency, Molecular and Cellular Biology 2(9) (1982) 1145-1154.
[139] T.K. Kim, J.H. Eberwine, Mammalian cell transfection: the present and the future, Analytical and Bioanalytical Chemistry 397(8) (2010) 3173-3178.

Chapter 2

Preparation of circular micro-patterns having different size for investigation of cell size influences on MSCs osteogenic commitment and phenotype maintenance

2.1 Summary

Osteogenic differentiation and commitment of MSCs is a complex process which is induced and regulated by various biological factors and biophysical cues. Although cell size, as one of the biophysical cues, plays a critical role on regulation of osteogenic differentiation of MSCs, its influence on maintenance of osteogenically differentiated phenotype of MSCs is still not clear. In this study, PVA was micro-patterned on TCPS surface and the micro-patterned surfaces were applied for manipulate MSCs size. The effects of cell size on osteogenic commitment and maintenance of differentiated phenotype of MSCs was investigated. Large MSCs showed higher degree of osteogenic differentiation, slower losing of osteogenically differentiated phenotype and slower recovery of stem cell marker than did small MSCs. Therefore, large cell size was beneficial for osteogenic differentiation and maintenance of osteogenically differentiated phenotype of MSCs.

2.2 Introduction

Regeneration of deficient or injured tissues through tissue engineering and regenerative medicine approaches has been well developed for several decades [1]. Stem cells are attractive cell sources for these approaches. In particular, MSCs which possess self-renewability and multipotency to differentiate into osteoblast [2], smooth muscle cells [3-5], chondrocytes [6-8] and adipocytes [9-11] have been demonstrated as one of the very useful cell sources [12, 13]. The challenging issue for utilization of MSCs for tissue engineering and regenerative medicine is how to control stem cell differentiate into desirable somatic cells and how to maintain the differentiated phenotype after transplantation. Osteogenic differentiation and osteogenesis of MSCs have been broadly investigated by using various osteogenic induction factors under different conditions.

Osteogenic induction factors including dexamethasone, BMP and transforming growth factor have been frequently used for osteogenic differentiation and osteogenesis of MSCs. However, osteogenic differentiation and commitment of MSCs are extremely complicate processes that may be affected by various factors [14, 15]. Except these biological induction factors, biophysical cues have also been reported to play a critical role on stem cell differentiation [16, 17]. Combination of biological factors and biophysical cues has been proposed to exhibit their

synergistic effects on promotion of stem cell differentiation. Cell size is one of the typical biophysical cues, which has been extensively studied for controlling stem cell functions. Cell size has shown regulative functions on cell proliferation [18], migration [19-21], differentiation [9] and reprogramming [22]. Cell morphology and size can be precisely controlled by using a variety of micro-patterning techniques such as microcontact printing , photolithography [23] and stencil patterning [24].

Although many researches have elucidated the influence of biophysical cues on stem cell differentiation, their influence on maintaining the differentiated phenotype of stem cells after removal of biological induction factors is unclear. Maintenance of differentiated states after stem cell differentiation is a critical issue for functional tissue regeneration because stem cell differentiation has been shown as a reversible process [25] and it may be difficult to maintain the differentiated or committed phenotype after removal of biological induction factors [26]. Disclosure of morphological influence of stem cells on maintenance of the phenotype of osteogenically differentiated MSCs is strongly anticipated. Therefore, in this study, micro-patterned surfaces were prepared through UV-lithography and used for culture of MSCs to manipulate cell spreading area and further investigate the influence of cell size on osteogenic commitment and maintenance of the osteogenically differentiated phenotype of MSCs.

2.3 Materials & methods

2.2.1 Synthesis and characterization of photo-reactive AzPhPVA

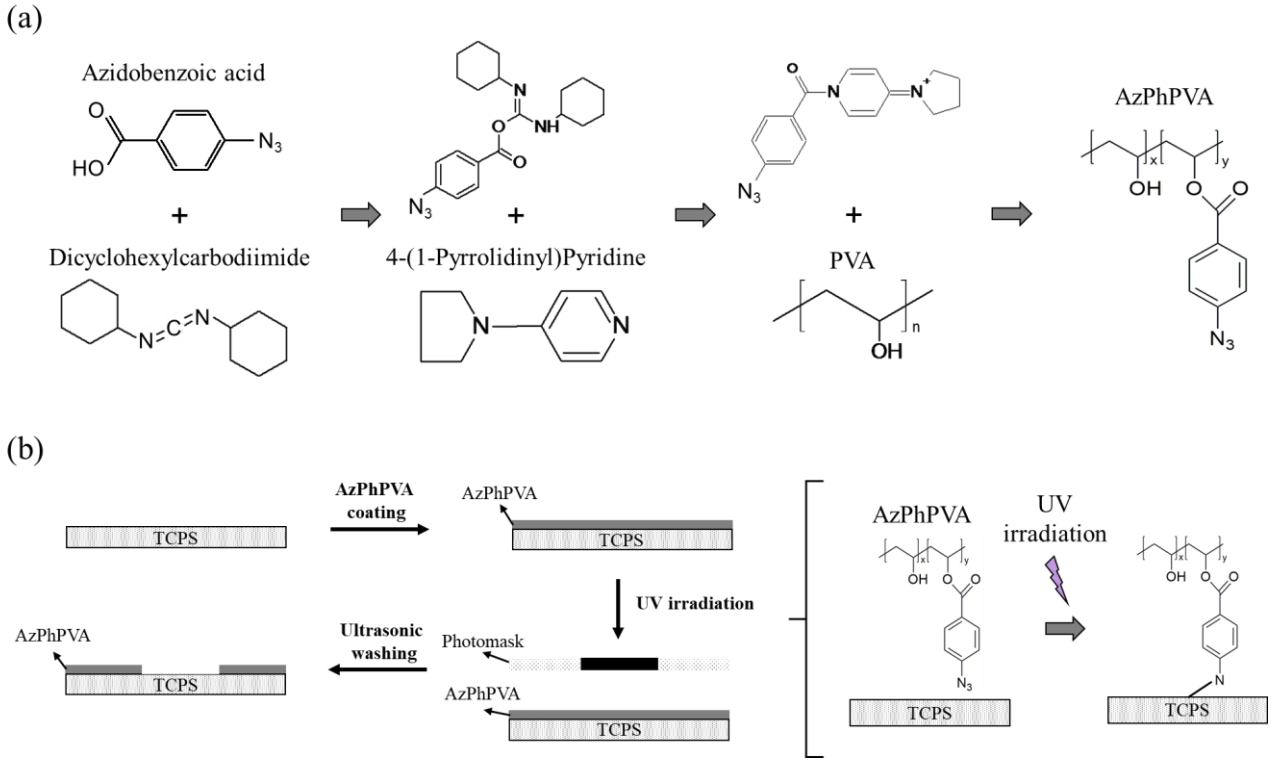

Figure 2.1 Preparation of micro-patterned surfaces through UV lithography by using photo-reactive AzPhPVA. (a) Synthesis of photo-reactive PVA through Steglich esterification. (b) Preparation scheme of micro-patterned surfaces through UV-lithography.

Photo-reactive AzPhPVA was synthesized through Steglich esterification (Figure 2.1a) reaction between carboxyl groups of azidobenzoic acid and hydroxyl groups of PVA [27]. Briefly, 10 mL 1.13 mM dicyclohexylcarbodiimide (Watanabe Chemical Industries, Ltd., Japan) solution in dimethyl sulfoxide

(DMSO), 10 mL 0.113 mM 4-pyrrolidinpyridine solution in DMSO and 40 mL 2.26 mM PVA solution in DMSO were sequentially dropwise added into 25 mL 1.13 mM 4-azidobenzoic acid (Tokyo Chemical Industry Co, Ltd., Japan) solution in DMSO. Reaction mixture was filtered after being stirred at room temperature in dark for 24h. The filtrate was harvested and dropwise added into methanol. 10 mL DMSO was applied to dissolve the precipitant again. Then, the DMSO solution was dropwise added into methanol to purify the synthesized photo-reactive PVA. The purified precipitate was dissolved in Milli-Q water to prepare the aqueous solution of AzPhPVA at a concentration for following experiments. The AzPhPVA aqueous solutions were characterized by ultraviolet-visible (UV-Vis) absorbance analysis (JASCO V-660 Spectrophotometer). The UV spectra of azidobenzoic acid, PVA and the mixture of PVA and azidobenzoic acid were measured to confirm the reaction between PVA and azidobenzoic acid. The AzPhPVA aqueous solutions were freeze dried and re-dissolved in deuterium oxide (D_2O, Sigma-Aldrich Co. LLC., USA). The AzPhPVA D_2O solutions were characterized by ^{1}H-NMR to calculate the grafting efficiency.

2.2.2 Preparation and characterization of micro-patterns

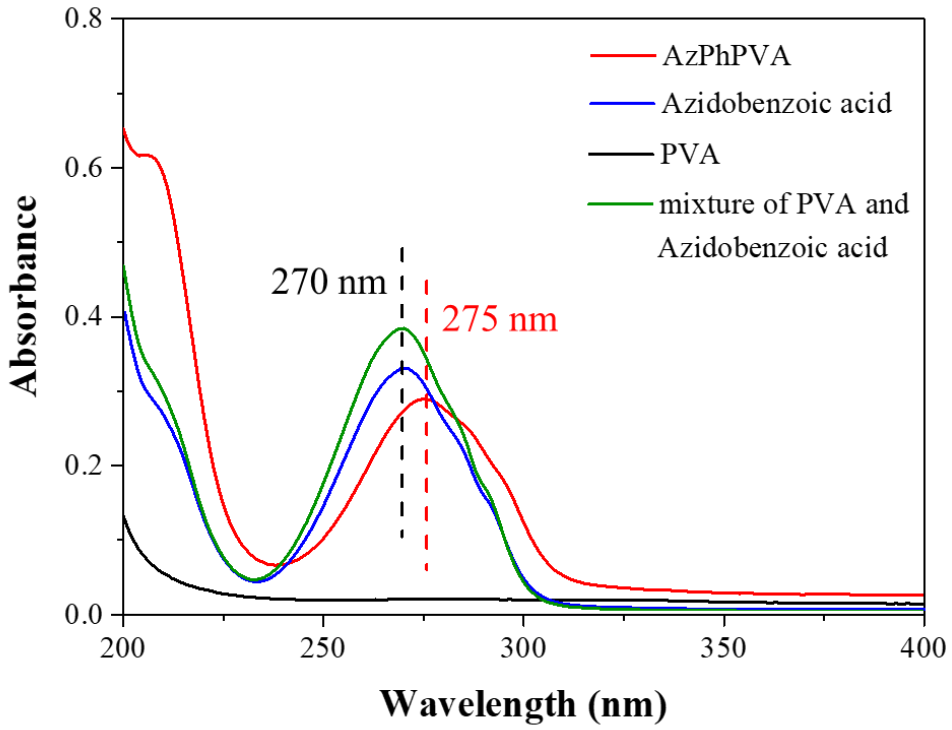

Figure 2.2 UV spectra of AzPhPVA, azidobenzoic acid, PVA and mixture of PVA and azidobenzoic acid.

Photo-reactive AzPhPVA was used to prepare PVA micro-patterns on tissue culture polystyrene (TCPS) discs through photo-lithography. TCPS discs were cut from Falcon™ tissue culture treated flask. 200 μL of 0.3 g/L AzPhPVA aqueous solution was dropped on each TCPS discs. After the AzPhPVA aqueous solution was air-dried in room temperature under dark, the AzPhPVA-coated TCPS discs were irradiated by ultraviolet light (UV, Funa-UV-linker FS-1500, 0.25 J/cm^2) through a micro-patterned photomask (Figure 2.1b). The photomask was a quartz wafer containing non-transparent micro-dots with a diameter of 20, 40, 60 and 80 μm , respectively. After UV irradiation, the unreacted AzPhPVA molecules below non-transparent micro-dots of the photomask were completely removed after ultrasonic washing in Milli-Q water. The micro-patterned discs were sterilized by immersing in 70% ethanol aqueous solution for 20 min and rinsed by aseptic Milli-Q water before cell culture.

The micro-patterned surfaces were observed by a phase-contrast microscope (BX51, Olympus, Tokyo, Japan) and characterized by an MFP-3D-BIO atomic force microscope (AFM, Asylum Research Corporation, Santa Barbara, CA). For AFM characterization, a cantilever with a nitride tip was used. Contact mode in Milli-Q water was performed during scanning process.

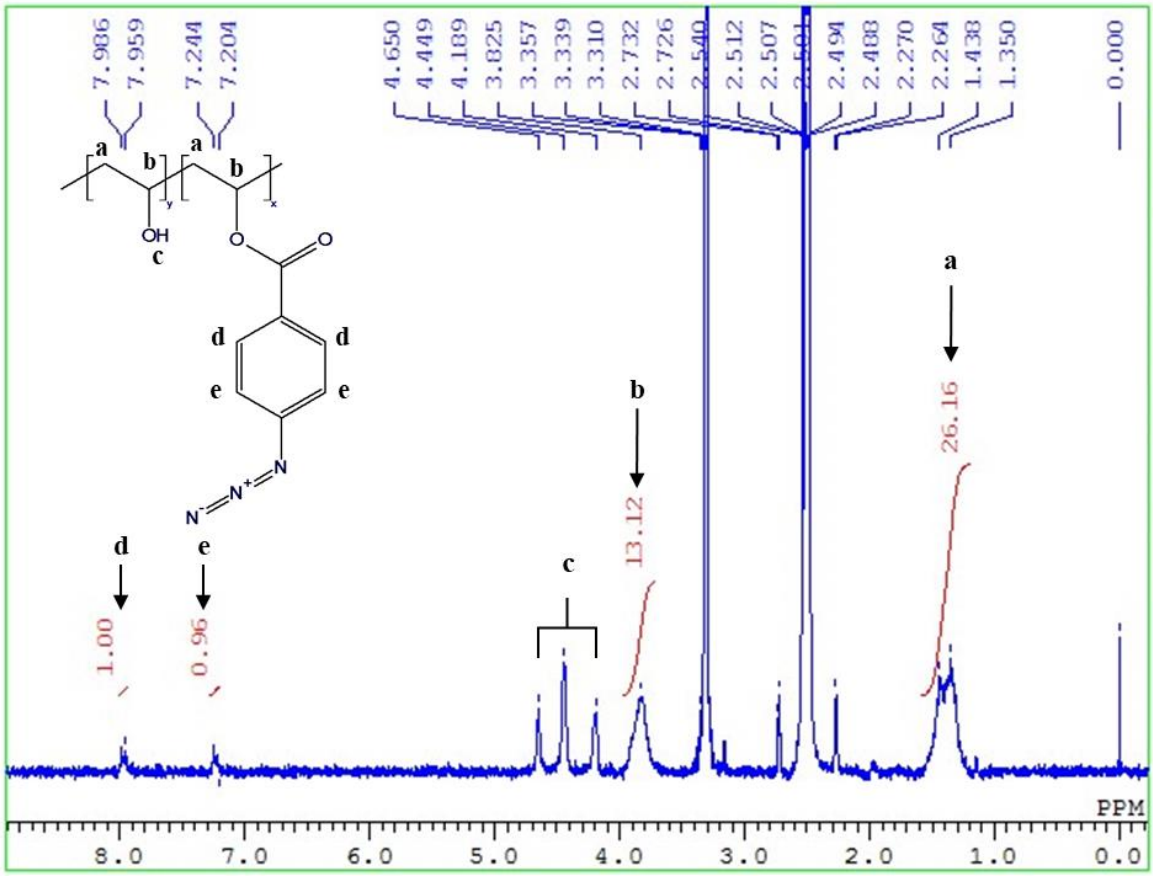

Figure 2.3 ^{1}H-NMR spectrum of synthesized AzPhPVA

2.2.3 Cell culture

Human bone marrow-derived mesenchymal stem cells (MSCs) were purchased from Lonza Walkersville, Inc at passage 2. Cell colony from single MSCs was used for the following cell culture experiments. Cell colony of MSCs was obtained by a previously reported method [28]. Briefly, less than 30 cells were seeded onto a cell culture dish (d = 10 cm) and proliferated in MSCGM^{TM} medium for 3 weeks to obtain cell colonies. Cell colonies were collected and subcultured in 25 cm^2 TCPS flask for another 3 weeks to obtain the homogeneous cell mass. The purified MSCs at passage 4 were used for following experiments. The sterilized micro-patterned discs were placed in 6-well TCPS plates and added with 3 mL MSCGM^{TM} per well. Glass rings with 1.5 cm inner diameter were placed on each micro-patterned disc to constrain the seeded cells on the micro-patterns. Cell suspension including around 5000 cells was added inner each glass ring. Glass rings were removed after the cells were cultured on the micro-patterned surfaces in a CO_2 incubator at 37 °C for 6 hours. After another 18 hours culture, cell attachment on the micro-patterned surfaces was observed by a phase-contrast microscope.

After MSCs were cultured on the micro-patterned surfaces in MSCGM^{TM} for 24 hours, the culture medium was replaced by osteogenic induction medium (complete DMEM serum medium supplied with 100 nM DEX and 10 mM GP. The osteogenic induction culture was continued for 3 days, 1 week, 2 weeks and 3 weeks. To investigate if the osteogenically differentiated cells could maintain their differentiated phenotype, the osteogenic induction

medium was changed to proliferation medium without osteogenic induction factors. After osteogenic induction culture for designated time, the osteogenic induction medium was replaced to proliferation medium MSCGM™ and the cells were further cultured for 1 week or 2 weeks under 37 °C and 5% CO_2 in a humidified incubator. The medium was refreshed every 3 days.

2.2.4 Fluorescence staining of actin and nuclei

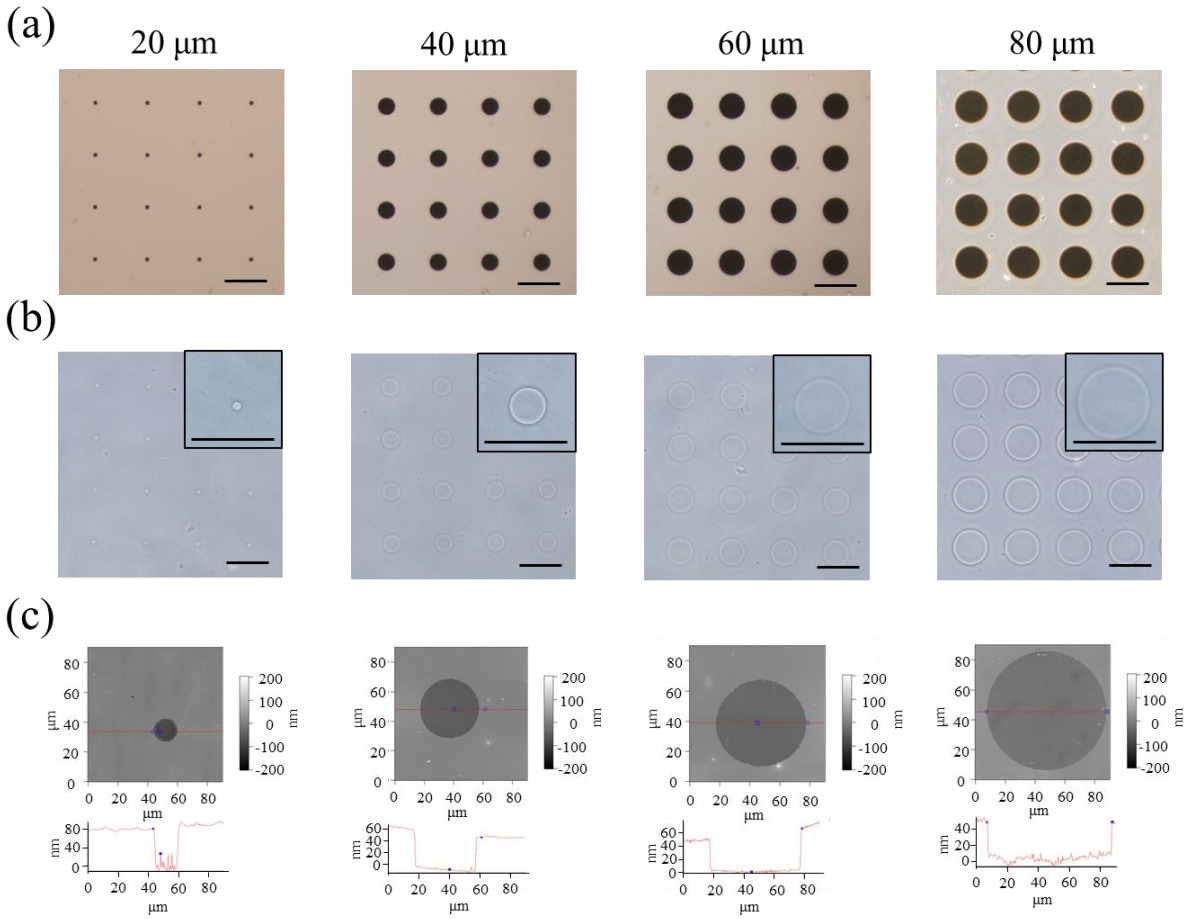

Figure 2.4 Characterization of PVA/TCPS micro-patterned surfaces. Representative photomicrographs of micro-patterned photomask. Scale bar: 100 μm. (b) Representative photomicrographs of micro-patterned surfaces. Scale bar: 100 μm. (c) Representative height images (up) and section images (down) of micro-patterned surfaces characterized by AFM.

After the MSCs were cultured on micro-patterned surfaces in proliferation medium for 1 day, the cells were fixed by paraformaldehyde aqueous solution. The fixed samples were permeabilized by Triton™ X-100 and blocked by immersing in BSA aqueous solution in room temperature. Then, the cells were stained by Alexa Fluor-488® phalloidin in room temperature under dark for 20 minutes. After being rinsed by PBS solution, the samples were air dried in room temperature and mounted with VECTASHEILD®. Fluorescence images of each sample were captured through an Olympus fluorescence microscope.

2.2.5 Immunofluorescence staining of stem cell marker

A representative marker of MSCs, CD105 (endoglin), was stained after MSCs were cultured on the micro-patterned surfaces at the above-mentioned conditions. Samples were fixed by paraformaldehyde aqueous solution

and blocked by BSA and glycine for 30 minutes in room temperature. Samples were incubated with a primary CD105 antibody (Invitrogen, CA, USA) aqueous solution diluted at 1:500 in 1% BSA. After being rinsed with PBS, the samples were incubated with an Alexa Fluor-488® conjugated goat anti-mouse IgG antibody (Invitrogen, CA, USA) at a dilution ratio of 1:1000 in PBS in room temperature. After being rinsed for by PBS and dried in room temperature under dark, the samples were mounted by VECTASHEILD® (with DAPI, Vector Laboratories, Inc.). The fluorescent images of stained cells were obtained through a fluorescence Olympus BX51 microscope at a fixed parameter (5s, ISO:200). The corrected total fluorescence (CTF_{Cell}) of CD105 was calculated through an ImageJ software. The area (A_{Cell}) and integrated intensity (I_{Cell}) of each micro-patterned cell were measured. The area ($A_{Background}$) and integrated intensity ($I_{Background}$) of micro-patterns without cells were also measured and set as background. The *CTF* of CD105 in micro-patterned cells was calculated as $CTF_{Cell} = (I_{Cell}/A_{Cell} - I_{Background}/A_{Background}) \times A_{Cell}$. The *CTF* of micro-patterned cells which were only incubated with secondary antibody (Alexa Fluor-488® conjugated goat anti-mouse IgG antibody) without incubation with first antibody were calculated and set as a control group ($CTF_{Control}$). CD105 positive cells were defined as the cells having 50 times higher fluorescence intensity than control group ($CTF_{Cell}/CTF_{Control} > 50$). The ratio of CD105 positive cell number to the total cell number was calculated to evaluate the stemness of MSCs. More than 150 cells from 3 independent experiments were used for the analysis.

2.2.6 Alkaline phosphatase and Alizarin Red S staining

Osteogenic differentiation of MSCs on the micro-patterned surfaces during osteogenic induction culture was evaluated by alkaline phosphatase (ALP) staining and alizarin red S (ARS) staining. After MSCs were culture for designated time, the cells were rinsed with pre-warmed PBS solution for twice and fixed with 4% cold paraformaldehyde aqueous solution and rinsed with PBS. Then, the fixed samples were immersed in staining solution of ALP or ARS in room temperature for 10 minutes. ALP staining solution was composed of 56 mM 2-amino-2-methyl-1,3-propanediol (Sigma-Aldrich Co. LLC., USA), 0.1 wt% naphthol AS-MX phosphate (Sigma-Aldrich Co. LLC., USA) and 0.1 wt% Fast Blue RR salt (Sigma-Aldrich Co. LLC., USA). ARS staining solution was 0.1% ARS solution. Optical images of the stained cells were obtained through a phase-contrast microscope. The optical images were analyzed by Color Deconvolution plugin of ImageJ to discriminate ALP positive and negative cells. In the original optical images, color-specific vectors were assigned as purple and brown channels. The percentage of ALP or ARS positively stained cells was calculated. More than 150 cells from 3 independent experiments were analyzed.

2.2.7 Statistical analysis

The quantitative data are reported as means ± standard deviation (SD). The significant difference was confirmed through multiple comparisons of one-way ANOVA. The significant difference was defined when $p < 0.05$.

2.3 Result

2.3.1 Characterization of synthesized photo-reactive AzPhPVA

The photo-reactive AzPhPVA was synthesized according to the previous articles [27]. The photo-reactive azido

groups were introduced into PVA through the reaction between carboxyl groups of azidobenzoic acid and hydroxyl groups of PVA. Compared with PVA absorbance curve, the absorbance peak at 275 nm in AzPhPVA absorbance curve indicated the benzenoid structure was included in the AzPhPVA aqueous solution (Figure 2.2). To confirm the azidophenyl groups were successfully introduced into the PVA through the esterification, the azidobenzoic acid aqueous solution and the mixture of PVA and azidobenzoic acid aqueous solution were measured. The benzenoid structure absorbance peak in the curves of unreacted azidobenzoic acid was appeared at 270 nm. The bathochromic shift of benzenoid absorbance peak was related with the configuration change of benzoic acid [29]. The percentage of azidophenyl groups in AzPhPVA was calculated through spectrum of ^{1}H-NMR (Figure 2.3). The peaks between 7.0 and 8.0 ppm represented the protons of benzenoid structure. The peaks at 1.4 and 3.8 ppm represented the methylene and methylidyne protons on PVA, respectively. The grafting degree was calculated through integration of each peak.

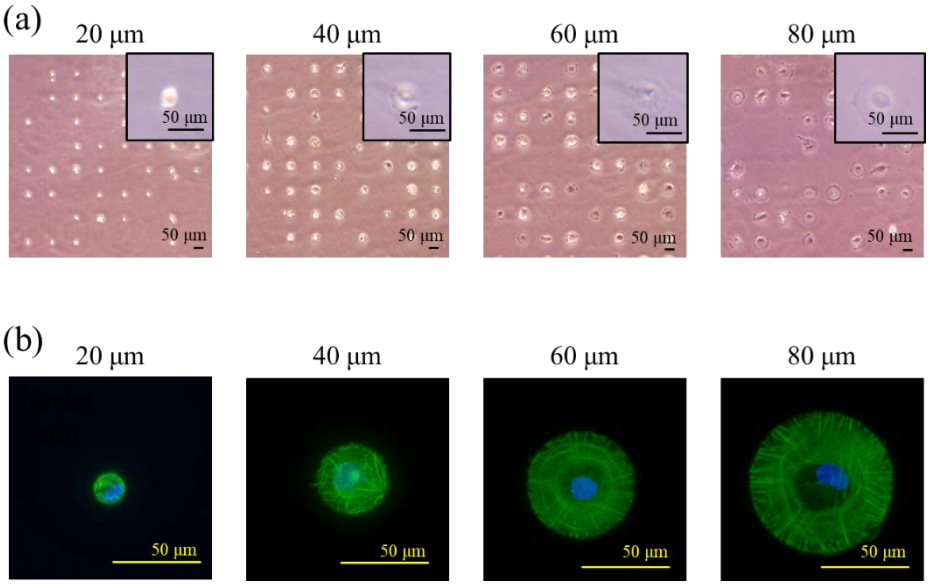

Figure 2.5 Cell adhesion and morphology on micro-patterned surfaces. (a) Representative photomicrographs of MSCs adhered on micro-patterned surfaces after culture in proliferation medium for 1 day. (b) Representative images of actin (green) and nuclei (blue) staining images of MSCs shown in (a).

2.3.2 Preparation and characterization of micro-patterned surfaces

As shown at Figure 2.1b, the PVA/TCPS micro-patterned surfaces were prepared through UV-lithography. A thin layer of photo-reactive AzPhPVA was firstly coated on cell adhesive TCPS discs. The AzPhPVA-coated TCPS discs were UV irradiated through a transparent quartz photomask with non-transparent micro-patterns. After UV irradiation, the AzPhPVA molecules below transparent regions of the photomask were grafted on the TCPS disc surface. The AzPhPVA molecules below non-transparent micro-patterns of the photomask were easily stripped from the TCPS surfaces after washing procedure. After washing, micro-patterned TCSP surfaces were obtained. Microdots of cell adhesive TCPS were surrounded with cell repellent PVA layer. The circular micro-dot patterns prepared with a photomask having a micro-dot diameter of 20, 40, 60 and 80 μm showed the same micro-pattern structure as that of the photomask (Figure 2.4 b, Figure 2.4 c). As characterized by AFM, the micro-patterned micro-dots had a diameter of 20.2 ± 0.5, 41.3 ± 0.4, 60.7 ± 1.4 and 82.1 ± 1.4 μm , respectively. The area of each type of circular micro-patterns was 321.5 ± 17.2, 1338.6 ± 23.0, 2894.0 ± 134.9 and 5294.4 ± 184.7 μm^2 , respectively. The depth of PVA layer in the four types of micro-dot patterns was 64.6 ± 3.1, 58.4 ± 3.4, 58.3 ± 3.2 and 60.6 ± 4.9 nm ,

respectively. All the micro-dot patterns had almost the same thickness of surrounding PVA layer, which could protect protein adhesion and protect cell adhesion. Cells could only adhere on the TCPS micro-dots to form micro-patterned cells.

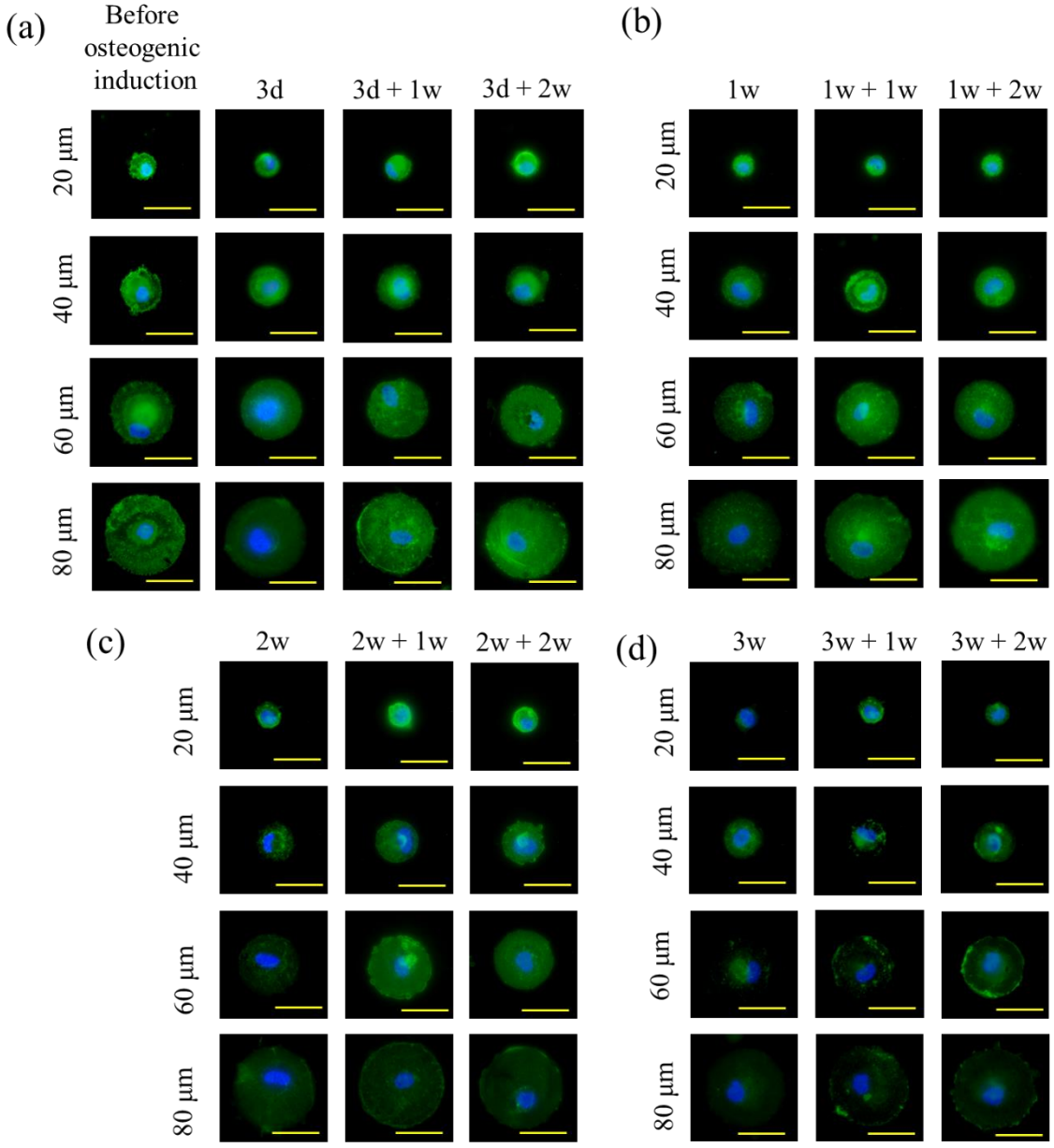

Figure 2.6 Representative images of CD105 immunofluorescence staining of (a) Micro-patterned MSCs cultured in osteogenic induction medium for 3 days (3d) and re-cultured in proliferation medium for 1 (3d + 1w) and 2 (3d + 2w) weeks; (b) Micro-patterned MSCs cultured in osteogenic induction medium for 1 week (1w) and re-cultured in proliferation medium for 1 (1w + 1w) and 2 (1w + 2w) weeks; (c) Micro-patterned MSCs cultured in osteogenic induction medium for 2 weeks (2w) and re-cultured in proliferation medium for 1 (2w + 1w) and 2 (2w + 2w) weeks. (d) Micro-patterned MSCs cultured in osteogenic induction medium for 3 weeks (3w) and re-cultured in proliferation medium for 1 (1w + 1w) and 2 (1w + 2w) weeks. Scale bar: 50 µm.

2.3.3 Cell morphology and actin filaments structure

The PVA/TCPS circular micro-patterns were used for culture of MSCs to control cell size and spreading area.

MSCs adhered on the TCPS micro-dots of the micro-patterned surfaces, not on the PVA-grafted regions (Figure 2.5 a). MSCs on the small TCPS micro-dots having a diameter of 20 μm did not spread, while MSCs on the large TCPS micro-dots with 40, 60 and 80 μm in diameter spread along the micro-dots. The cells showed the same circular morphology as that of the micro-dots. The spreading area was almost the same as that of the micro-dots. Therefore, cell morphology and size were precisely controlled by the micro-patterned surfaces. Staining of actin filaments and nuclei showed actin filament structure was different when the size of micro-dots was changed (Figure 2.5 b). The actin filaments of micro-patterned MSCs with a diameter of 20 μm showed random structure without clear alignment. When the spreading area of micro-patterned MSCs increased, alignment of actin filaments became more evident. The micro-patterned MSCs with a diameter of 80 μm had highly aligned actin filaments that were well assembled along the radial and concentric directions.

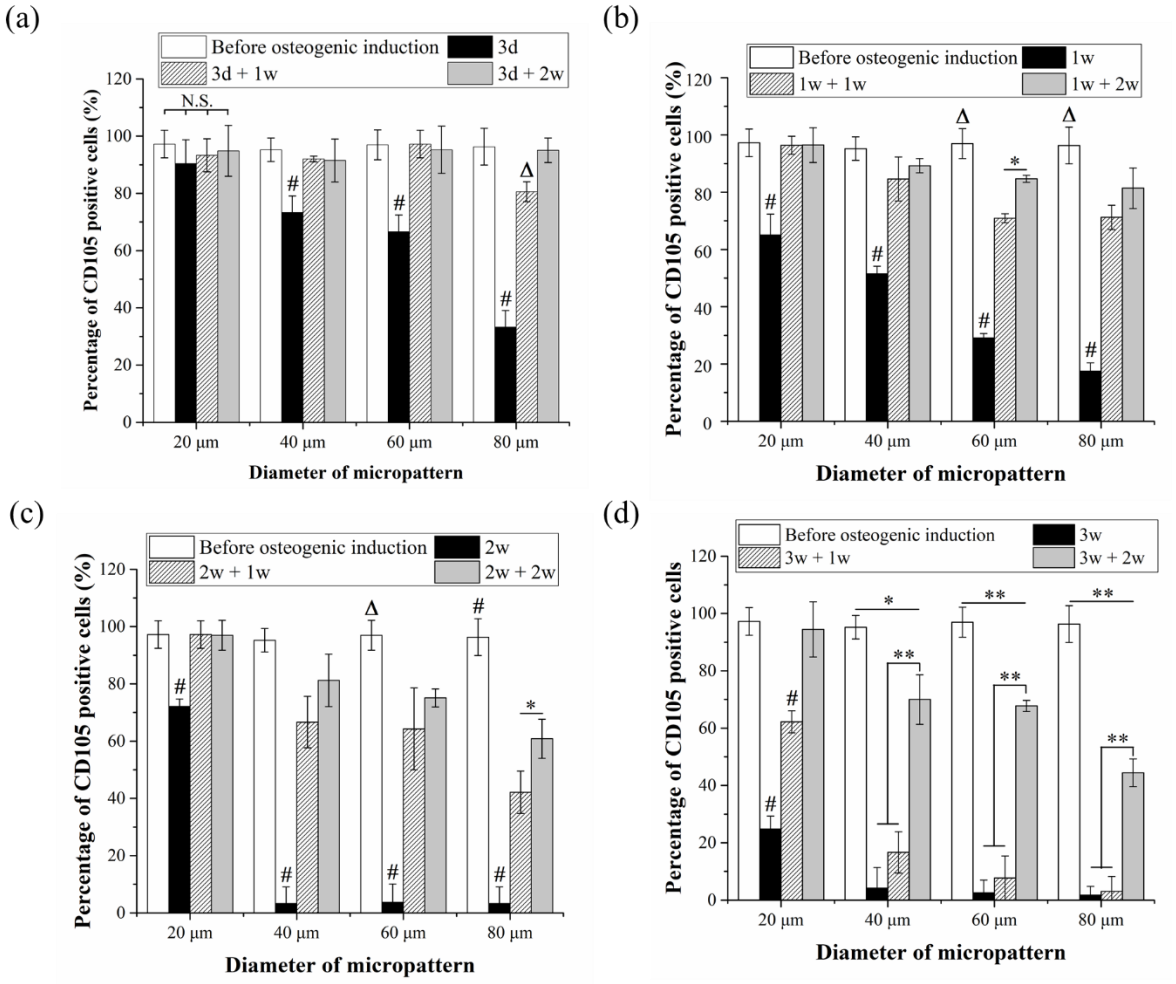

Figure 2.7 Percentage of CD105 positively stained micro-patterned MSCs. Cell culture condition was the same as that shown in Figure 2.6. Data are reported as mean ± SD, n = 3, *$p < 0.01$, **$p < 0.001$. # or Δ represented $p < 0.01$ or $p < 0.001$ in comparison between the respect percentage of CD105 positively stained MSCs and the other three groups with same cell spreading area and different cell culture conditions.

2.3.4 Influence of cell size on CD105 expression

CD105 is a representative marker of MSCs. CD105 expression was analyzed during cell culture to evaluate

the stemness of MSCs. The micro-patterned MSCs cultured at different conditions were immunofluorescently stained with CD105 antibody. The representative images of immunofluorescence staining of CD105 of MSCs cultured in proliferation medium before osteogenic induction (without induction culture); cultured in osteogenesis differentiation medium for 3 days, 1, 2 and 3 weeks (osteogenic induction); cultured in osteogenesis differentiation medium for 3 days, 1, 2 and 3 weeks followed with culture in proliferation medium for 1 and 2 weeks (re-culture in proliferation medium after initial osteogenic induction) are shown in Figure 2.6. Nearly all of the micro-patterned MSCs' CD105 was positively stained when they were cultured in proliferation medium before osteogenic induction culture. When MSCs were cultured in osteogenic induction medium, the fluorescence of CD105 staining became weak. When the culture medium was changed from osteogenic induction medium to proliferation medium after initial osteogenic induction culture for a certain period, the fluorescence intensity of stained CD105 slightly increased again.

CD105 positive MSCs were counted from the immunofluorescent staining of CD105 and percentage of CD105 positive MSCs was calculated to show CD105 expression level (Figure 2.7). After osteogenic induction culture for 3 days, CD105 expression of MSCs having a diameter of 20 μm was at the same level as that of MSCs without induction culture. CD105 expression level of MSCs after induction culture decreased significantly when the size of MSCs increased. MSCs having a diameter of 80 μm expressed the least CD105. When the 3 day inducted MSCs were re-cultured in proliferation medium after osteogenic induction, CD1045 expression level increased and reached the initial level after 2 weeks re-culture. The rebound of CD105 expression was slower when the cells were larger. When the initial osteogenic induction culture time lasted for 1, 2 and 3 weeks, decrease of CD105 expression became more evident. Even for MSCs having a diameter of 20 μm, CD105 expression level of MSCs after osteogenic induction culture for 1, 2 and 3 weeks was significantly lower than that of MSCs without induction culture. When cell size was larger, decrease of CD105 expression level became more evident. When osteogenic induction period was longer than 2 weeks, almost no CD105 expression could be detected except for the cells having a diameter of 20 μm.

When the initially inducted MSCs were re-cultured in proliferation medium, expression level of CD105 showed some rebound. The rebound degree was higher and quicker for smaller cells and shorter induction culture time. MSCs having a diameter of 80 μm showed the lowest expression of CD105 and slowest rebound. CD105 expression recovery capacity of micro-patterned MSCs was weakened by the extended osteogenic induction. After MSCs were cultured in initial induction condition for 1, 2 and 3 weeks, the rebound of CD105 expression in cells with 60 and 80 μm in diameter were very limited and could not reach the level without initial induction. However, MSCs having a smaller diameter showed higher CD105 expression recovery capacity after re-culture in proliferation medium. In particular, CD105 expression of MSCs having a diameter of 20 μm could be totally recovered even after initial induction culture for 3 weeks

2.3.5 Influence of cell size on ALP activity and calcium deposition

ALP is a maker to indicate the osteogenic differentiation activity of MSCs. ALP staining of micro-patterned MSCs was conducted to analyze the early osteogenic differentiation at different time point. The ALP positively expressed cells were stained in purple and negatively stained cells appear in brown (Figure 2.9). ALP staining was not evident when cell size was small and osteogenic induction culture time was short, while it became evident when the cell size was large and induction time was extended.

Percentage of ALP positively expressed cells was calculated from the images of ALP staining (Figure 2.9). After osteogenic induction culture for 3 days, ALP positive MSCs were not detected from the small MSCs having a diameter of 20 μm, while a small amount of ALP positive cells was detected in large MSCs. ALP positive MSCs cannot been observed when culture medium was changed to proliferation medium. ALP activity increased when

osteogenic induction period was extended to 1 and 2 weeks. Compared with MSCs osteogenically induced for 2 weeks, ALP activity of micro-patterned MSCs was slightly decreased after osteogenic induction culture for 3 weeks. ALP activity could decrease slowly when osteogenic differentiation proceeded to late stage. Among all the ALP activity results after initial osteogenic induction, larger MSCs showed higher ALP activity. Meanwhile, ALP activity decreased significantly when osteogenic induction medium was changed to proliferation medium.

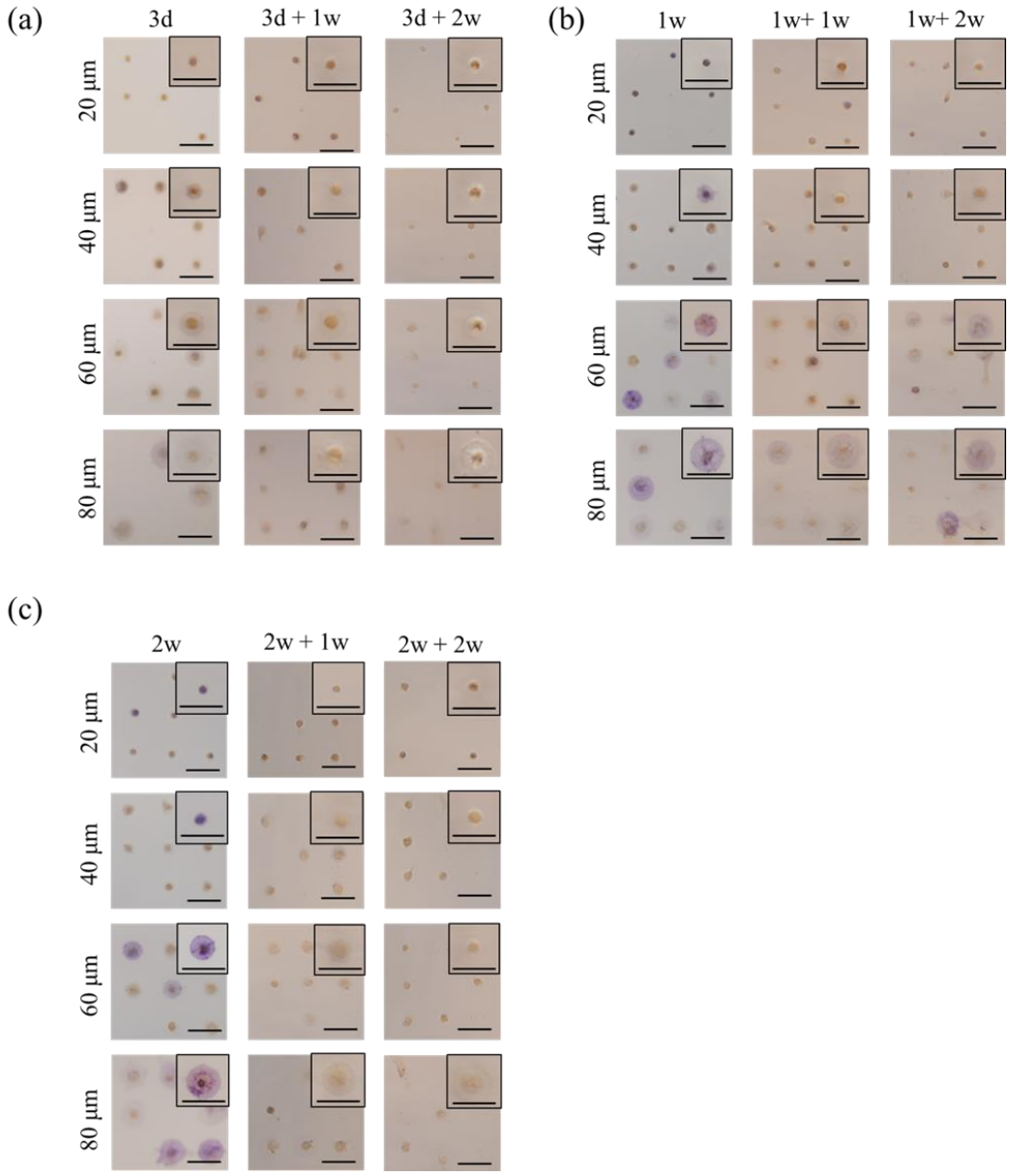

Figure 2.8 Representative images of ALP stained micro-patterned MSCs. Cell culture condition was same as that shown in Figure 2.6. Scale bar: 100 µm.

Calcium deposition is a mature marker of MSCs osteogenesis. Calcium deposition of micro-patterned MSCs was stained by ARS to further investigate their osteogenic differentiation. ARS positive MSCs appeared as red spots and ARS negative cells appeared in brown (Figure 2.10 a). Calcium deposition was not detected when osteogenic induction culture time was short (3 days and 1 week). Only after osteogenic induction culture for 2 weeks, calcium deposition was detected. More cells showed calcium deposition when osteogenic induction culture time became longer and cell size was larger. Percentage of ARS positive cells was calculated from the images of ARS staining (Figure 2.10 b). After osteogenic induction culture for 2 weeks, calcium deposition was detected in large MSCs having a diameter of 60 and 80 µm. More calcium deposition was observed after MSCs were osteogenically induced

for 3 weeks. Percentage of ARS positive cells increased with the size of MSCs. When the initially inducted MSCs were re-cultured in proliferation medium, percentage of ARS positive cells was significantly decreased.

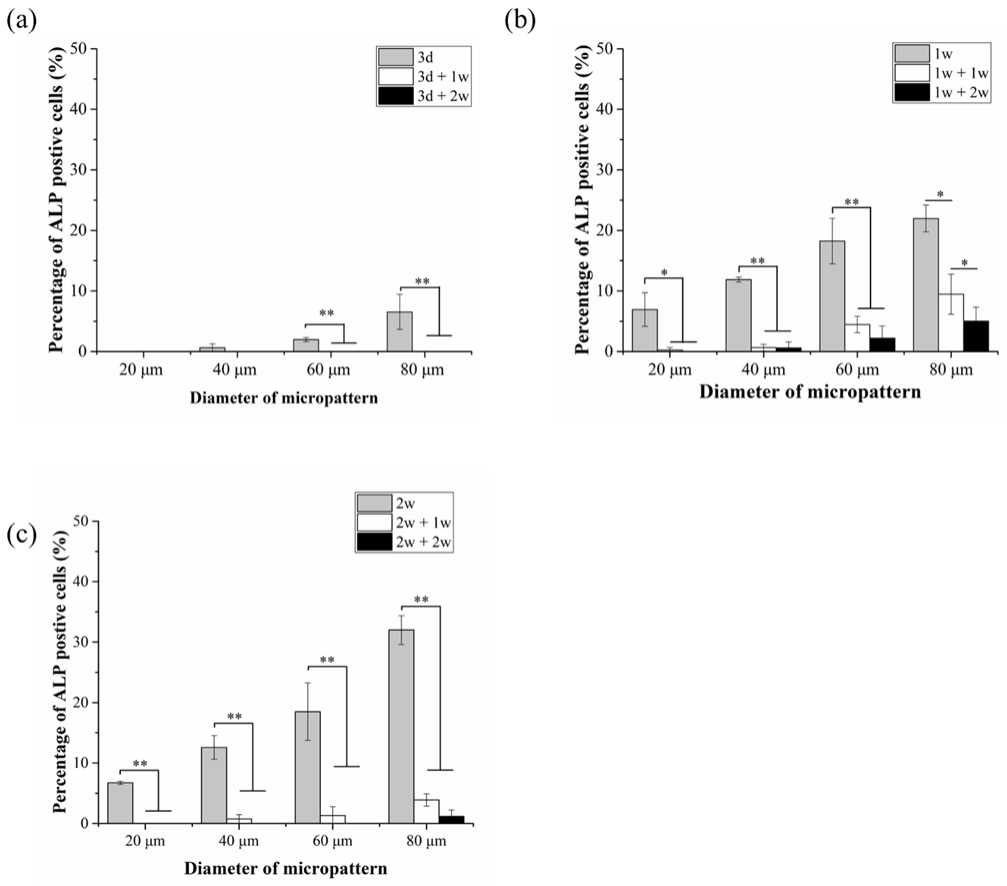

Figure 2.9 Percentage of ALP positively stained micro-patterned MSCs Cell culture condition was same as that shown in Figure 2.6. Data are reported as mean ± SD, n = 3, *$p < 0.01$, **$p < 0.001$.

2.4 Discussion

PVA/TCPS micro-dots patterns were used for culture of MSCs to control cell size for investigation of cell size influence on osteogenic commitment and maintenance of differentiated phenotype of MSCs. Not only cell size influence on osteogenic differentiation of MSCs was analyzed, but also its influence on de-differentiation of the initially differentiated cells and re-expression of stem cell marker was investigated. After MSCs were cultured on the PVA/TCPS micro-patterned surfaces, the spreading area of MSCs was precisely manipulated and cell size was determined by the diameter of TCPS micro-dots. The cells had almost the same diameter as that of the micro-dots (20, 40, 60 and 80 µm). The well aligned and organized actin filaments presented in large MSCs indicated that actin polymerization was promoted by cell spreading (Figure 2.5 b). Well organized actin filaments can lead to high cell contractility [30] which is critical in regulation of osteogenic differentiation [27, 31] and stemness maintenance [28] of MSCs.

Stemness and osteogenic commitment of MSCs on the micro-patterned surfaces were investigated by staining stem cell marker and osteogenic differentiation markers. CD105 is a surface marker to identify mesenchymal stem cells [32] and to evaluate their multipotency [33]. Expression level of CD105 on membrane surface of MSCs has been reported to be associated with the process of osteogenesis [34-36]. In this research, expression of CD105 was

used to evaluate the stemness of micro-patterned MSCs of different size during initial osteogenic induction culture and re-culture in proliferation medium. Alkaline phosphate (ALP) and calcium deposition which are the respective early and late markers of osteogenic differentiation of MSCs were used to evaluate osteogenic differentiation.

Expression of CD105 in the micro-patterned MSCs decreased as the osteogenic induction period was extended. At each group, larger MSCs showed lower CD105 expression level and higher ALP activity and calcium deposition. As previously reported that large MSCs can promote osteogenesis [37], the high level of CD105 expression by small MSCs in this study should be due to the inhibition of osteogenesis. The result was also consistent with the previous results that multipotency of MSCs decreases during osteogenesis process [36] and small spreading area is beneficial for maintenance of stemness [28].

After the osteogenic induction medium was replaced by proliferation medium, osteogenesis of micro-patterned MSCs was immediately inhibited and the CD105 expression was partially or fully recovered. Recoverability of stemness was related with cell size and osteogenic induction period. The fully recovered CD105 expression was only observed in small MSCs or MSCs were osteogenically induced for a short period. The results indicated that stemness recoverability could be compromised by promoted osteogenesis or stemness could only be recovered at the initial stage of osteogenesis. Cell size could not only affect osteogenic differentiation of MSCs, but also affected the de-differentiation of the initially differentiated cells and recovered expression of stem cell marker. Large MSCs facilitated osteogenic differentiation of MSCs more strongly than did small MSCs, while small MSCs could return to stem cell stage more easily than did large cells.

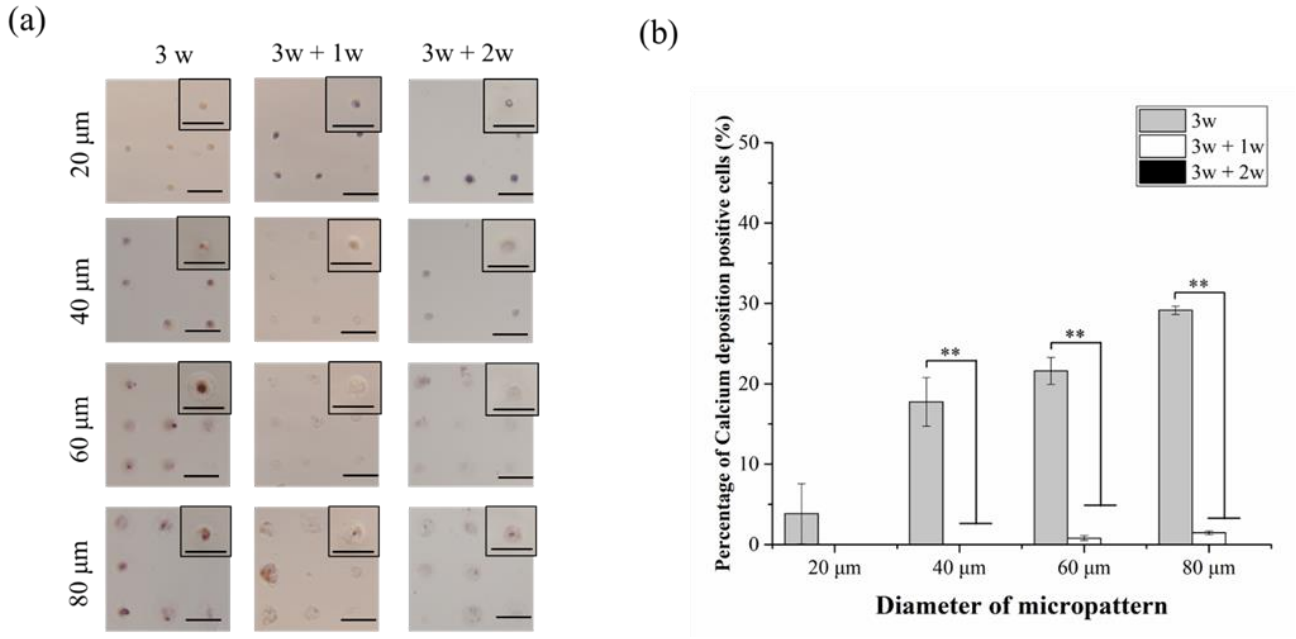

Figure 2.10 (a) Representative images of ARS stained micropatterned MSCs cultured in osteogenic induction medium for 3 weeks (3w) and re-cultured in proliferation medium for 1 (1w + 1w) and 2 (1w + 2w) weeks. Scale bar: 100 µm. (b) Percentage of ARS positively stained micropatterned MSCs.

2.5 Conclusions

In summary, by using UV-lithography and photoreactive AzPhPVA, PVA/TCPS micro-patterned surfaces were prepared and used to control the size of MSCs for investigation of the influence of cell morphological cues on

osteogenic differentiation and commitment of MSCs. Large MSCs promoted osteogenic differentiation while suppressed recoverability of stem cell marker expression. On the contrast, small MSCs inhibited osteogenic differentiation but facilitated recovering of stem cell marker expression. The results indicated that cell size was an important factor for stem cell differentiation and commitment.

2.6 References

[1] F.J. O'Brien, Biomaterials & scaffolds for tissue engineering, Materials Today 14(3) (2011) 88-95.
[2] L. Guo, Y. Fan, N. Kawazoe, H. Fan, X. Zhang, G. Chen, Fabrication of gelatin-micropatterned surface and its effect on osteogenic differentiation of hMSCs, Journal of Materials Chemistry B 6(7) (2018) 1018-1025.
[3] Y. Yang, X. Wang, T.-C. Huang, X. Hu, N. Kawazoe, W.-B. Tsai, Y. Yang, G. Chen, Regulation of mesenchymal stem cell functions by micro–nano hybrid patterned surfaces, Journal of Materials Chemistry B 6(34) (2018) 5424-5434.
[4] T. Nakamoto, X. Wang, N. Kawazoe, G. Chen, Influence of micropattern width on differentiation of human mesenchymal stem cells to vascular smooth muscle cells, Colloids and surfaces. B, Biointerfaces 122 (2014) 316-323.
[5] J.S. Park, J.S. Chu, A.D. Tsou, R. Diop, Z. Tang, A. Wang, S. Li, The effect of matrix stiffness on the differentiation of mesenchymal stem cells in response to TGF-beta, Biomaterials 32(16) (2011) 3921-30.
[6] L.A. Solchaga, K.J. Penick, J.F. Welter, Chondrogenic differentiation of bone marrow-derived mesenchymal stem cells: tips and tricks, Methods in molecular biology 698 (2011) 253-78.
[7] G.S. Huang, L.G. Dai, B.L. Yen, S.H. Hsu, Spheroid formation of mesenchymal stem cells on chitosan and chitosan-hyaluronan membranes, Biomaterials 32(29) (2011) 6929-45.
[8] L. Bian, D.Y. Zhai, E. Tous, R. Rai, R.L. Mauck, J.A. Burdick, Enhanced MSC chondrogenesis following delivery of TGF-beta3 from alginate microspheres within hyaluronic acid hydrogels in vitro and in vivo, Biomaterials 32(27) (2011) 6425-34.
[9] G. Abagnale, M. Steger, V.H. Nguyen, N. Hersch, A. Sechi, S. Joussen, B. Denecke, R. Merkel, B. Hoffmann, A. Dreser, U. Schnakenberg, A. Gillner, W. Wagner, Surface topography enhances differentiation of mesenchymal stem cells towards osteogenic and adipogenic lineages, Biomaterials 61 (2015) 316-26.
[10] J. Li, J. Zhang, Y. Chen, N. Kawazoe, G. Chen, TEMPO-Conjugated Gold Nanoparticles for Reactive Oxygen Species Scavenging and Regulation of Stem Cell Differentiation, ACS applied materials & interfaces 9(41) (2017) 35683-35692.
[11] X. Wang, W. Song, N. Kawazoe, G. Chen, Influence of cell protrusion and spreading on adipogenic differentiation of mesenchymal stem cells on micropatterned surfaces, Soft Matter 9(16) (2013) 4160.
[12] A.I. Caplan, Adult mesenchymal stem cells for tissue engineering versus regenerative medicine, Journal of cellular physiology 213(2) (2007) 341-7.
[13] A. Higuchi, Q.D. Ling, S.T. Hsu, A. Umezawa, Biomimetic cell culture proteins as extracellular matrices for stem cell differentiation, Chemical reviews 112(8) (2012) 4507-40.
[14] C.M. Kolf, E. Cho, R.S. Tuan, Mesenchymal stromal cells. Biology of adult mesenchymal stem cells: regulation of niche, self-renewal and differentiation, Arthritis Res Ther 9(1) (2007) 204.
[15] D. Li, J. Zhou, F. Chowdhury, J. Cheng, N. Wang, F. Wang, Role of mechanical factors in fate decisions of stem cells, Regenerative Medicine 6(2) (2011) 229-240.
[16] Y.M. Chen, L.H. Chen, M.P. Li, H.F. Li, A. Higuchi, S.S. Kumar, Q.D. Ling, A.A. Alarfaj, M.A. Munusamy, Y. Chang, G. Benelli, K. Murugan, A. Umezawa, Xeno-free culture of human pluripotent stem cells on oligopeptide-grafted hydrogels with various molecular designs, Scientific reports 7 (2017) 45146.

[17] A. Higuchi, Q.D. Ling, Y. Chang, S.T. Hsu, A. Umezawa, Physical cues of biomaterials guide stem cell differentiation fate, Chemical reviews 113(5) (2013) 3297-328.
[18] R.G. Thakar, Q. Cheng, S. Patel, J. Chu, M. Nasir, D. Liepmann, K. Komvopoulos, S. Li, Cell-shape regulation of smooth muscle cell proliferation, Biophysical journal 96(8) (2009) 3423-32.
[19] L. Chin, Y. Xia, D.E. Discher, P.A. Janmey, Mechanotransduction in cancer, Current opinion in chemical engineering 11 (2016) 77-84.
[20] X. Wang, F. Lv, T. Li, Y. Han, Z. Yi, M. Liu, J. Chang, C. Wu, Electrospun Micropatterned Nanocomposites Incorporated with Cu2S Nanoflowers for Skin Tumor Therapy and Wound Healing, ACS nano 11(11) (2017) 11337-11349.
[21] H. Xu, F. Lv, Y. Zhang, Z. Yi, Q. Ke, C. Wu, M. Liu, J. Chang, Hierarchically micro-patterned nanofibrous scaffolds with a nanosized bio-glass surface for accelerating wound healing, Nanoscale 7(44) (2015) 18446-52.
[22] T.L. Downing, J. Soto, C. Morez, T. Houssin, A. Fritz, F. Yuan, J. Chu, S. Patel, D.V. Schaffer, S. Li, Biophysical regulation of epigenetic state and cell reprogramming, Nature materials 12(12) (2013) 1154-62.
[23] X. Wang, X. Hu, J. Li, A.C. Russe, N. Kawazoe, Y. Yang, G. Chen, Influence of cell size on cellular uptake of gold nanoparticles, Biomaterials science 4(6) (2016) 970-8.
[24] J. Yuan, G. Sahni, Y.C. Toh, Stencil Micropatterning for Spatial Control of Human Pluripotent Stem Cell Fate Heterogeneity, Methods in molecular biology 1516 (2016) 171-181.
[25] M. Tagami, S. Ichinose, K. Yamagata, H. Fujino, S. Shoji, M. Hiraoka, S. Kawano, Genetic and ultrastructural demonstration of strong reversibility in human mesenchymal stem cell, Cell Tissue Res 312(1) (2003) 31-40.
[26] K.C. Murphy, A.I. Hoch, J.N. Harvestine, D. Zhou, J.K. Leach, Mesenchymal Stem Cell Spheroids Retain Osteogenic Phenotype Through alpha2beta1 Signaling, Stem Cells Transl Med 5(9) (2016) 1229-37.
[27] X. Wang, X. Hu, I. Dulinska-Molak, N. Kawazoe, Y. Yang, G. Chen, Discriminating the Independent Influence of Cell Adhesion and Spreading Area on Stem Cell Fate Determination Using Micropatterned Surfaces, Scientific reports 6 (2016) 28708.
[28] X. Wang, T. Nakamoto, I. Dulińska-Molak, N. Kawazoe, G. Chen, Regulating the stemness of mesenchymal stem cells by tuning micropattern features, J. Mater. Chem. B 4(1) (2016) 37-45.
[29] H.B. Guo, F. He, B. Gu, L. Liang, J.C. Smith, Time-dependent density functional theory assessment of UV absorption of benzoic acid derivatives, J Phys Chem A 116(48) (2012) 11870-9.
[30] A. Pitaval, Q. Tseng, M. Bornens, M. Thery, Cell shape and contractility regulate ciliogenesis in cell cycle-arrested cells, The Journal of cell biology 191(2) (2010) 303-12.
[31] K.A. Kilian, B. Bugarija, B.T. Lahn, M. Mrksich, Geometric cues for directing the differentiation of mesenchymal stem cells, Proceedings of the National Academy of Sciences of the United States of America 107(11) (2010) 4872-7.
[32] M. Dominici, K. Le Blanc, I. Mueller, I. Slaper-Cortenbach, F. Marini, D. Krause, R. Deans, A. Keating, D. Prockop, E. Horwitz, Minimal criteria for defining multipotent mesenchymal stromal cells. The International Society for Cellular Therapy position statement, Cytotherapy 8(4) (2006) 315-7.
[33] D. Zhang, K.A. Kilian, The effect of mesenchymal stem cell shape on the maintenance of multipotency, Biomaterials 34(16) (2013) 3962-9.
[34] H.J. Jin, S.K. Park, W. Oh, Y.S. Yang, S.W. Kim, S.J. Choi, Down-regulation of CD105 is associated with multi-lineage differentiation in human umbilical cord blood-derived mesenchymal stem cells, Biochem Biophys Res Commun 381(4) (2009) 676-81.
[35] B. Levi, D.C. Wan, J.P. Glotzbach, J. Hyun, M. Januszyk, D. Montoro, M. Sorkin, A.W. James, E.R. Nelson, S. Li, N. Quarto, M. Lee, G.C. Gurtner, M.T. Longaker, CD105 protein depletion enhances human adipose-derived stromal cell osteogenesis through reduction of transforming growth factor beta1 (TGF-beta1) signaling, The Journal of biological chemistry 286(45) (2011) 39497-509.

[36] T. Na, J. Liu, K. Zhang, M. Ding, B.Z. Yuan, The notch signaling regulates CD105 expression, osteogenic differentiation and immunomodulation of human umbilical cord mesenchymal stem cells, PloS one 10(2) (2015) e0118168.
[37] W. Song, N. Kawazoe, G. Chen, Dependence of Spreading and Differentiation of Mesenchymal Stem Cells on Micropatterned Surface Area, Journal of Nanomaterials 2011 (2011) 1-9.

Chapter 3

Preparation of micro-patterns having different size and aspect ratio for investigation of cell morphology on MSCs transfection efficiency

3.1 Summary

Gene transfection has broad applications in bioengineering and biomedical fields. Although many gene carrier materials and transfection methods have been developed, it remains unclear how cell morphology including cell spreading and elongation affect gene transfection. In this study, human bone marrow-derived mesenchymal stem cells (MSCs) were cultured on micro-patterns and transfected with cationic pAcGFP1-N1 plasmid complexes. Relationship between cell morphology of MSCs and gene transfection was investigated by using micro-patterning technique. Spreading and elongation of MSCs were precisely controlled by micro-patterned surfaces. The results showed that well spread and elongated MSCs had high transfection efficiency. Analysis of exogenous genes uptake and DNA synthesis activity indicated that the well spread and elongated cell morphology promoted gene transfection through enhanced uptake of the cationic complexes and accelerated DNA synthesis. The results should provide useful information for understanding of cell morphology on gene transfection and development of efficient gene transfection methods.

3.2 Introduction

Transfection, a technique that introduces exogenous nucleic acid into targeted cells to obtain transgenic cells, has been well developed for over 30 years. It has been commonly applied in gene therapy [1, 2], pharmacy [3], biological analysis [4] and creation of induced multipotent stem cells [5]. Nowadays, a variety of new techniques have been developed to increase transfection efficiency. Since delivery capacity of exogeneous nuclei acid is the primary factor in gene transfection, most researches have been focused on development of novel carrier materials and delivery methods. Cationic liposome [6-8] , polymer [9-11] and particles [1, 12, 13] are commonly applied to enhance the delivery efficacy of exogenous genes. However cationic carrier-associated transfection is accompanied with low transfection efficiency and limited cell types [14]. Although virus-mediated transfection can significantly improve transfection efficiency [15, 16], induction of oncogenesis and inflammatory responses has shown tremendous concerns for the safety in clinical applications. Physical methods including microinjection [17],

electroporation [18] and sonoporation [19] can directly deliver the naked nucleic acid into cells. However they may induce harmful effects on cells [20].

In contrast to the tremendous efforts in designing new carrier materials and transfection method, influence of cell morphology on transfection of exogenous genes has rarely been studied. Many recent researches have shown that cell morphology can affect cell contractility [21], proliferation [22], migration [23, 24] and differentiation [25-28]. Although influence of cell morphology on endocytosis of exogenous nanoparticles has been reported[29], it remains unclear how cell morphology such as cell spreading and elongation affects uptake of exogenous genes and gene transfection efficiency. Precise controlling of cell morphology and understanding of their influence on gene transfection can provide useful information for development of new gene transfection techniques and methods.

Benefit from the self-renewability and multipotency, human bone marrow-derived mesenchymal stem cells (MSCs) are a very useful cell source for tissue engineering and regenerative medicine [30-32]. It is noteworthy that, since MSCs can avoid immune response, genetically modified MSCs are the ideal gene carriers for applications of gene therapy [33]. Additionally, because stem cell differentiation can be selectively enhanced by specific exogenous genes, genetically modified MSCs have promising prospect in contribution to tissue engineering [34]. However, as one of the typical difficult-to-transfect types of cells, successful transfection of exogeneous gene into MSCs remains challenge by using traditional transfection technique [7]. Elucidation of influence of stem cells morphology on exogenous gene transfection is strongly desired for development of efficient transfection techniques for stem cells and further broad applications of stem cells. Therefore, in this study, micro-patterned surfaces were prepared by UV lithography with photomasks having well deigned micro-patterns. The micro-patterned surfaces were used to control cell spreading area and elongation of MSCs. Influence of MSCs spreading are and elongation on transfection efficiency cellular uptake of cationic complexes and DNA synthesis activity were investigated

3.3 Materials and methods

3.3.1 Preparation of micro-patterns and characterization

Photo-reactive PVA, AzPhPVA, was synthesized through the Steglich esterification between hydroxyl groups of PVA and carboxyl groups of 4-azidobenzoic acid as previously reported.[35] AzPhPVA was dissolved in Milli-Q water to prepare its aqueous solution. TCPS discs were cut from cell culture flask (BD Falcon^{TM}). 200 μL of the 0.3 mg/mL AzPhPVA aqueous solution was coated within 2.25 cm^2 square on each TCPS disc surface and dried in room temperature air in dark. The AzPhPVA-coated TCPS disc was irradiated by an ultraviolet light (UV, Funa-UV-linker FS-1500, 0.25 J/cm^2) through a photomask. The micro-patterns of the photomask were designed as circular micro-patterns of different diameter (20, 40, 60 and 80 μm) and ellipse micro-patterns of different aspect ratio (1:1, 2:1, 4:1 and 8:1) while the same area of 5027 μm^2. After UV irradiation, the discs were sonicated in Milli-Q water to remove uncrosslinked AzPhPVA. The micro-patterned disc was sterilized by immersing in 70% ethanol aqueous solution for 20 min and rinsed by aseptic Milli-Q water. To enhance cell adhesion, the sterilized micro-patterned surfaces were coated with fibronectin (Sigma-Aldrich Co. LLC., USA) by dropping 300 μL fibronectin aqueous solution (20 μg/mL in $NaHCO_3$ aqueous solution, pH 8.4) on each micro-patterned surface and incubating at 37 °C for 1 h in a CO_2 cell incubator. The fibronectin-coated micro-patterned plates were washed with sterile $NaHCO_3$ aqueous solution and sterile Milli-Q water for following experiments.

The micro-patterned surfaces were observed by a phase-contrast microscope (Olympus BX51, Tokyo, Japan). The character of micro-patterned surfaces was analyzed by an atom force microscope (AFM, Asylum Research Corporation MFP-3D-BIO, Santa Barbara, CA). A cantilever with a nitride tip was used for scanning of the micro-patterned surfaces in Milli-Q water by a contact mode.

3.3.2 Cell culture

The human bone-marrow derived MSCs were purchased at passage 2 from Lonza Walkersville and proliferated in MSCGM™ medium. The cells at passage 4 were harvested for cell seeding. The fibronectin-coated micro-patterned discs were placed in cell culture dishes and added with 3 mL complete DMEM serum mediums previously reported [35]. Glass ring having an inner diameter of 1.5 cm was placed on each micro-patterned disc for constraint of cell suspension solution on the micro-patterned surfaces. 200 μL of MSCs suspension (2.5×10^4 cells/mL) was added in each glass ring. Glass ring was removed after the cells were cultured in a CO_2 cell incubator for 6 h. After another 18 h culture, cell attachment on the micro-patterned surfaces was observed by a phase-contrast microscope.

3.3.3 Plasmid amplification and purification

A commercially available pAcGFP1-N1 vector that encodes a green fluorescent protein (GFP) was used. It was purchased from Clontech Laboratories, Inc and amplified by using Escherichia coli DH5α (*E. coli*, TAKARA BIO INC. Japan). The pAcGFP1-N1 was transformed into *E. coli* through heat shock. Transformed *E. coli* was seeded on Agar-LB plate containing kanamycin (30 μg/mL, Sigma-Aldrich Co. LLC., USA) and incubated in 37 °C overnight. The colonies formed on the Agar-LB plate were picked and re-seeded in 3 mL LB broth miller (25 mg/mL, Nacalai Tesque, Inc., Kyoto, Japan) with 30 μg/mL kanamycin and then incubated in 37 °C with shaking for 18 h. The amplified pAcGFP1-N1 was harvested and purified by using Plasmid Mini Kit (QIAGEN, CA, USA) according to the product protocol. The concentration of amplified pAcGFP1 was assayed by spectrophotometry (Nanodrop, Thermo Fisher Scientific Inc., USA) at 260 nm. The integrity of amplified pAcGFP1-N1 was confirmed by DNA electrophoresis in agarose gels and stained by ethidium bromide solution (Bio-Rad Laboratories, Inc., USA).

3.3.4 Transfection

Lipofectamine™ 2000 Transfection Reagent (Invitrogen, CA, USA) was applied to enhance plasmid delivery efficacy. To prepare Lipofectamine™ 2000/pAcGFP1-N1 complexes, 1 μL Lipofectamine™ 2000 and 500 ng pAcGFP1-N1 was diluted in 50 μL Opti-MEM® (Thermo Fisher Scientific Inc., USA) separately and incubated in room temperature for 5 min. The Lipofectamine™ 2000 and plasmid solutions were gently mixed. The mixture solution was incubated for another 30 min to prepare cationic plasmid complexes. Before addition of the cationic plasmid complexes, MSCs were starved in Opti-MEM® for 2 h after 24 h culture in DMEM serum medium. Glass rings with an inner diameter of 1.5 cm were placed on the micro-patterned surfaces to prevent leakage of cationic plasmid complexes during transfection. 100 μL cationic plasmid complexes solution was added on the cells in the glass ring. The plasmid complexes were incubated with the micro-patterned MSCs for 6 h in a CO_2 cell incubator. And then, the medium containing the cationic plasmid complexes was replaced by DMEM serum medium and further incubated for 18 h. After that, the samples were rinsed by pre-warmed PBS twice and fixed by paraformaldehyde aqueous solution (4%, 4°C, 10 min). The cells were treated by 1% Triton™ X-100 and blocked by BSA. Finally, the actin and nuclei of transfected MSCs were stained by Alexa Fluor-594 phalloidin (Invitrogen) and Hoechst 33258 (Wako Pure Chemical Industries, Ltd.) as previously reported.[25] The stained samples were observed and recorded through a fluorescence microscope (Olympus, Japan) with a 10X objective lens at fixed parameters (11s, ISO: 200). The GFP fluorescence intensity was calculated through an ImageJ software. The corrected total fluorescence (*CTF*) of each cell was calculated as $CTF = I - (A \times M)$ (A: area of selected cell; I: integrated intensity of selected cell; M: mean fluorescence intensity of micro-patterns without cells). *CTF was* considered as corrected fluorescence intensity of GFP. The *CTF* of plasmid untreated MSCs was also calculated by

the same method. Fluorescence intensity threshold to distinguish positive or negative GFP expression is generally set at the intensity where more than 99.5% of plasmid untreated cells are considered fluorescence-negative.[36] In the present study, GFP positive cells were defined as the cells which *CTF* of GFP was 50 times higher than that of plasmid untreated cells on the same micro-patterns. To evaluate transfection efficiency, GFP positive cells were counted and percentage of GFP positive cell number was calculated. Only single cell on the micro-patterns was used for the analysis. From each sample, more than 150 cells were counted and 5 samples were used for each analysis.

3.3.5 Cellular uptake of cationic complexes

Fluoresbrite® carboxylate microspheres (d = 500 nm, Funakoshi Co., Ltd., Japan) were applied to evaluate the capacity of cellular uptake. 0.1 μL microsphere stock solution and 1 μL Lipofectamine™ 2000 were separately added into 50 μL Opti-MEM® medium to prepare microspheres dilution solution and Lipofectamine™ 2000 dilution solution, respectively. The two solutions were mixed and added in the micro-patterned MSCs for 6 h culture by the above-mentioned method. To evaluate the quantity of endocytosed microspheres, the samples were firstly rinsed by pre-warmed PBS for 3 times and extracellular fluorescence of microspheres was quenched by 0.4% trypan blue solution (Sigma-Aldrich Co. LLC., USA). Then, the samples were fixed with paraformaldehyde aqueous solution. To confirm the position of cationically modified microspheres, plasma membrane of MSCs was stained by CellMask™ Deep Red (0.25 μg/mL, Invitrogen, CA, USA) and observed under a fluorescence confocal microscope (Zeiss, Germany). Actin filaments and nuclei were stained. Similar with the evaluation of GFP fluorescence intensity, the total fluorescence yield of FITC was calculated from the *CTF* of microspheres fluorescence within the micro-patterned MSCs as previously described. Fifteen cells from 5 independent experiments (3 cells from each independent experiment) were analyzed.

3.3.6 BrdU staining

Before cell seeding on the micro-patterned surfaces, MSCs were starved in FBS-free DMEM for 24 h to keep cells staying in G0 phase as previously reported.[37] And then, MSCs were seeded on the micro-patterned surfaces and incubated in complete growth medium for 24 h in a CO_2 cell incubator before transfection. After MSCs were incubated with the cationic plasmid complexes for 6 h, Opti-MEM® with cationic plasmid complexes was replaced by growth medium supplemented with 1% BrdU labelling reagent (v/v, Thermo Fisher Scientific Inc., USA). The cells were incubated with BrdU labelling reagents under 37 °C in a CO_2 cell incubator for 18 h. And then, the samples were rinsed by pre-warmed PBS, fixed by 70% (v/v) ethanol aqueous solution and denatured by 2 M HCl. After being rinsed by PBS, the samples were permeabilized by 1% Triton™ X-100 for 10 min and blocked by 2% BSA for 30 min. The primary anti-BrdU antibody (1/200 in 2% BSA, Abcam, plc.) was incubated with samples for 1.5 h at room temperature. And then, the samples were incubated with Alexa Fluor® 488-conjugated anti-mouse IgG antibody (1/500 in PBS, Thermo Fisher Scientific Inc., USA) for 1 h and Hoechst 33258 (1/1000 in PBS) at room temperature. Finally, the percentage of BrdU positively stained cells were counted through fluorescence microscopy images. From each sample, more than 150 cells were counted and 5 samples were used for each analysis.

3.3.7 Fluorescence staining of actin and nuclei

After the cells were cultured on micro-patterned surfaces for 24 h, the actin and nuclei of micro-patterned MSCs were stained. Fluorescence images of each sample were captured through a fluorescence microscope and a confocal fluorescence microscope (Zeiss, Germany).

3.3.8 Measurement of cell stiffness

The stiffness of living MSCs was measured through nanoindentation of MFP-3D-BIO AFM as previously reported[24]. A cantilever with a silica sphere (d = 600 nm) was applied as a probe for nanoindentation. The spring constant of cantilever was proofed before measurement. The position of cells or cantilever was observed through a phase-contrast microscope. The cells were directly used for measurement after being seeded on the micro-patterned surfaces and cultured in DMEM serum medium for 1 day. Measurement time for each sample was controlled less than 2 h to maximize cell viability. During nanoindentation, 2 nN trigger force and 4 μm/s indentation rate were performed to avoid any damage on cells. Young's modulus of each micro-patterned cell was calculated by fitting force-distance curves obtained at a central region of cells to a Hertz contact model. For each sample, 20 force-distance curves from each cell were measured and analyzed. The average of Young's modulus from 10 cells was calculated.

3.3.9 Statistical analysis

The quantitative data are reported as mean ± standard deviation (SD). The significant difference was confirmed through multiple comparisons of one-way ANOVA. The significant difference was defined when $p < 0.05$.

3.4 Results

3.4.1 Preparation and characterization of micro-patterns and controlling of cell morphology by micro-patterns

PVA micro-patterns were fabricated on TCPS surfaces through UV lithography by using AzPhPVA. The micro-patterned circles and ellipses of TCPS, which were surrounded by cell-repellent PVA, were formed to control MSCs spreading and elongation. The typical diameter of MSCs is around 20 μm [38] and their spreading area is less than 5000 μm^2 [39]. Hence, 4 types of circle micro-patterns of different diameter (20, 40, 60 and 80 μm) were prepared to control cell size and spreading area. Another 4 types of ellipse micro-patterns of different aspect ratio (1:1, 2:1, 4:1 and 8:1) while the same surface area as that of 80 μm circle micro-pattern were prepared to control cell aspect ratio and elongation. Observation by a photo-contrast microscope and AFM confirmed formation of the micro-patterns (Figure 3.1 a and b). AFM measurement indicated that the average thickness of PVA thin layer was 66.8 ± 1.8 nm. The 4 types of micro-patterned circles had a diameter of 21.7 ± 0.6, 41.4 ± 0.2, 61.4 ± 0.6 and 81.5 ± 0.9 μm, which were measured from the AFM images. Their respective area was calculated to be 368.6 ± 18.7, 1346.8 ± 13.5, 2962.1 ± 58.3 and 5221.1 ± 120.1 μm^2. The 4 types of micro-patterned ellipses had the same surface area of 5199.8 ± 174.0 μm^2 while different aspect ratio of 1.0 ± 0.1, 2.0 ± 0.1, 4.1 ± 0.3 and 7.6 ± 0.5. The micro-

patterns were coated with fibronectin and applied for MSCs culture. After 24 h culture, MSCs attached on the micro-patterns and their morphology was controlled by the micro-patterns (Figure 3.1 c).

3.4.2 Influence of cell spreading area and elongation on gene transfection efficiency

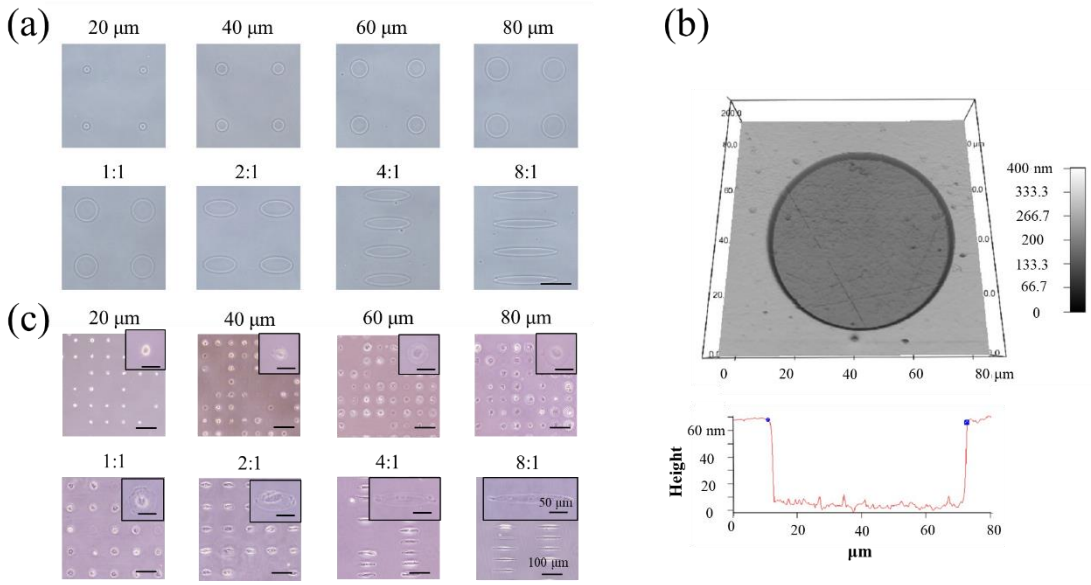

Figure 3.1 Characterization of micro-patterned surfaces. (a) Phase-contrast microscope images of micro-patterned surfaces having different diameter circles or different aspect ratio ellipses. (b) Representative AFM 3D view and cross section of micro-pattern of 60 μm diameter circle. (c) Phase-contrast micrographs of MSCs adhered on the micro-patterned surfaces. Scale bar at the bottom is 100 μm and scale bar in the insets is 50 μm.

The influence of cell morphology on gene transfection efficiency was investigated. Actin filament staining (red) indicated that the spreading area and aspect ratio of MSCs were confined by the different size and shape of micro-patterns (Figure 3.2 a and c). Since pAcGFP1-N1 plasmid is encoded with GFP as a reporter gene, the transfected cells could be confirmed by a fluorescence microscope. Percentage of GFP positive cells to the total cell number (transfection efficiency) was considered (Figure 3.2 b and d). The results showed that gene transfection efficiency increased with the increasing of cell size and aspect ratio. Larger MSCs had a higher transfect efficiency. When cell spreading area was controlled at the same level, high aspect ratio of cells promoted gene transfection. The results indicated that cell spreading and elongation were beneficial for gene transfection

3.4.3 Influence of cell spreading area and elongation on cellular uptake of cationic complexes

The influence of cell morphology on cellular uptake capacity of cationic complexes was investigated through evaluation of endocytosed quantity of Lipofectamine™ 2000-modified Fluoresbrite® microspheres. The negatively charged Fluoresbrite® microspheres with carboxyl groups were modified by Lipofectamine™ 2000 to prepare the fluorescent cationic microsphere complexes. After incubation with the cationic microsphere complexes, actin (red) and nuclei (blue) were stained to confirm cell morphology. Microspheres (green) were observed within all the micro-patterned cells (Figure 3.3 a). Cytoplasm membrane of the micro-patterned cells was stained and observed

by a laser confocal microscope (Figure 3.3 b). All the microspheres (green) were observed inside the cytoplasm membrane (red), indicating cellular uptake of the microspheres.

The cellular uptake capacity was evaluated through calculation of the FITC fluorescence yield of endocytosed microspheres in each single MSCs on the micro-patterns (Figure 3.3 c and d). The total amount of endocytosed microspheres increased when cells had a high level of spreading and elongation. The results indicated that cellular uptake capacity of cationic complexes was promoted by cell spreading and elongation.

3.4.4 Influence of cell spreading area and elongation on DNA synthesis

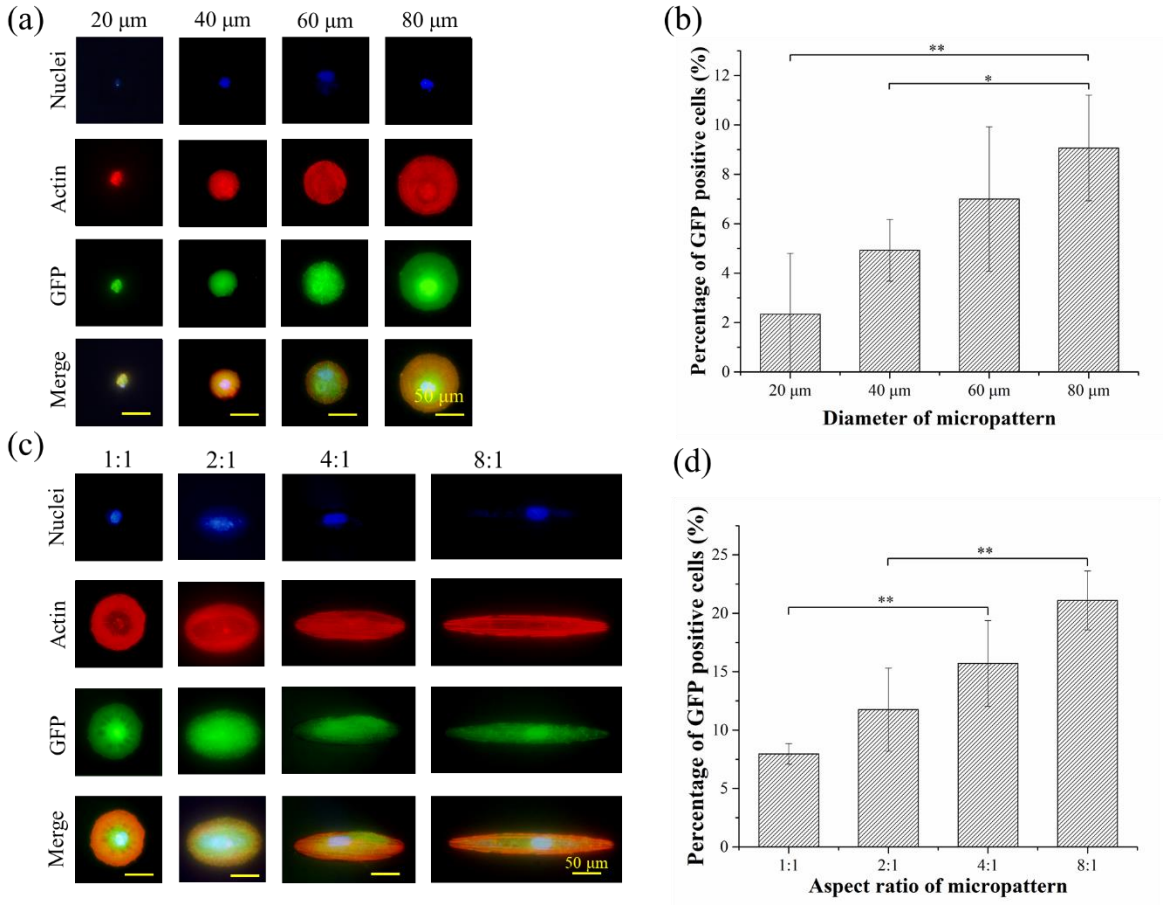

Figure 3.2 Gene transfection of MSCs on micro-patterned surfaces. (a) Representative fluorescent images of nuclei (blue), actin (red) and GFP (green) expression and (b) transfection efficiency of MSCs cultured on micro-patterns having different diameter circles. (c) Representative fluorescent images of nuclei (blue), actin (red) and GFP (green) expression and (d) transfection efficiency of the cells were cultured on micro-patterns having different aspect ratio ellipses. The means and standard deviations are shown in the figure (n = 5, $*p < 0.05$, $**p < 0.01$).

DNA synthesis activity of the micro-patterned MSCs was evaluated by incorporation of BrdU. Percentage of BrdU positively stained cells was calculated (Figure 3.4). The results presented that micro-patterned MSCs with large cell size had high DNA synthesis activity (Figure 3.4 b). Meanwhile, the high aspect ratio showed promotive effect on DNA synthesis (Figure 3.4 c). Therefore, DNA synthesis could be promoted by the cell spreading and elongation.

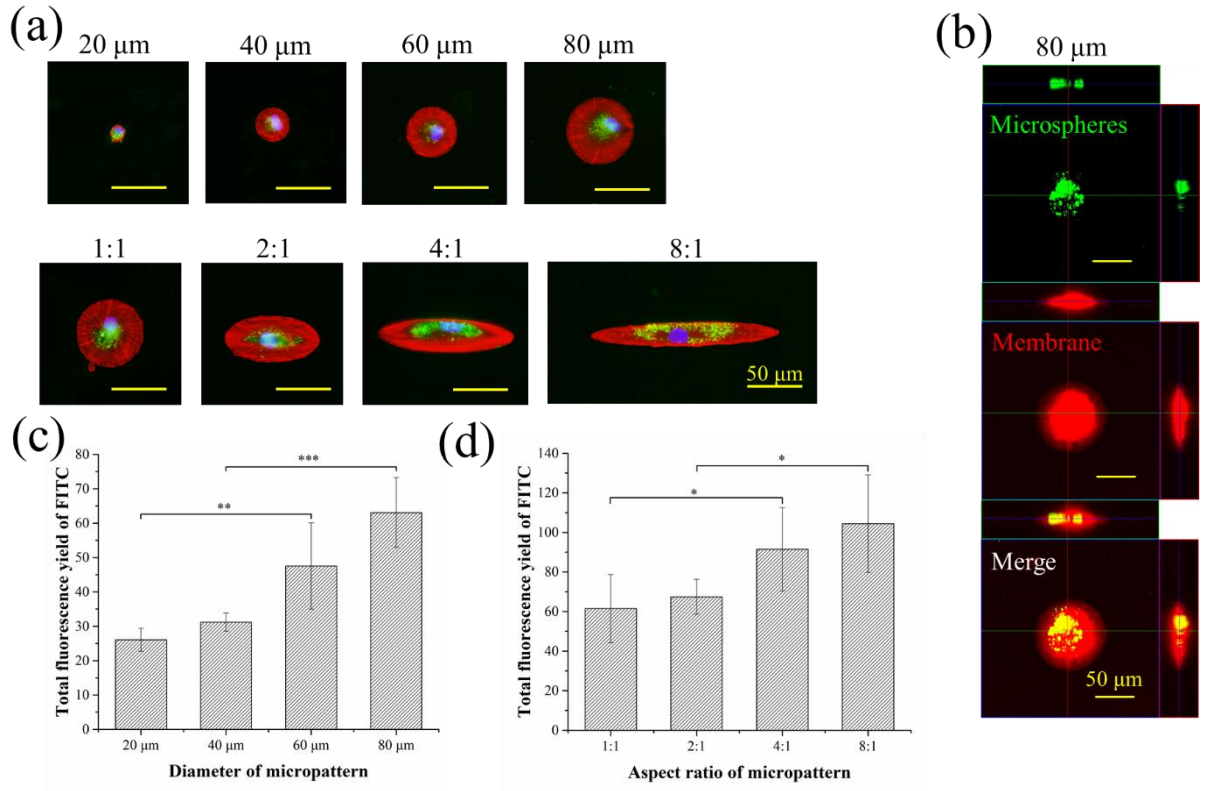

Figure 3.3 Influence of MSCs spreading area and aspect ratio on cellular uptake capacity of cationic complexes. (a) Representative fluorescent images of MSCs cultured on the micro-patterns showing cellular uptake of cationically modified Fluoresbrite® carboxylate microspheres (green). Nuclei were stained blue and actin was stained red. (b) Fluorescent confocal images of MSCs cultured on 80 μm diameter circle micro-pattern with cationically modified Fluoresbrite® carboxylate microspheres (green). Cell membrane was stained red. (c) Total FITC fluorescence yield of microspheres in MSCs cultured on micro-patterns having different diameter circles. (d) Total FITC fluoresce yield of microspheres in MSCs cultured on micro-patterns having different aspect ratio ellipses. All values represent mean value and all error bars represent standard deviation, n = 5, $*p < 0.05$, $**p < 0.01$.

3.4.5 Actin filaments structure and cellular stiffness

Actin filament structure was observed through actin (green) and nuclei (blue) staining fluorescence images (Figure 3.5 a and b). Actin filament organization and orientation of MSCs on micro-patterned circles having a diameter of 20 μm were not clear. Actin filaments were well organized and oriented when MSCs had large spreading area. The organization and orientation level of actin filaments increased when cell spreading area increased. When MSCs were cultured on the micro-patterns having different aspect ratios, actin filaments also showed different orientation. Actin filaments were assembled along the radial and concentric direction when aspect ratio was 1:1. As the aspect ratio of MSCs increased, actin filaments were assembled and oriented along the major axis of cells. In particular, when MSCs elongated with an aspect ratio of 8:1, the well aligned perinuclear actin filaments spanned above the nuclei (Figure 3.5 b). The stiffness of MSCs on the micro-patterns was calculated through force-distance curves from nanoindentation (Figure 3.5 c and e). The Young's modulus increased significantly when cell spreading

area and aspect ratio increased (Figure 3.5 d and f). The well organization and orientation of actin filaments were accompanied with the increase of cell Young's modulus.

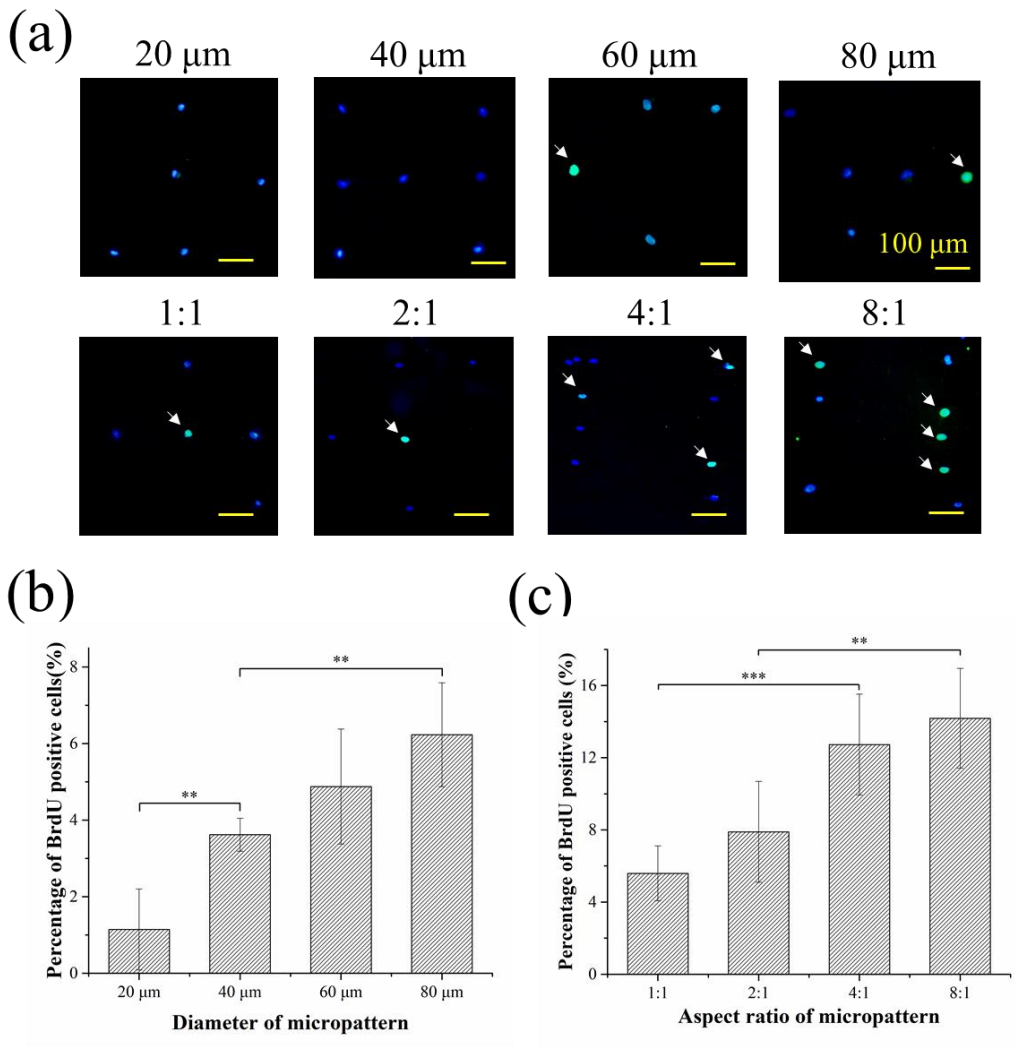

Figure 3.4 Influence of MSCs spreading area and elongation on DNA synthesis activity. (a) Representative fluorescent images of nuclei (blue) and BrdU (green, white arrow indicated) staining of MSCs on the micro-patterns. (b) Percentage of BrdU positively stained MSCs cultured on micro-patterns having different diameter circles. (c) Percentage of BrdU positively stained MSCs cultured on micro-patterns having different aspect ratio ellipses. The means and standard deviations are shown in the figure (n = 5, $*p < 0.05$, $**p < 0.01$).

3.5 Discussion

By using PVA/PS micro-patterned surfaces, MSCs adhered on the micro-patterned circles and ellipses. The fibronectin-coated PS circles and ellipses of the micro-patterns supported cell adhesion while the PVA thin layers surrounding the PS circles and ellipses inhibited cell adhesion. Therefore, cell spreading area and elongation could be precisely controlled by the micro-patterns (Figure 3.1 and Figure 3.2). After the micro-patterned single MSCs were transfected with the Lipofectamine™ 2000 modified pAcGFP1-N1 plasmid, the cells having different spreading area and aspect ratio showed different degree of transfection. Cells having larger spreading area and

higher aspect ratio showed higher transfection efficiency of GFP genes (Figure 3.2). Both spreading area and aspect ratio had dominant influence on gene transfection efficiency. Additionally, compared with 10 - 15% transfection efficiency of MSCs by using conventional chemical-based transfection techniques [7, 40], over 20% transfection efficiency was achieved for the well spread and elongated MSCs on the micro-patterned surfaces.

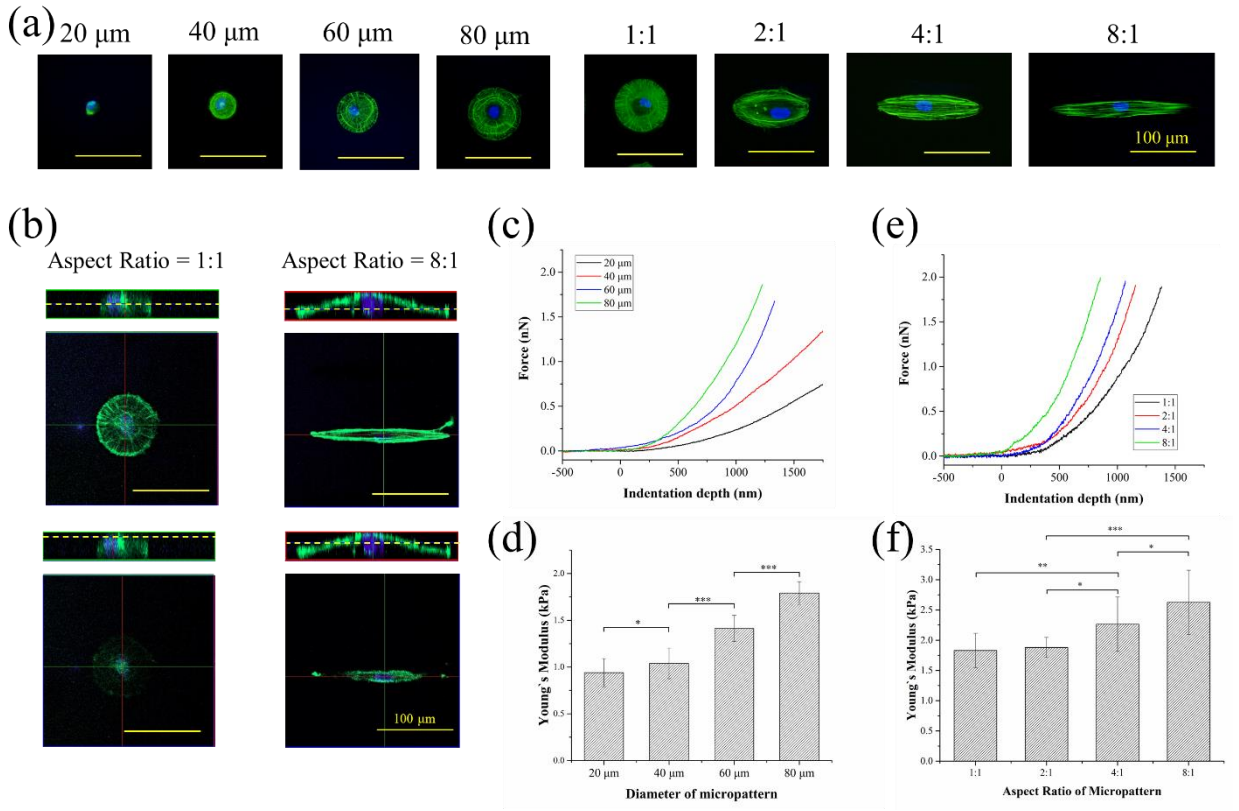

Figure 3.5 Influence of MSCs spreading area and elongation on cytoskeleton organization. (a) Representative fluorescent images of actin (green) and nuclei (blue) staining of MSCs on the micro-patterns. (b) Representative fluorescent confocal microscope images of MSCs cultured on the micro-patterns having respect aspect ratios of 1:1 and 8:1. (c) Representative force-distance curves and (d) Young's modulus of MSCs having different size. (e) Representative force-distance curves and (f) Young's modulus of micro-patterned MSCs having different aspect ratio ellipses. All values represent mean value and all error bars represent standard deviation, n = 5, $*p < 0.05$, $**p < 0.01$.

It is interesting that the transfection efficiency was positively correlated with Young's modulus of micro-patterned MSCs. Actin fluorescence staining (Figure 3.5 a and b) and Young's modulus measurement (Figure 3.5 d and f) indicated the close relationship between the structure of actin filaments and cell stiffness. As one of the steps of gene transfection, plasmid endocytosis has been demonstrated a vital step to affect gene transfection efficiency [9, 14, 41, 42]. The influence of cell morphology on cellular uptake capacity was investigated by using fluorescence-labelled microspheres. The diameter of cationic liposome modified plasmid complexes has been reported in a range from 300 nm to 2 μm [43, 44]. The fluorescence-labelled microspheres with 500 nm in mean diameter were used to mimic the exogeneous gene. More microspheres were uptaken by the MSCs having larger spreading area and higher aspect ratio. Therefore, endocytosis of cationic complexes could be enhanced by cell spreading and elongation (aspect ratio) of the micro-patterned cells. Cellular uptake of cationic liposome-modified plasmid has been reported to be dominantly dependent on clathrin mediate endocytosis (CME) which is associated with actin filaments [45-47]. In the present study, the actin filaments organization and orientation were shown to be

related to cell spreading area and aspect ratio. More actin filaments were better organized in larger MSCs and the actin caps between nucleus and cytoplasm membrane were formed in the elongated MSCs (Figure 3.5 a and b). The well organized and oriented actin filaments could increase the stiffness of the MSCs and also promote endocytosis of cationic complexes, which is in a good agreement with previous reports [48, 49].

Except plasmid uptake, DNA synthesis is extremely important for efficient gene transfection [50]. DNA synthesis activity of the micro-patterned MSCs was evaluated to investigate the effect of cell morphology on plasmid replication. The results indicated that DNA synthesis was facilitated by large cell spreading area. Cell spreading area has been reported to have positive effect on stimulation of cell proliferation [37, 51, 52]. Well spread cells can lead to enlargement of nuclei volume and activation of DNA synthesis [53, 54]. Regarding to the influence of cell elongation, an increasing of cell aspect ratio resulted in high DNA synthesis activity (Figure 3.4 c). Cellular contractility through cytoskeleton organization has been demonstrated effective in regulation of cells proliferation [52, 55]. Cells with a high elongation showed well-organized actin filaments and actin cap formation, which suggested formation of contractile actin bundles along their apical surface (Figure 3.5 b) [56]. The apically posited actin cap leads the nucleus-centrosome axis towards the ventral surface which can inhibit primary cilium growth [57]. The suppressed cilium will facilitate cell resume to cell cycle and promote cell proliferation [58].

The critical role of plasmid uptake and replication in regulation of mammalian cells transfection has also been revealed by other researchers [59-62]. The results in the present study demonstrated cell spreading area and elongation could affect gene transfection of MSCs through regulating uptake capacity of plasmid and DNA replication activity. Large and elongated cells were beneficial for gene transfection.

3.6 Conclusions

The PVA/PS micro-patterned surfaces prepared through UV lithography were successfully applied to manipulate MSCs spreading area and elongation. The micro-patterned MSCs were applied to investigate the influence of cell morphology on gene transfection. Highly spread and elongated MSCs on micro-patterns having 80 μm in diameter or 8:1 in aspect ratio had well organized actin filaments and high transfection efficiency through promoted uptake capacity of cationic gene complexes and accelerated activity of DNA synthesis. The results will provide a valuable new insight for design and development of new methods and biomaterials for gene transfection.

3.7 References

[1] T. Liu, A. Tang, G. Zhang, Y. Chen, J. Zhang, S. Peng, Z. Cai, Calcium phosphate nanoparticles as a novel nonviral vector for efficient transfection of DNA in cancer gene therapy, Cancer biotherapy & radiopharmaceuticals 20(2) (2005) 141-9.

[2] R.S. Goomer, L.J. Deftos, R. Terkeltaub, T. Maris, M.C. Lee, F.L. Harwood, D. Amiel, High-efficiency non-viral transfection of primary chondrocytes and perichondrial cells for ex-vivo gene therapy to repair articular cartilage defects, Osteoarthritis and cartilage 9(3) (2001) 248-56.

[3] Y. Wang, S. Zhao, L. Bai, J. Fan, E. Liu, Expression systems and species used for transgenic animal bioreactors, BioMed research international 2013 (2013) 580463.

[4] A. Reynolds, D. Leake, Q. Boese, S. Scaringe, W.S. Marshall, A. Khvorova, Rational siRNA design for RNA interference, Nature biotechnology 22(3) (2004) 326-30.

[5] L. Warren, P.D. Manos, T. Ahfeldt, Y.H. Loh, H. Li, F. Lau, W. Ebina, P.K. Mandal, Z.D. Smith, A. Meissner, G.Q. Daley, A.S. Brack, J.J. Collins, C. Cowan, T.M. Schlaeger, D.J. Rossi, Highly efficient reprogramming to pluripotency and directed differentiation of human cells with synthetic modified mRNA, Cell stem cell 7(5) (2010)

618-30.
[6] X. Gao, L. Huang, A novel cationic liposome reagent for efficient transfection of mammalian cells, Biochemical and biophysical research communications 179(1) (1991) 280-285.
[7] C. Madeira, R.D. Mendes, S.C. Ribeiro, J.S. Boura, M.R. Aires-Barros, C.L. da Silva, J.M. Cabral, Nonviral gene delivery to mesenchymal stem cells using cationic liposomes for gene and cell therapy, Journal of biomedicine & biotechnology 2010 (2010) 735349.
[8] Z. Zhou, C. Li, M. Zhang, Q. Zhang, C. Qian, D. Oupicky, M. Sun, Charge and Assembly Reversible Micelles Fueled by Intracellular ATP for Improved siRNA Transfection, ACS applied materials & interfaces 10(38) (2018) 32026-32037.
[9] A. Rémy-Kristensen, J.-P. Clamme, C. Vuilleumier, J.-G. Kuhry, Y. Mély, Role of endocytosis in the transfection of L929 fibroblasts by polyethylenimine/DNA complexes, Biochimica et Biophysica Acta (BBA) - Biomembranes 1514(1) (2001) 21-32.
[10] S.C. De Smedt, J. Demeester, W.E. Hennink, Cationic polymer based gene delivery systems, Pharmaceutical Research 17(2) (2000) 113-126.
[11] T. Wu, Z. Li, Y. Zhang, J. Ji, Y. Huang, H. Yuan, F. Feng, K.S. Schanze, Remarkable Amplification of Polyethylenimine-Mediated Gene Delivery Using Cationic Poly(phenylene ethynylene)s as Photosensitizers, ACS applied materials & interfaces 10(29) (2018) 24421-24430.
[12] K.K. Sandhu, C.M. McIntosh, J.M. Simard, S.W. Smith, V.M. Rotello, Gold Nanoparticle-Mediated Transfection of Mammalian Cells, Bioconjugate Chemistry 13(1) (2002) 3-6.
[13] M.N.V.R. Kumar, M. Sameti, S.S. Mohapatra, X. Kong, R.F. Lockey, U. Bakowsky, G. Lindenblatt, C.H. Schmidt, C.M. Lehr, Cationic Silica Nanoparticles as Gene Carriers: Synthesis, Characterization and Transfection Efficiency <I>In vitro</I> and <I>In vivo</I>, Journal of Nanoscience and Nanotechnology 4(7) (2004) 876-881.
[14] T.K. Kim, J.H. Eberwine, Mammalian cell transfection: the present and the future, Analytical and Bioanalytical Chemistry 397(8) (2010) 3173-3178.
[15] D.A. Rubinson, C.P. Dillon, A.V. Kwiatkowski, C. Sievers, L. Yang, J. Kopinja, D.L. Rooney, M. Zhang, M.M. Ihrig, M.T. McManus, F.B. Gertler, M.L. Scott, L. Van Parijs, A lentivirus-based system to functionally silence genes in primary mammalian cells, stem cells and transgenic mice by RNA interference, Nature Genetics 33(3) (2003) 401-406.
[16] L. Naldini, U. Blomer, P. Gallay, D. Ory, R. Mulligan, F.H. Gage, I.M. Verma, D. Trono, In Vivo Gene Delivery and Stable Transduction of Nondividing Cells by a Lentiviral Vector, Science 272(5259) (1996) 263-267.
[17] Y.M. Shen, R.R. Hirschhorn, W.E. Mercer, E. Surmacz, Y. Tsutsui, K.J. Soprano, R. Baserga, Gene transfer: DNA microinjection compared with DNA transfection with a very high efficiency, Molecular and Cellular Biology 2(9) (1982) 1145-1154.
[18] G. Covello, K. Siva, V. Adami, M.A. Denti, An electroporation protocol for efficient DNA transfection in PC12 cells, Cytotechnology 66(4) (2014) 543-53.
[19] Y. Zhang, R. Tachibana, A. Okamoto, T. Azuma, A. Sasaki, K. Yoshinaka, Y. Tei, S. Takagi, Y. Matsumoto, Ultrasound-mediated gene transfection in vitro: effect of ultrasonic parameters on efficiency and cell viability, International journal of hyperthermia : the official journal of European Society for Hyperthermic Oncology, North American Hyperthermia Group 28(4) (2012) 290-9.
[20] A.J. Mellott, M.L. Forrest, M.S. Detamore, Physical non-viral gene delivery methods for tissue engineering, Annals of biomedical engineering 41(3) (2013) 446-68.
[21] I. Lilge, S. Jiang, D. Wesner, H. Schonherr, The Effect of Size and Geometry of Poly(acrylamide) Brush-Based Micropatterns on the Behavior of Cells, ACS applied materials & interfaces 8(36) (2016) 23591-603.
[22] G. Abagnale, M. Steger, V.H. Nguyen, N. Hersch, A. Sechi, S. Joussen, B. Denecke, R. Merkel, B. Hoffmann, A. Dreser, U. Schnakenberg, A. Gillner, W. Wagner, Surface topography enhances differentiation of mesenchymal

stem cells towards osteogenic and adipogenic lineages, Biomaterials 61 (2015) 316-26.
[23] X. Jiang, D.A. Bruzewicz, A.P. Wong, M. Piel, G.M. Whitesides, Directing cell migration with asymmetric micropatterns, Proc Natl Acad Sci U S A 102(4) (2005) 975-8.
[24] X. Wang, X. Hu, N. Kawazoe, Y. Yang, G. Chen, Manipulating Cell Nanomechanics Using Micropatterns, Advanced Functional Materials 26(42) (2016) 7634-7643.
[25] Y. Yang, X. Wang, T.-C. Huang, X. Hu, N. Kawazoe, W.-B. Tsai, Y. Yang, G. Chen, Regulation of mesenchymal stem cell functions by micro–nano hybrid patterned surfaces, Journal of Materials Chemistry B 6(34) (2018) 5424-5434.
[26] L. Guo, Y. Fan, N. Kawazoe, H. Fan, X. Zhang, G. Chen, Fabrication of gelatin-micropatterned surface and its effect on osteogenic differentiation of hMSCs, Journal of Materials Chemistry B 6(7) (2018) 1018-1025.
[27] A. Higuchi, Q.D. Ling, Y. Chang, S.T. Hsu, A. Umezawa, Physical cues of biomaterials guide stem cell differentiation fate, Chemical reviews 113(5) (2013) 3297-328.
[28] B. Chang, C. Ma, X. Liu, Nanofibers Regulate Single Bone Marrow Stem Cell Osteogenesis via FAK/RhoA/YAP1 Pathway, ACS applied materials & interfaces 10(39) (2018) 33022-33031.
[29] X. Wang, X. Hu, J. Li, A.C. Russe, N. Kawazoe, Y. Yang, G. Chen, Influence of cell size on cellular uptake of gold nanoparticles, Biomaterials science 4(6) (2016) 970-8.
[30] A.I. Caplan, Adult mesenchymal stem cells for tissue engineering versus regenerative medicine, Journal of cellular physiology 213(2) (2007) 341-7.
[31] A. Higuchi, S. Suresh Kumar, Q.-D. Ling, A.A. Alarfaj, M.A. Munusamy, K. Murugan, S.-T. Hsu, G. Benelli, A. Umezawa, Polymeric design of cell culture materials that guide the differentiation of human pluripotent stem cells, Progress in Polymer Science 65 (2017) 83-126.
[32] A. Higuchi, Q.-D. Ling, S.S. Kumar, Y. Chang, A.A. Alarfaj, M.A. Munusamy, K. Murugan, S.-T. Hsu, A. Umezawa, Physical cues of cell culture materials lead the direction of differentiation lineages of pluripotent stem cells, Journal of Materials Chemistry B 3(41) (2015) 8032-8058.
[33] D. Baksh, L. Song, R.S. Tuan, Adult mesenchymal stem cells: characterization, differentiation, and application in cell and gene therapy, Journal of Cellular and Molecular Medicine 8(3) (2004) 301-316.
[34] X. Meng, M. Chen, W. Su, X. Tao, M. Sun, X. Zou, R. Ying, W. Wei, B. Wang, The differentiation of mesenchymal stem cells to vascular cells regulated by the HMGB1/RAGE axis: its application in cell therapy for transplant arteriosclerosis, Stem Cell Res Ther 9(1) (2018) 85.
[35] X. Wang, X. Hu, I. Dulinska-Molak, N. Kawazoe, Y. Yang, G. Chen, Discriminating the Independent Influence of Cell Adhesion and Spreading Area on Stem Cell Fate Determination Using Micropatterned Surfaces, Scientific reports 6 (2016) 28708.
[36] M.R. Soboleski, J. Oaks, W.P. Halford, Green fluorescent protein is a quantitative reporter of gene expression in individual eukaryotic cells, FASEB J 19(3) (2005) 440-2.
[37] X. Wang, T. Nakamoto, I. Dulińska-Molak, N. Kawazoe, G. Chen, Regulating the stemness of mesenchymal stem cells by tuning micropattern features, J. Mater. Chem. B 4(1) (2016) 37-45.
[38] J. Ge, L. Guo, S. Wang, Y. Zhang, T. Cai, R.C. Zhao, Y. Wu, The size of mesenchymal stem cells is a significant cause of vascular obstructions and stroke, Stem Cell Rev 10(2) (2014) 295-303.
[39] R.A. Marklein, J.L. Lo Surdo, I.H. Bellayr, S.A. Godil, R.K. Puri, S.R. Bauer, High Content Imaging of Early Morphological Signatures Predicts Long Term Mineralization Capacity of Human Mesenchymal Stem Cells upon Osteogenic Induction, Stem Cells 34(4) (2016) 935-47.
[40] T. Gonzalez-Fernandez, B.N. Sathy, C. Hobbs, G.M. Cunniffe, H.O. McCarthy, N.J. Dunne, V. Nicolosi, F.J. O'Brien, D.J. Kelly, Mesenchymal stem cell fate following non-viral gene transfection strongly depends on the choice of delivery vector, Acta biomaterialia 55 (2017) 226-238.
[41] S. Pan, D. Cao, R. Fang, W. Yi, H. Huang, S. Tian, M. Feng, Cellular uptake and transfection activity of DNA

complexes based on poly(ethylene glycol)-poly(l-glutamine) copolymer with PAMAM G2, Journal of Materials Chemistry B 1(38) (2013) 5114.
[42] Z. Kadlecova, Y. Rajendra, M. Matasci, L. Baldi, D.L. Hacker, F.M. Wurm, H.A. Klok, DNA delivery with hyperbranched polylysine: a comparative study with linear and dendritic polylysine, Journal of controlled release : official journal of the Controlled Release Society 169(3) (2013) 276-88.
[43] K.K. Son, D.H. Patel, D. Tkach, A. Park, Cationic liposome and plasmid DNA complexes formed in serum-free medium under optimum transfection condition are negatively charged, Biochimica et Biophysica Acta (BBA) - Biomembranes 1466(1-2) (2000) 11-15.
[44] E.K. Wasan, D.L. Reimer, M.B. Bally, Plasmid DNA is protected against ultrasonic cavitation-induced damage when complexed to cationic liposomes, Journal of pharmaceutical sciences 85(4) (1996) 427-33.
[45] A. Collins, A. Warrington, Kenneth A. Taylor, T. Svitkina, Structural Organization of the Actin Cytoskeleton at Sites of Clathrin-Mediated Endocytosis, Current Biology 21(14) (2011) 1167-1175.
[46] S. Loebrich, The role of F-actin in modulating Clathrin-mediated endocytosis: Lessons from neurons in health and neuropsychiatric disorder, Communicative & integrative biology 7 (2014) e28740.
[47] O.L. Mooren, B.J. Galletta, J.A. Cooper, Roles for actin assembly in endocytosis, Annual review of biochemistry 81 (2012) 661-86.
[48] M. Kaksonen, C.P. Toret, D.G. Drubin, Harnessing actin dynamics for clathrin-mediated endocytosis, Nature reviews. Molecular cell biology 7(6) (2006) 404-14.
[49] B. Qualmann, M.M. Kessels, R.B. Kelly, Molecular Links between Endocytosis and the Actin Cytoskeleton: Figure 1, The Journal of cell biology 150(5) (2000) F111-F116.
[50] Y. Gluzman, SV40-transformed simian cells support the replication of early SV40 mutants, Cell 23(1) (1981) 175-182.
[51] C.S. Chen, Geometric Control of Cell Life and Death, Science 276(5317) (1997) 1425-1428.
[52] D.M. Pirone, W.F. Liu, S.A. Ruiz, L. Gao, S. Raghavan, C.A. Lemmon, L.H. Romer, C.S. Chen, An inhibitory role for FAK in regulating proliferation: a link between limited adhesion and RhoA-ROCK signaling, The Journal of cell biology 174(2) (2006) 277-88.
[53] R.G. Thakar, Q. Cheng, S. Patel, J. Chu, M. Nasir, D. Liepmann, K. Komvopoulos, S. Li, Cell-shape regulation of smooth muscle cell proliferation, Biophysical journal 96(8) (2009) 3423-32.
[54] P. Roca-Cusachs, J. Alcaraz, R. Sunyer, J. Samitier, R. Farre, D. Navajas, Micropatterning of single endothelial cell shape reveals a tight coupling between nuclear volume in G1 and proliferation, Biophysical journal 94(12) (2008) 4984-95.
[55] C.M. Nelson, C.S. Chen, VE-cadherin simultaneously stimulates and inhibits cell proliferation by altering cytoskeletal structure and tension, J Cell Sci 116(Pt 17) (2003) 3571-81.
[56] S.B. Khatau, C.M. Hale, P.J. Stewart-Hutchinson, M.S. Patel, C.L. Stewart, P.C. Searson, D. Hodzic, D. Wirtz, A perinuclear actin cap regulates nuclear shape, Proceedings of the National Academy of Sciences of the United States of America 106(45) (2009) 19017-22.
[57] A. Pitaval, Q. Tseng, M. Bornens, M. Thery, Cell shape and contractility regulate ciliogenesis in cell cycle-arrested cells, The Journal of cell biology 191(2) (2010) 303-12.
[58] E.N. Pugacheva, S.A. Jablonski, T.R. Hartman, E.P. Henske, E.A. Golemis, HEF1-dependent Aurora A activation induces disassembly of the primary cilium, Cell 129(7) (2007) 1351-63.
[59] K.L. Douglas, C.A. Piccirillo, M. Tabrizian, Cell line-dependent internalization pathways and intracellular trafficking determine transfection efficiency of nanoparticle vectors, European journal of pharmaceutics and biopharmaceutics : official journal of Arbeitsgemeinschaft fur Pharmazeutische Verfahrenstechnik e.V 68(3) (2008) 676-87.
[60] I.A. Khalil, K. Kogure, H. Akita, H. Harashima, Uptake pathways and subsequent intracellular trafficking in

nonviral gene delivery, Pharmacological reviews 58(1) (2006) 32-45.
[61] M.A. van der Aa, U.S. Huth, S.Y. Hafele, R. Schubert, R.S. Oosting, E. Mastrobattista, W.E. Hennink, R. Peschka-Suss, G.A. Koning, D.J. Crommelin, Cellular uptake of cationic polymer-DNA complexes via caveolae plays a pivotal role in gene transfection in COS-7 cells, Pharm Res 24(8) (2007) 1590-8.
[62] M.J. Mahon, Vectors bicistronically linking a gene of interest to the SV40 large T antigen in combination with the SV40 origin of replication enhance transient protein expression and luciferase reporter activity, BioTechniques 51(2) (2011) 119-28.

Chapter 4

Preparation of micro-nano hybrid pattern surfaces for regulation of MSCs differentiation

4.1 Summary

Micro- and nano-structured substrates have been widely applied in biomedical engineering field. Their precise control on cell morphology makes them promise to investigate various cell behavior. However, regulation of cell functions using micro-nano hybrid pattern surfaces is rarely achieved. Since cell microenvironment *in vivo* has complex micro- and nano-structures, it is desirable to use micro-nano hybrid pattern surfaces to mimic the microenvironment to control cell morphology and disclose its influence on stem cell differentiation. In this study, poly (vinyl alcohol) (PVA) micro-stripes with different spacing (50 μm, 100 μm and 200 μm) were constructed on polystyrene (PS) nano-grooves to prepare micro-nano hybrid pattern surfaces where direction of PVA micro-stripes and PS nano-grooves was parallelly or orthogonally arranged. Human bone marrow-derived mesenchymal stem cells (MSCs) cultured on the micro-nano hybrid pattern surfaces showed different cell alignment and elongation dependent on PVA micro-stripe spacing and orientation of PS nano-grooves. Comparison of the cell alignment and aspect ratio effects on differentiation of MSCs indicated that myogenic differentiation was dominantly regulated by cell alignment and osteogenic differentiation by cell elongation, while adipogenic differentiation neither by cell alignment nor by cell elongation.

4.2 Introduction

Stem cells, such as mesenchymal stem cells (MSCs), are the ideal cell source for tissue engineering and regenerative medicine due to their ability of self-renewal and the multipotency [1, 2]. Regulation of stem cell functions, especially inducing stem cells to differentiate into specific lineage, attracts extensive interests. *In vivo*, stem cells are surrounded and affected by various soluble biomolecules, extracellular matrix (ECM) and adjacent cells. In recent years, biophysical factors [3, 4], such as the constraint from adjacent cells [5] and electrostatic or mechanical properties of ECM [6], have been demonstrated to play a vital role in regulating cell behaviours through cell-cell or cell-ECM interactions [7]. Cell morphology is known as one of the most important biophysical factors in regulation of cell functions [8]. Cell elongation has been demonstrated to be critical in regulating cell proliferation [9], reprogramming [10], stemness [11] and differentiation [12]. Additionally, unified cell alignment is effective in muscle [13, 14], liver [15] and blood vessel [16] generation. However, manipulation of cell alignment has been always accompanied with

change of cell elongation in previous works [17, 18]. It is still not clear whether cell alignment and elongation have different roles in regulation of cell functions.

To investigate the effects of cell morphology on their functions, micro- and nano-patterned surfaces have been used [19, 20]. Micro-patterning techniques [21, 22] provide an easy approach to precisely control cell spreading area [11, 23-25], shape [26, 27], polarity [28] and aspect ratio [9, 11, 12] through confining cell adhesion region. Meanwhile, nano-structured surfaces have been applied to unify cell orientation, promote elongation and control cell spreading though regulating the structure of focal adhesion (FA) [29-32] and actin filament [33]. However, by using micro-patterns or nano-structured surfaces, cell elongation is always positively correlated with the state of cell alignment. Cell alignment and elongation cannot be separately controlled.

Therefore, in this study, micro-nano hybrid pattern surfaces were prepared to control cell alignment and elongation. The hybrid pattern surfaces were prepared by introducing PVA micro-stripes on PS nano-grooves through UV lithography and nanoimprinting method. The PVA micro-stripes were controlled to be parallelly or orthogonally oriented to the PS nano-grooves. The micro-nano hybrid pattern surfaces were applied for culture of MSCs to control their alignment and elongation. The influence of cell alignment and elongation on stem cell differentiation was compared.

4.3 Materials and methods

4.3.1 Preparation of micro-nano hybrid pattern surfaces

PS nano-grooved substrate was fabricated by a nanoimprinting method[14]. A nanotextured polydimethyl-siloxane (PDMS) mold having nano-grooves with a ridge depth of 400 nm, a ridge width of 800 nm and a spacing distance of 800 nm was prepared after casting on a pre-fabricated silicon master and cured at 60 °C. One drop of a 3 (w/v) % PS toluene solution was dropped on polyethylene terephthalate (PET) substrate (1×1 cm^2) and directly pressed by the nanostructured PDMS mold with a constant pressure (10 kPa). PDMS mold was peeled off after air-drying for 12 h to prepare the nano-grooved PS substrate (PS nano-grooves). The PS nano-grooves were treated by oxygen plasma for 100 s under 40 w and 100 sccm oxygen gas flow rate with a plasma asher (PB-006I, Mory Engineering Co, Ltd.).

To prepare the micro-nano hybrid pattern surfaces, 50 μL 4 mg/mL AzPhPVA solution was dropped on the PS nano-grooves and air dried overnight. A photomask containing micro-stripes with various equal width and spacing (50/50 μm, 100/100 μm and 200/200 μm) was covered on the AzPhPVA coated PS nano-grooves during UV irradiation (Funa-UV-linker FS-1500, 0.25 J/cm^2). The photomask micro-stripes were parallelly or orthogonally oriented along the PS nano-grooves to obtain the different micro-nano hybrid pattern surfaces. PVA micro-stripes on the PS nano-grooves were obtained after ultrasonic washing in Milli-Q water. To promote cell adhesion during cell culture experiments, the micro-nano hybrid pattern surfaces were coated with fibronectin after sterilization by incubating the substrates in fibronectin solution (20 μg/mL, Sigma-Aldrich Co. LLC., USA) diluted with $NaHCO_3$ (pH 8.4) buffer solution at 37 °C. The fibronectin coated substrates were then rinsed with a sterile aqueous solution of $NaHCO_3$ for three times and sterile water for another three times.

The micro-nano hybrid pattern surfaces were characterized by an atomic force microscope (AFM) and a scanning electron microscope (SEM, Hitachi S-4800, Japan). For AFM observation, a cantilever (DNP, Bruker) with a nitride tip was used. A contact mode in Milli-Q water was performed during scanning process.

4.3.2 Cell culture

The MSCs were directly purchased from Lonza Walkersville and proliferated in MSCGM™ in a CO_2 incubator at 37 °C. The MSCs at passage 4 were harvested for following experiments. The subcultured MSCs were suspended in complete DMEM serum medium containing 4500 mg/L glucose at a concentration of 6×10^4 cells/mL. The sterile fibronectin coated micro-nano hybrid pattern substrates were placed in 24-well plates and covered with glass rings having an inner diameter of 8 mm to constrain cell suspension medium within the micro-nano hybrid pattern surfaces. To each glass ring, 50 μL of the cell suspension solution was added to seed MSCs on the micro-nano hybrid pattern surfaces. The glass rings were removed after culture in the humidified incubator at 37 °C and 5% CO_2 atmosphere for 6 h to allow initial cell adhesion. Then, 1 mL growth medium was added into each well for continual culture in the incubator.

4.3.3 Actin, vinculin and nuclei staining

After the cells were cultured for 24 h, they were fixed with paraformaldehyde and successively treated with Triton X-100 and Tween-20 at room temperature. The BSA solution was applied to block the fixed sample at room temperature to avoid non-specific binding of antibodies during the following staining procedures. And then, an aqueous solution of mouse anti-vinculin antibody (Merck KGaA, Darmstadt, Germany) at a dilution ratio of 1:100 in 2% BSA was added on the blocked samples and incubated at 37 °C for 1 h. The samples were rinsed with 0.02% Tween-20 aqueous solution. After being rinsed by PBS for three times, the samples were incubated in an aqueous solution of Alexa Fluor-488 labelled goat anti-mouse IgG antibody (Invitrogen, CA, USA) at a dilution ratio of 1:1000 at 37 °C for 1 h. Finally, actin was stained by incubating the samples with Alexa Fluor-594 phalloidin (Invitrogen, CA, USA) at a dilution ratio of 1:40 in PBS at room temperature for 20 min. Nuclei were stained by Hoechst 33258 at room temperature in dark for 1 h. After being washed by 0.02% Tween-20 and PBS for each three times, the fluorescence images of each sample were observed and recorded by an Olympus fluorescence microscope.

4.3.4 Analysis of cell morphology

Cellular morphology was characterized through analysis of actin and nuclei staining images by an ImageJ software. For cell alignment, the angle between cell major axis and PVA stripes was calculated. Aligned cells were defined as those with an angle less than 10°. The ratio of aligned cells to the total cells was calculated to evaluate cell alignment. Cell aspect ratio was calculated by dividing the length of cell major axis by the width of minor axis which was vertical to the major axis. More than 50 cells from 3 independent experiments of each micro-nano hybrid pattern surfaces were analyzed for these measurements.

4.3.5 Myogenesis, osteogenesis and adipogenesis induction culture of MSCs

After cultured for 24 h, proliferation medium was substituted by myogenesis, osteogenesis or adipogenesis medium for myogenic, osteogenic and adipogenic differentiation, respectively. Myogenic induction medium was MesenPRO RS medium (Invitrogen, CA, USA) supplied with 1 ng/mL transforming growth factor β1 (TGF-β1, R&D systems, Minneapolis, MN). Osteogenic induction medium was complete

DMEM serum medium supplied with 100 nM DEX and 10 mM GP. Adipogenesis medium was complete DMEM serum medium supplied with 4500 mg/L glucose 1 μM dexamethasone, 0.5 mM IBMX, 10 μg/mL insulin and 10 μM indomethacin. For myogenic and adipogenic differentiation, 1 mL induction medium was added into each well. For osteogenic differentiation, 0.5 mL osteogenic medium was added into each well. All the induction media were refreshed every 3 days. Cells were incubated with the induction media for 2 weeks.

4.3.6 Analysis of myogenic, osteogenic and adipogenic differentiation of MSCs

After incubation with myogenic induction medium for 2 weeks, the cells were washed with PBS twice and fixed with 4% cold paraformaldehyde for 10 min. The samples were treated with Triton X-100 (Sigma-Aldrich Co. LLC., USA) for 2 min and blocked in 2% BSA at room temperature for 30 min. And then, the samples were incubated with mouse anti-human smooth muscle actin (SMA, Dako, Carpinteria, CA) at a dilution ratio of 1:100 in 2% BSA at 37°C for 1 h. After washing in PBS for 3 times, the samples were incubated with Alexa Fluor-488 labelled goat anti-mouse IgG antibody (Invitrogen, CA, USA) at a dilution ratio of 1:1000 in PBS at 37°C for 1 h. Nuclei were stained with 10 μg/ml of Hoechst 33258. Images of stained cells were obtained through an Olympus BX51 microscope with a DP-70 CCD camera (Olympus, Tokyo, Japan). The ratio of SMA positively stained cells to the total cells was calculated to indicate the potential of myogenesis. Average fluorescence intensity (*AFI*) per unit area of each cell was calculated through an ImageJ software as previously reported[34]. During ImageJ analysis, the regions near each nucleus were selected to calculate area (*A*) and integrated intensity (*I*). Corrected total fluorescence (*CTF*) was calibrated as $CTF = I - A \times M$ by using mean fluorescence intensity (*M*) as background. The mean fluorescence intensity was measured at PS regions without cells. Average fluorescence intensity (*AFI*) was calculated through $AFI = CTF / A$. The average value of *AFI* from all cells in the same image was calculated and set as a threshold. The cell which possessed higher *AFI* than threshold was defined as SMA positively expressed cell. More than 100 cells from 3 independent samples of each micro-nano hybrid pattern surfaces were analyzed. The percentage of SMA positively expressed MSCs on each micro-nano hybrid pattern surfaces was calculated.

Osteogenic differentiation was analyzed by staining alkaline phosphatase (ALP). The ALP was firstly stained according previous introduced in chapter 1. Finally, the cells were rinsed by PBS for three times and treated by 1% Triton-X-100 for 2 min followed by incubation with Hoechst 33258 at room temperature for. Optical images of the stained cells were obtained through an Olympus BX51 microscope with a DP-70 CCD camera (Olympus, Tokyo, Japan). Every 2 optical images from each of 3 independent samples were taken and the ALP positively stained cells were counted. More than 100 cells from each sample were analyzed and the percentage of ALP positively expressed cells was used to indicate the potential of osteogenic differentiation.

For adipogenic differentiation, lipid vacuoles were stained by Oil Red O. After induction culture in the adipogenic induction medium for 2 weeks, the cells were washed with PBS twice and fixed with paraformaldehydes. The fixed cells were immersed in 60% isopropanol at room temperature and then stained by Oil Red O solution. The fresh Oil Red O solution was prepared by dissolving Oil Red O powder (Sigma-Aldrich Co. LLC., USA) in 60% isopropanol. Finally, the cells were treated with Triton-X 100 and incubated with Hoechst 33258 for 10 min. The percentage of lipid vacuoles presenting cells was used to define the level of adipogenic differentiation. More than 100 cells from 3 independent samples of each micro-nano hybrid pattern surfaces were used for calculation.

4.3.7 Statistical analysis

The quantitative data are reported as mean ± standard deviation (SD). The significant difference was confirmed through multiple comparisons of one-way ANOVA. The significant difference was defined when *p* value was lower than 0.05.

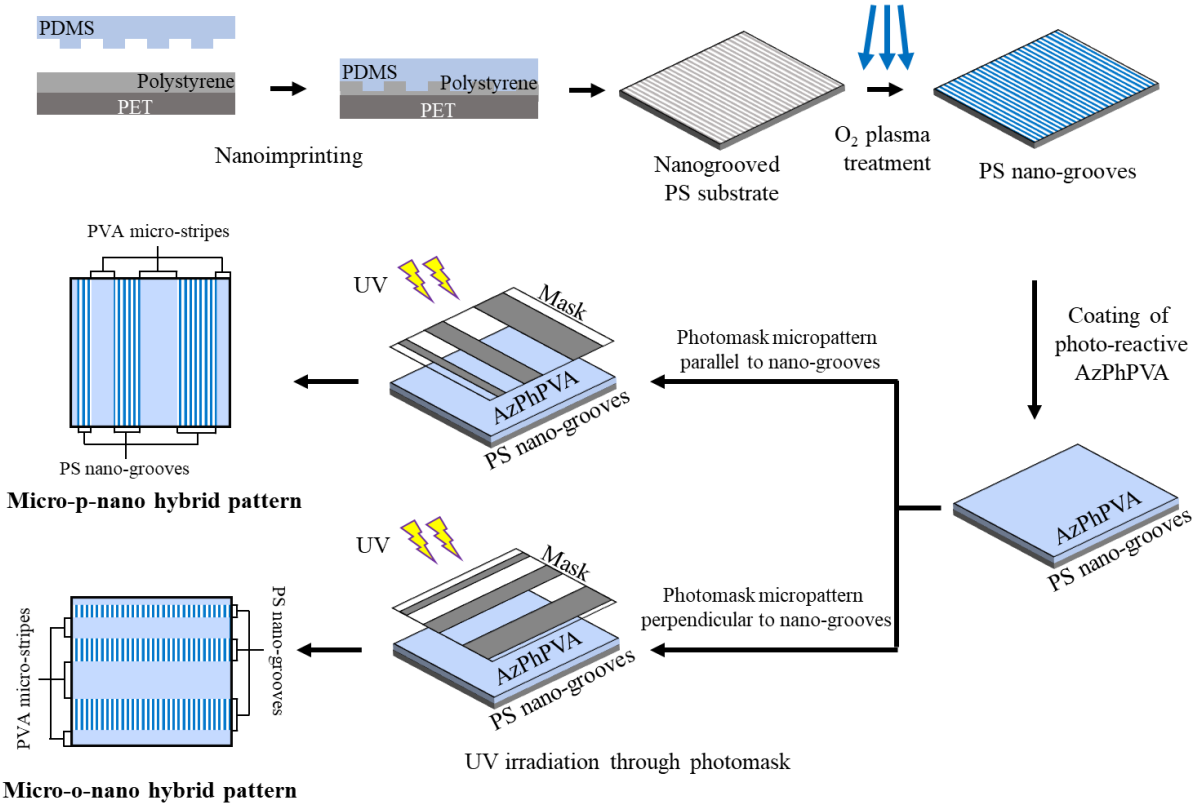

Figure 4.1 Preparation scheme of micro-nano hybrid pattern surfaces through nanoimprinting and UV lithography.

4.4 Results

4.4.1 Micro-nano hybrid pattern surfaces

PS substrates with micro-nano hybrid pattern surfaces were prepared as shown in Figure 4.1. The PS nano-grooves were firstly prepared by pressing a nanotextured PDMS mold on a PS toluene solution through a nanoimprinting method. Subsequently, the PS nano-grooves were treated with oxygen plasma and micro-patterned with PVA. PVA was used as a cell adhesion repellent to confine cell adhesion and spreading region on the PS nano-grooves.

To prepare PVA micro-patterns, the plasma-treated nano-grooves were coated with photo-reactive AzPhPVA aqueous solution. After drying, the AzPhPVA coated PS nano-grooves were covered with a photomask containing transparent and nontransparent alternate micro-stripes and irradiated by UV light. During UV irradiation, AzPhPVA molecules under transparent micro-stripes of mask were inter- or intramolecularly crosslinked and grafted to the PS nano-grooves. On the contrary, AzPhPVA molecules under non-transparent micro-stripes were resisted from UV activation and then washed away to expose PS

nano-grooves surface. Three sets of PVA micro-stripe patterns with equal width and spacing were prepared. The equal width and spacing of the three sets of PVA micro-stripes were 50 μm, 100 μm and 200 μm. By changing the photomask angle during UV irradiation, PVA micro-stripes parallelly aligned to PS nano-grooves (micro-p-nano hybrid pattern) and PVA micro-stripes orthogonally aligned to PS nano-grooves (micro-o-nano hybrid pattern) were prepared.

The PS nano-grooves and micro-nano hybrid pattern surfaces were observed by SEM and AFM (Figure 4.2). The PS nano-grooves had an average convex width of 781.3 ± 39.1 nm, an average concave width of 823.5 ± 39.2 nm (spacing of the convex ridge) and an average depth of 338.9 ± 11.1 nm (Figure 4.2 a). SEM and AFM observation

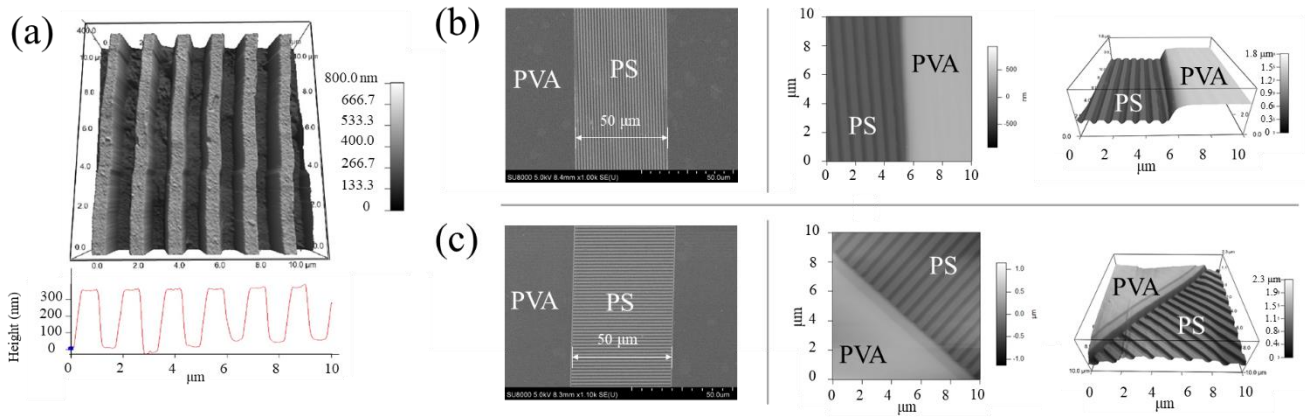

Figure 4.2 Characterization of micro-nano hybrid pattern surfaces. (a) AFM 3D and section images of PS nano-grooves. (b) SEM (left) and AFM (right two) images of parallelly oriented micro-p-nano hybrid pattern having 50 μm PVA micro-stripes spacing. (c) SEM (left) and AFM (right two) images of orthogonally oriented micro-o-nano hybrid pattern having 50 μm PVA micro-stripes spacing.

of the micro-p-nano and micro-o-nano hybrid pattern surfaces having a PVA stripe width of 50 μm showed that the PVA micro-stripe patterns were formed on the PS nano-grooves (Figure 4.2 b and c). The height of PVA terrace over PS nano-grooves was 565.6 ± 64.9 nm. The PVA micro-stripes in the micro-p- nano hybrid pattern surfaces were parallel to the PS nano-grooves, while those in the micro-o-nano hybrid pattern were orthogonal to the PS nano-grooves.

4.4.2 Cell alignment and elongation on micro-nano hybrid pattern surfaces

The micro-p-nano and micro-o-nano hybrid pattern surfaces were used for culture of MSCs. Staining of actin filaments and nuclei of MSCs after 1 day culture showed the cells spread and had different morphology on the hybrid pattern surfaces (Figure 4.3 a). Cells adhered on the PS nano-grooves and were constrained within the PVA micro-stripe spacing. Cells aligned more regularly on the narrow and parallel hybrid pattern surfaces than did on the wide and orthogonal hybrid pattern surfaces. The morphology of MSCs was analyzed through the stained images of actin and nuclei by using an ImageJ Software.

The percentage of aligned cells to the total cells is shown in Figure 4.3 b and c. Both PVA micro-stripe spacing and PS nano-groove orientation influenced cell alignment. When PS nano-groove orientation was fixed at parallel or orthogonal direction, PVA micro-stripe spacing showed significant effect on cell alignment (Figure 4.3 b). The cells showed the highest alignment percentage when PVA micro-stripe spacing was 50 μm, while the lowest when PVA micro-stripe spacing was 200 μm. Cell alignment percentage on micro-o-nano hybrid pattern surfaces increased significantly with the decrease of PVA micro-stripe spacing. Cell alignment percentage on micro-p-nano hybrid pattern surfaces having PVA

micro-stripe spacing of 50 and 100 μm was almost the same. When PVA micro-stripe spacing was fixed, influence of nano-groove orientation on cell alignment was dependent on PVA micro-stripe spacing (Figure 4.3 c). At a spacing of 50 μm, cell alignment was almost the same regardless of parallelly or orthogonally oriented nano-grooves. When PVA micro-stripe spacing was 100 or 200 μm, the aligned cell percentage on

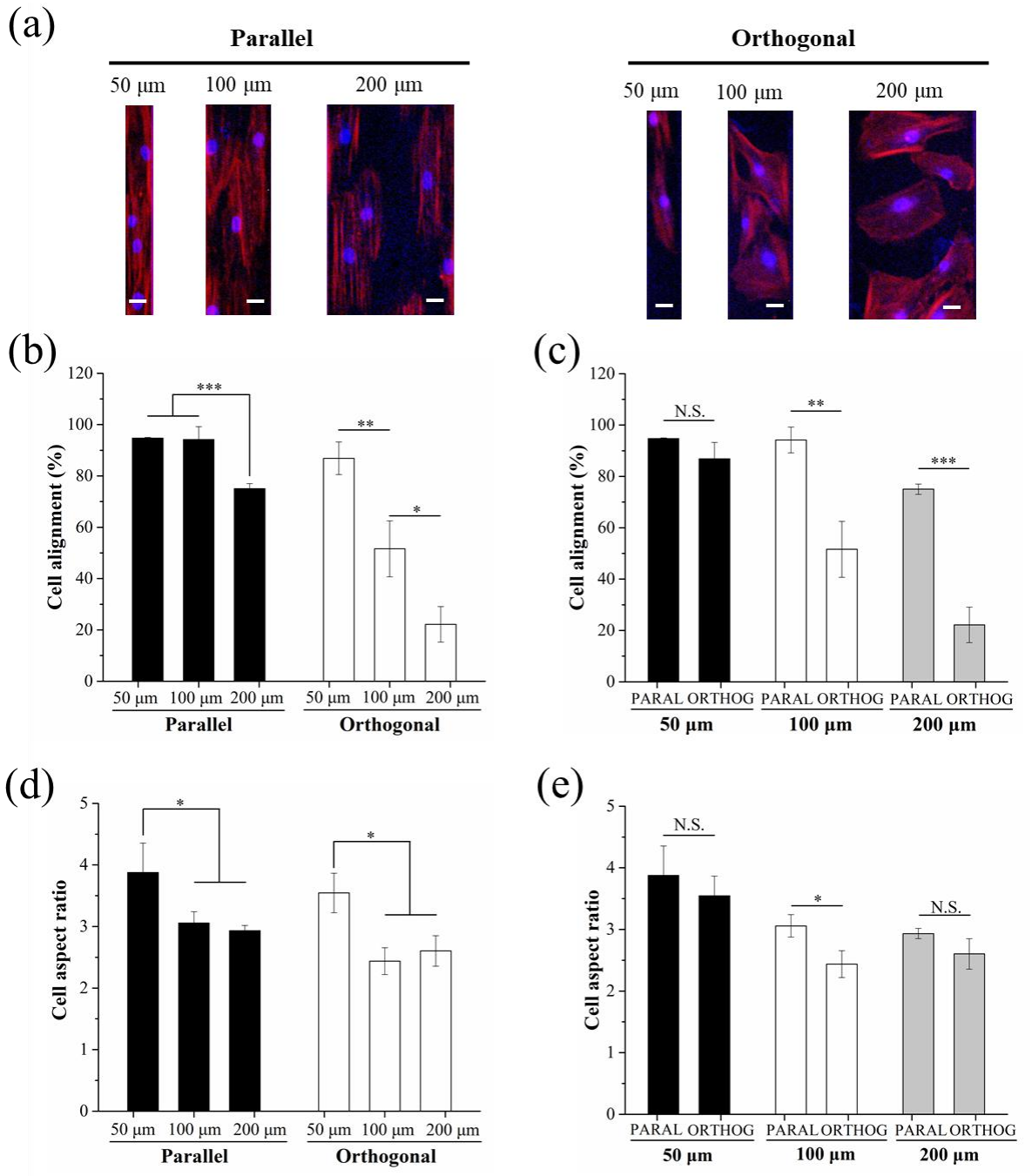

Figure 4.3 Morphological characterization of MSCs after 1 day culture on micro-nano hybrid pattern surfaces. (a) Representative fluorescence images of actin (red) and nuclei (blue) stained MSCs. (b) and (c) Percentage of aligned MSCs to the total cells. (c) Aspect ratio of MSCs. Data are reported as mean ± SD (n = 3). *$p < 0.05$, **$p < 0.01$, ***$p < 0.001$. Scale bar: 25 μm.

micro-p-nano hybrid pattern surfaces was significantly higher than that on micro-o-nano hybrid pattern surfaces.

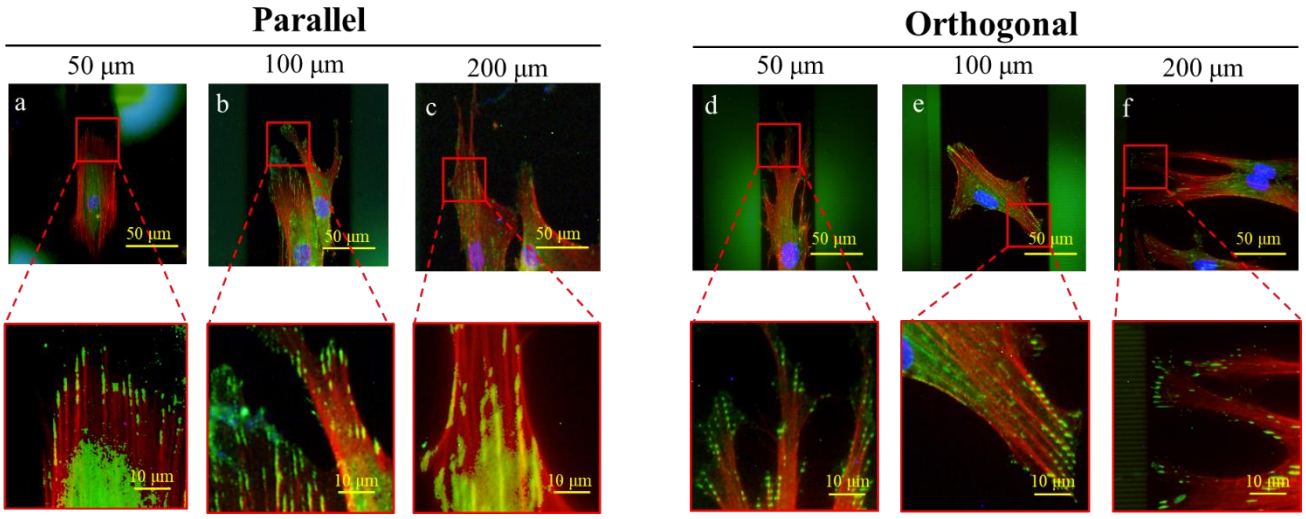

Figure 4.4 Representative immunofluorescence images of actin (red), nuclei (blue) and vinculin (green) staining of MSCs after 1 day culture on micro-nano hybrid pattern surfaces.

Cell aspect ratio was also analyzed (Figure 4.3 d and e). Cell aspect ratio on micro-nano hybrid pattern surfaces having PVA micro-stripe spacing of 50μm was higher than that on micro-nano hybrid pattern surfaces having PVA micro-stripe spacing of 100 or 200 μm (Figure 4.3 d). Cell aspect ratio on micro-nano hybrid pattern surfaces having PVA micro-stripe spacing of 100 or 200 μm was almost the same. When PVA micro-stripe spacing was fixed at 50 or 200μm, cell aspect ratio on the micro-p-nano hybrid pattern surfaces and micro-o-nano hybrid pattern surfaces had no significant difference Figure 4.3 e). When PVA micro-stripe spacing was 100μm, cell aspect ratio on micro-p-nano hybrid pattern surfaces was significantly higher than that on micro-o-nano hybrid pattern surfaces.

The cell alignment and aspect ratio results indicated that both cell alignment percentage and aspect ratio were dominantly controlled by PVA micro-pattern spacing when PVA micro-stripe spacing was narrow (50 μm). Cell alignment became more random and cell aspect ratio decreased as the spacing of PVA stripes increased and the effects from PS nano-groove orientation came into play. When PVA micro-stripe spacing was 50 μm, cells on both micro-p-nano hybrid pattern surfaces and micro-o-nano hybrid pattern surfaces had the same level of high alignment and high aspect ratio. At PVA micro-stripe spacing of 100 μm, cells on micro-p-nano hybrid pattern surfaces had significantly higher alignment and higher aspect ratio than those on micro-o-nano hybrid pattern surfaces. When PVA micro-stripe spacing became 200 μm, cells on micro-p-nano hybrid pattern and micro-o-nano hybrid pattern had significantly different alignment, but the same level of aspect ratio. Cell alignment and aspect ratio could be separately controlled by the spacing of PVA micro-stripes and orientation of PS nano-grooves.

Focal adhesion (FA) structure of MSCs cultured on micro-nano hybrid pattern surfaces was observed through immunofluorescence staining of vinculin (green fluorescence, Figure 4.4). FA was formed along PS nano-grooves when MSCs were cultured on micro-p-nano hybrid pattern surfaces (Figure 4.4 a-c). An interesting phenomenon was observed when MSCs were cultured on micro-o-nano hybrid pattern surfaces. When PVA micro-stripe spacing was 200 μm, FA was assembled along PS nano-grooves (Figure 4.4 f). However, when PVA micro-stripe spacing became narrow (50 μm and 100 μm), FA spanned over the PS nano-grooves and was assembled along PVA spacing direction (Figure 4.4 d-e).

4.4.3 Myogenic differentiation of MSCs on micro-nano hybrid pattern surfaces

Smooth muscle actin (SMA), an early smooth muscle cell marker, was stained and analyzed to evaluate myogenic differentiation potential after MSCs were seeded on the hybrid pattern surfaces in myogenic induction medium for 2 weeks (Figure 4.5 a). Percentage of SMA positively expressed cells was calculated (Figure 4.5 b and c). At first, the influence of PVA micro-stripe spacing was compared by fixing the orientation of PS nano-grooves in micro-nano hybrid patterns (Figure 4.5 b). The results showed myogenic differentiation level of MSCs increased with the decrease of PVA micro-stripe spacing. MSCs cultured on micro-nano hybrid pattern surfaces having PVA micro-stripe spacing of 50 μm showed the highest level of myogenic differentiation regardless of the orientation of PS nano-grooves. Difference between myogenic differentiation level of MSCs on micro-p-nano hybrid pattern surfaces having PVA micro-stripe spacing of 50 and 100 μm was not significant.

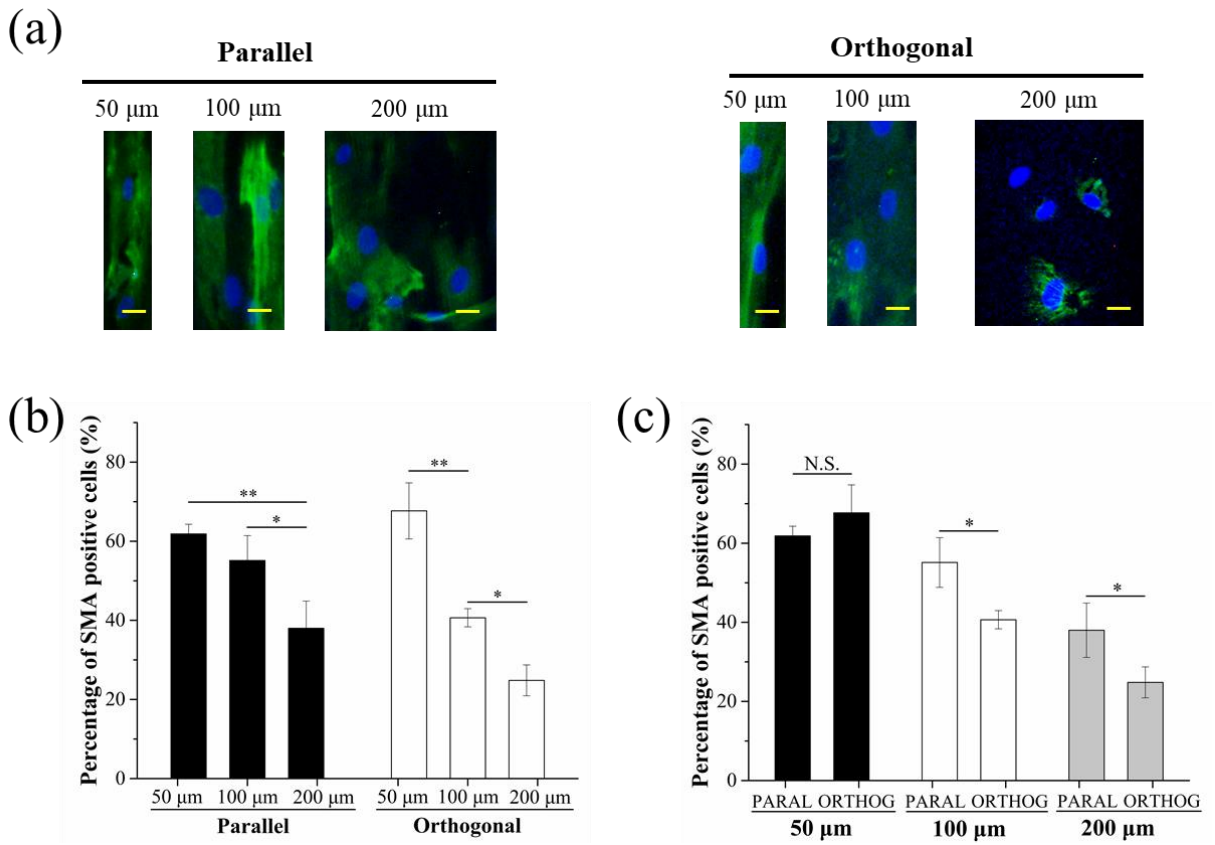

Figure 4.5 Analysis of myogenic differentiation of MSCs on micro-nano hybrid patterns by SMA expression after myogenic induction culture for 2 weeks. (a) Representative immunofluorescence images of SMA stained cells. (b) and (c) Percentage of SMA positively stained cells. Data are reported as mean ± SD (n = 3). *$p < 0.05$, **$p < 0.01$. Scale bar: 25 μm.

And then, the influence of orientation of PS nano-grooves was compared by fixing the spacing of PVA micro-stripes (Figure 4.5 c). When PVA micro-stripe spacing was fixed at 50 μm, orientation of PS nano-grooves did not affect the myogenic differentiation of MSCs. When PVA micro-stripe spacing increased to 100 or 200 μm, myogenic differentiation level of MSCs on micro-p- nano hybrid pattern was significantly higher than that on micro-o-nano hybrid pattern. These results indicated that myogenic differentiation was regulated by both PVA micro-stripe spacing and PS nano-groove orientation. Narrow PVA micro-stripe

spacing and parallel orientation of PS nano-grooves promoted, while wide PVA micro-stripe spacing and orthogonal orientation of PS nano-grooves inhibited myogenic differentiation of MSCs.

By comparing the results shown in Figure 4.3 b-e and Figure 4.5 b-c, it can be found that cell alignment and myogenic differentiation level of MSCs on micro-nano hybrid pattern surfaces had exactly the same trend. However, there was some difference between cell aspect ratio and myogenic differentiation level. Although high cell aspect ratio had some promotive influence on myogenic differentiation of MSCs, its influence was not as evident as that of cell alignment. When MSCs were cultured on the micro-nano hybrid pattern surfaces having the same orientation of PS nano-grooves but different PVA micro-stripe spacing of 100 and 200 μm, or the same PVA micro-stripe spacing of 200 μm but different orientation of PS nano-grooves, cell aspect ratio had no significant difference, while myogenic differentiation level was significantly different. Therefore, myogenic differentiation of MSCs on micro-nano hybrid pattern surfaces was dominantly regulated by cell alignment. High cell alignment was beneficial to myogenic differentiation. Cell aspect ratio was less important than cell alignment.

4.4.4 Osteogenic differentiation of MSCs on micro-nano hybrid pattern surfaces

After MSCs were cultured in osteogenic induction medium for 2 weeks, ALP was stained to evaluate osteogenic differentiation (Figure 4.6 a). Purple regions indicated ALP positively stained cells suggesting osteogenic differentiation of MSCs [35]. The positively stained cells were counted to calculate the percentage of ALP positively stained cells to the total cells (Figure 4.6 b and c). By comparing micro-nano hybrid pattern surfaces having the same parallel/orthogonal orientation but different PVA micro-stripe spacing, MSCs showed the highest osteogenic differentiation level when PVA micro-stripe spacing was 50 μm (Figure 4.6 b). Osteogenic differentiation level decreased when PVA micro-stripe spacing increased. Osteogenic differentiation level of MSCs on micro-nano hybrid pattern surfaces having PVA micro-stripe spacing of 100 and 200 μm had no significant difference.

However, when the PVA micro-stripe spacing was fixed at 50 or 200 μm, osteogenic differentiation level of MSCs on micro-o-nano and micro-p-nano hybrid pattern surfaces had no significant difference (Figure 4.6 c). Orientation of PS nano-grooves showed no influence on osteogenic differentiation of MSCs. On the micro-nano hybrid pattern having PVA micro-stripe spacing of 100 μm, parallelly oriented PS nano-grooves showed significantly higher promotive effect on osteogenic differentiation than did the orthogonally oriented PS nano-grooves. These results indicated that both PVA micro-stripe spacing and PS nano-groove orientation could influence osteogenic differentiation. Narrow PVA micro-stripe spacing and parallel orientation of PS nano-grooves showed promotive, while wide PVA micro-stripe spacing and orthogonal orientation of PS nano-grooves had inhibitory effect on osteogenic differentiation of MSCs.

When cell alignment and aspect ratio parameters shown in Figure 4.3 b-e and osteogenic differentiation data in Figure 4.6 b-c were compared, it is clear that osteogenic differentiation level of MSCs on micro-nano hybrid pattern surfaces had the same trend as that of cell aspect ratio. However, the changing trend of cell alignment was different from that of osteogenic differentiation level. In particular, when cell alignment was low, difference between the changing trends of cell alignment and osteogenic differentiation became evident. Cell alignment on the micro-nano hybrid pattern surfaces having the same orientation of PS nano-grooves but different PVA micro-stripe spacing of 100 and 200 μm, or the same PVA micro-stripe spacing of 200 μm but different orientation of PS nanogrooves was significantly different, osteogenic differentiation level had no significant difference. It could be concluded that osteogenic differentiation of MSCs was dominantly regulated by cell aspect ratio although cell alignment had some influence. High cell aspect ratio promoted osteogenic differentiation.

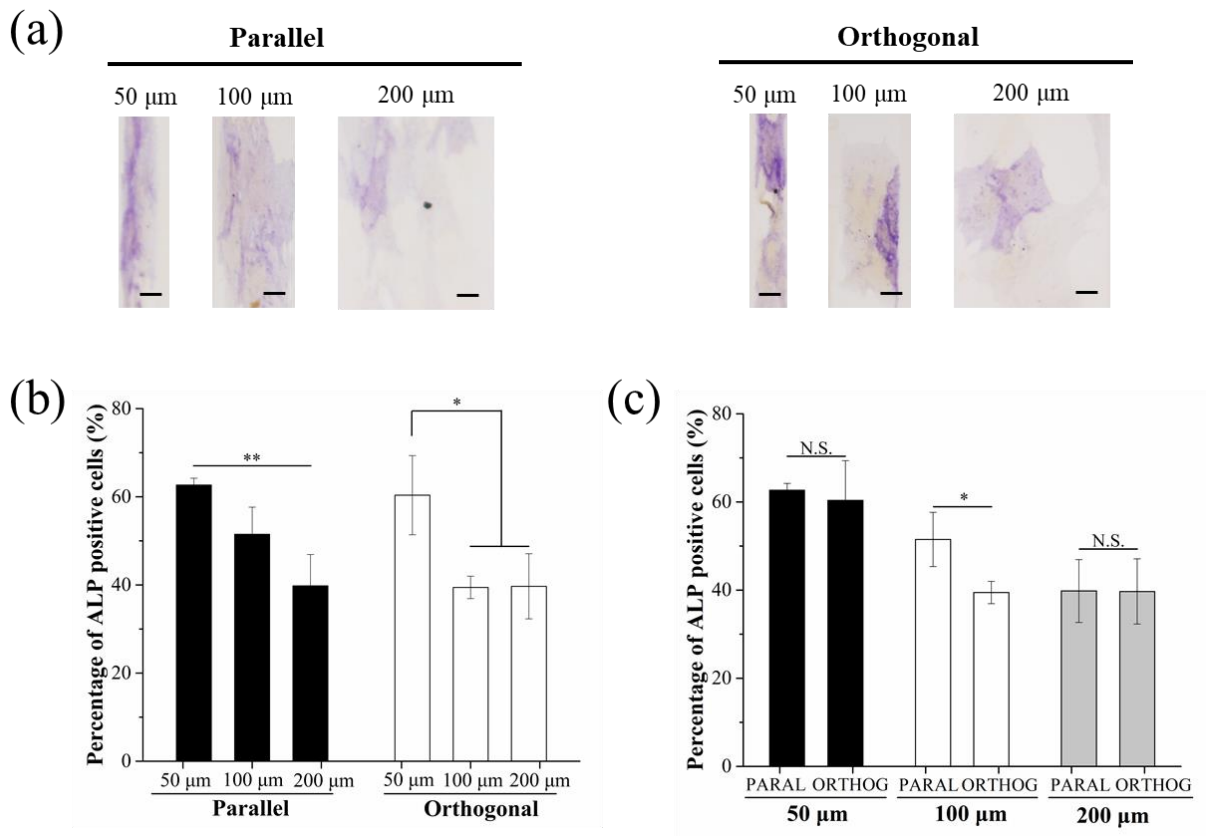

Figure 4.6 Analysis of osteogenic differentiation of MSCs on micro-nano hybrid patterns by ALP staining after osteogenic induction culture for 2 weeks. (a) Representative images of ALP stained cells. (b) and (c) Percentage of ALP positively stained cells. Data are reported as mean ± SD (n = 3). *$p < 0.05$, **$p < 0.01$. Scale bar: 25 μm.

4.4.5 Adipogenic differentiation of MSCs on micro-nano hybrid pattern surfaces

Lipid vacuoles is a key sign of adipocytes and used as a marker for adipogenic differentiation of MSCs [36]. Oil Red O solutions were applied to stain the lipid vacuoles in cytoplasm. After MSCs were cultured on micro-nano hybrid pattern surfaces in adipogenic induction medium for 2 weeks, the cells were stained by Oil Red O (Figure 4.7 a). Cells undergoing adipogenesis were stained red. Percentage of lipid vacuoles positively stained cells was used to evaluate degree of adipogenic differentiation of MSCs (Figure 4.7 b and c).

When micro-nano hybrid patterns having the same parallel or orthogonal orientation but different PVA micro-stripe spacing were compared, adipogenic differentiation potential of MSCs was dependent on both PVA micro-stripe spacing and PS nano-groove orientation (Figure 4.7 b). On the parallelly oriented micro-p-nano hybrid pattern surfaces, adipogenic differentiation level of MSCs on PVA micro-stripe spacing of 50 μm was the lowest. On the orthogonally orientated micro-o-nano hybrid pattern surfaces, MSCs had similar level of adipogenic differentiation level regardless of the PVA micro-stripe spacing.

On the other hand, when the PVA micro-stripe spacing was fixed at 50 or 100 μm, adipogenic differentiation level on micro-p-nano hybrid pattern was significantly lower than that on micro-o-nano hybrid pattern (Figure 4.7 c). When PVA micro-stripe spacing was fixed at 200 μm, adipogenic differentiation level had no significant difference. The results indicated that orthogonal orientation of PS nano-grooves and wide PVA micro-stripe spacing were beneficial to adipogenic differentiation, while

narrow PVA micro-stripe spacing and parallel orientation of PS nano-grooves had inhibitory effect on adipogenic differentiation.

Adipogenic differentiation level of MSCs on micro-nano hybrid pattern surfaces had no evident relationship with either cell alignment or cell aspect ratio although high cell alignment and high aspect ratio inhibited adipogenic differentiation of MSCs on parallelly oriented micro-p-nano hybrid pattern surfaces having PVA micro-stripes of 50 μm.

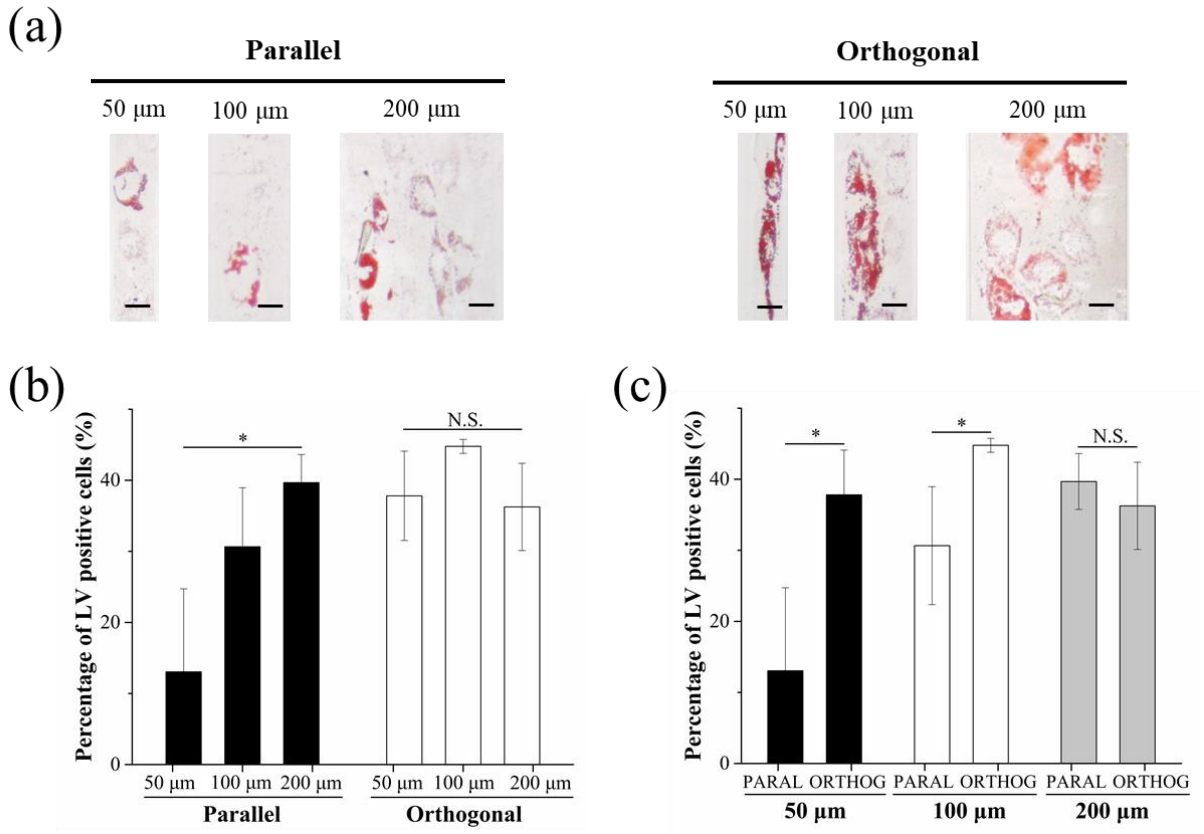

Figure 4.7 Analysis of adipogenesis of MSCs on micro-nano hybrid patterns by Oil Red O staining after adipogenic induction culture for 2 weeks. (a) Representative images of Oil Red O staining of MSCs. (b) and (c) Percentage of lipid vacuoles (LV) positively stained cells. Data are reported as mean ± SD (n = 3). *$p < 0.05$. Scale bar: 25 μm.

4.5 Discussion

By using the micro-nano hybrid pattern surfaces, alignment and aspect ratio (elongation) of MSCs could be simultaneously regulated. Cells cultured on micro-nano hybrid pattern surfaces having PVA micro-stripe spacing of 50 μm showed the same level of high alignment and high elongation regardless of the parallel or orthogonal orientation of PS nano-grooves. When PVA micro-stripe spacing increased to 100 μm, micro-p-nano hybrid pattern induced significantly higher cell alignment and elongation than did micro-o-nano hybrid pattern. When PVA micro-stripe spacing further increased to 200 μm, cell alignment on micro-nano hybrid pattern surfaces with different orientation of PS nano-grooves had significant difference, while cell elongation was kept at the same level.

The role of cell alignment and elongation on MSCs differentiation could be investigated by using the hybrid pattern surfaces for culture of MSCs. At the narrowest PVA micro-stripe spacing (50 μm), cell alignment and elongation were mainly affected by PVA stripe spacing because of the strong constraint that was resulted from the PVA micro-stripes. Narrow PVA micro-stripes spacing could limit cell width and unify cell alignment and promote cell elongation. On the other hand, wide PVA micro-stripe spacing could weaken the constraint effect of PVA micro-stripes and therefore influence of PS nano-grooves on cell alignment and elongation became evident.

The phenomena could be explained by the FA formation on the micro-nano hybrid pattern surfaces. On micro-nano hybrid pattern surfaces with the narrowest PVA micro-stripes (50 μm), FA was formed in the same direction of the PVA micro-stripes regardless of the orientation of PS nano-grooves. However, when PVA micro-stripe spacing increased, FA was assembled along the PS nano-grooves rather than following the PVA micro-stripe spacing. Therefore, cell morphology and FA formation were intimately related and dominantly regulated by both PVA micro-stripes and PS nano-grooves depending on the spacing of PVA micro-stripes.

The micro-nano hybrid pattern surfaces were used to investigate the influence of cell morphology such as cell alignment and elongation on myogenic, osteogenic and adipogenic differentiation of MSCs. Previous studies have reported that cell alignment and elongation are critical for the myogenic differentiation of MSCs [12, 37]. Cell alignment has been reported to enhance cell end-to-end contacts which are critical for the fusion of myotubes [38] and high cell aspect ratio has been reported to promote myogenic differentiation through up-regulation of RhoA/ROCK pathway [12]. However, the different weight of cell alignment and cell elongation on myogenic differentiation remains unclear. In this study, by using micro-nano hybrid pattern surfaces, influence of alignment and elongation on myogenic differentiation of MSCs was compared. As shown in Figure 4.3 and Figure 4.5, myogenic differentiation level had a good relationship with cell alignment. High cell alignment resulted in high level of myogenic differentiation and vice versa. However, influence of cell elongation was a little complicated. Although cells cultured on the micro-nano hybrid pattern surfaces with PVA micro-stripe spacing of 50 μm had high cell aspect ratio and high myogenic differentiation level, the relationship became unclear when PVA micro-stripe spacing increased to 100 or 200 μm. On the micro-nano hybrid pattern surfaces having PVA micro-stripe spacing of 100 or 200 μm, cells on the parallelly oriented micro-p-nano hybrid pattern surfaces had the same level of elongation as that on the orthogonal oriented micro-o-nano hybrid pattern surfaces, but significantly different level of myogenic differentiation. The results suggest influence of cell elongation on MSCs myogenic differentiation was weaker than that of cell alignment.

In contrast to the influence on myogenic differentiation, cell aspect ratio had a more important influence on osteogenic differentiation of MSCs than did cell alignment. The dominant influence of cell elongation on osteogenic differentiation should be due to high cytoskeleton tension in elongated cells. It has been reported that cytoskeleton tension can be regulated by cell elongation and can act a critical role in directing MSCs osteogenic differentiation [39]. This result was also consistent with previous work that elongated cells promoted osteogenic differentiation through increasing cytoskeleton contractility [25].

Combination of narrow PVA micro-stripe spacing and parallelly orientated PS nano-grooves had inhibitory influence on adipogenic differentiation. The lowest adipogenic differentiation level of MSCs on micro-p-nano hybrid pattern surfaces having PVA micro-stripe spacing of 50 μm group should be due to high cell alignment and elongation. It has been reported that high cell aspect ratio can result in cell contractility and inhibit adipogenic differentiation [40]. Grooved structure has been reported to facilitate adipogenesis through inhibition of FA formation and disturbance of cytoskeleton organization [38, 41, 42]. Punctiform FA on orthogonal nano-grooves can weaken the mechanical links between stress fibers and

ECM substrate and therefore promote adipogenic differentiation [43]. On the other hand, cells on micro-p-nano hybrid pattern surfaces having PVA micro-stripe spacing of 100 μm and micro-o-nano hybrid pattern surfaces having PVA micro-stripe spacing of 50 μm had high alignment and elongation, while their adipogenic differentiation potential was not low. The relationship between cell alignment and aspect ratio with adipogenic differentiation of MSCs was not as evident as those related to myogenic and osteogenic differentiation. Except for cell alignment and elongation, cell size has also been reported to be vital for adipogenic differentiation of MSCs. It has been reported that small cell size is more beneficial for adipogenic differentiation of MSCs than large cell size [28, 44].

4.6 Conclusions

Preparation of PS/PVA micro-nano hybrid pattern surfaces through nanoimprinting and photolithography provided a useful method to manipulate cell alignment and cell aspect ratio and to investigate their effects on myogenic, osteogenic and adipogenic differentiation of MSCs. Cell alignment and aspect ratio were simultaneously regulated by changing PVA micro-stripe spacing and orientation of PS nano-grooves of micro-nano hybrid pattern surfaces. On micro-nano hybrid pattern surfaces, cell alignment and cell aspect ratio showed different influence on MSCs differentiation. Myogenic differentiation of MSCs on micro-nano hybrid pattern surfaces was dominantly regulated by cell alignment, while osteogenic differentiation of MSCs was dominantly regulated by cell aspect ratio. Adipogenic differentiation level of MSCs on micro-nano hybrid pattern surfaces had no evident relationship with either cell alignment or cell aspect ratio.

4.7 References

[1] W. Wei, J. Li, S. Chen, M. Chen, Q. Xie, H. Sun, J. Ruan, H. Zhou, X. Bi, A. Zhuang, Z. You, P. Gu, X. Fan, In vitro osteogenic induction of bone marrow mesenchymal stem cells with a decellularized matrix derived from human adipose stem cells and in vivo implantation for bone regeneration, Journal of Materials Chemistry B 5(13) (2017) 2468-2482.

[2] R.S. Tuan, G. Boland, R. Tuli, Adult mesenchymal stem cells and cell-based tissue engineering, Arthritis Research & Therapy 5(1) (2003) 32.

[3] A. Higuchi, S. Suresh Kumar, Q.-D. Ling, A.A. Alarfaj, M.A. Munusamy, K. Murugan, S.-T. Hsu, G. Benelli, A. Umezawa, Polymeric design of cell culture materials that guide the differentiation of human pluripotent stem cells, Progress in Polymer Science 65 (2017) 83-126.

[4] A. Higuchi, Q.-D. Ling, S.S. Kumar, Y. Chang, A.A. Alarfaj, M.A. Munusamy, K. Murugan, S.-T. Hsu, A. Umezawa, Physical cues of cell culture materials lead the direction of differentiation lineages of pluripotent stem cells, Journal of Materials Chemistry B 3(41) (2015) 8032-8058.

[5] S. Wei, L. Hongxu, N. Kawazoe, C. Guoping, Gradient patterning and differentiation of mesenchymal stem cells on micropatterned polymer surface, Journal of Bioactive and Compatible Polymers 26(3) (2011) 242-256.

[6] A.J. Engler, S. Sen, H.L. Sweeney, D.E. Discher, Matrix elasticity directs stem cell lineage specification, Cell 126(4) (2006) 677-89.

[7] S.W. Lane, D.A. Williams, F.M. Watt, Modulating the stem cell niche for tissue regeneration, Nature biotechnology 32(8) (2014) 795-803.

[8] M. Thery, Micropatterning as a tool to decipher cell morphogenesis and functions, Journal of cell science 123(Pt 24) (2010) 4201-13.

[9] M. Versaevel, T. Grevesse, S. Gabriele, Spatial coordination between cell and nuclear shape within

micropatterned endothelial cells, Nature communications 3 (2012) 671.
[10] T.L. Downing, J. Soto, C. Morez, T. Houssin, A. Fritz, F. Yuan, J. Chu, S. Patel, D.V. Schaffer, S. Li, Biophysical regulation of epigenetic state and cell reprogramming, Nature materials 12(12) (2013) 1154-62.
[11] X. Wang, T. Nakamoto, I. Dulińska-Molak, N. Kawazoe, G. Chen, Regulating the stemness of mesenchymal stem cells by tuning micropattern features, J. Mater. Chem. B 4(1) (2016) 37-45.
[12] D. Zhang, M.B. Sun, J. Lee, A.A. Abdeen, K.A. Kilian, Cell shape and the presentation of adhesion ligands guide smooth muscle myogenesis, Journal of biomedical materials research. Part A 104(5) (2016) 1212-20.
[13] Y. Zhao, H. Zeng, J. Nam, S. Agarwal, Fabrication of skeletal muscle constructs by topographic activation of cell alignment, Biotechnology and bioengineering 102(2) (2009) 624-31.
[14] P.Y. Wang, H.T. Yu, W.B. Tsai, Modulation of alignment and differentiation of skeletal myoblasts by submicron ridges/grooves surface structure, Biotechnology and bioengineering 106(2) (2010) 285-94.
[15] S. Hoehme, M. Brulport, A. Bauer, E. Bedawy, W. Schormann, M. Hermes, V. Puppe, R. Gebhardt, S. Zellmer, M. Schwarz, E. Bockamp, T. Timmel, J.G. Hengstler, D. Drasdo, Prediction and validation of cell alignment along microvessels as order principle to restore tissue architecture in liver regeneration, Proceedings of the National Academy of Sciences of the United States of America 107(23) (2010) 10371-6.
[16] C.Y. Xu, R. Inai, M. Kotaki, S. Ramakrishna, Aligned biodegradable nanofibrous structure: a potential scaffold for blood vessel engineering, Biomaterials 25(5) (2004) 877-86.
[17] H. Aubin, J.W. Nichol, C.B. Hutson, H. Bae, A.L. Sieminski, D.M. Cropek, P. Akhyari, A. Khademhosseini, Directed 3D cell alignment and elongation in microengineered hydrogels, Biomaterials 31(27) (2010) 6941-6951.
[18] P.Y. Wang, J. Yu, J.H. Lin, W.B. Tsai, Modulation of alignment, elongation and contraction of cardiomyocytes through a combination of nanotopography and rigidity of substrates, Acta biomaterialia 7(9) (2011) 3285-93.
[19] A. Higuchi, Q.D. Ling, Y. Chang, S.T. Hsu, A. Umezawa, Physical cues of biomaterials guide stem cell differentiation fate, Chemical reviews 113(5) (2013) 3297-328.
[20] P.-Y. Wang, S. Ding, H. Sumer, R.C.-B. Wong, P. Kingshott, Heterogeneity of mesenchymal and pluripotent stem cell populations grown on nanogrooves and nanopillars, J. Mater. Chem. B 5(39) (2017) 7927-7938.
[21] L. Guo, Y. Fan, N. Kawazoe, H. Fan, X. Zhang, G. Chen, Fabrication of gelatin-micropatterned surface and its effect on osteogenic differentiation of hMSCs, Journal of Materials Chemistry B 6(7) (2018) 1018-1025.
[22] D. Falconnet, G. Csucs, H.M. Grandin, M. Textor, Surface engineering approaches to micropattern surfaces for cell-based assays, Biomaterials 27(16) (2006) 3044-63.
[23] X. Wang, X. Hu, N. Kawazoe, Y. Yang, G. Chen, Manipulating Cell Nanomechanics Using Micropatterns, Advanced Functional Materials 26(42) (2016) 7634-7643.
[24] W. Song, X. Wang, H. Lu, N. Kawazoe, G. Chen, Exploring adipogenic differentiation of a single stem cell on poly(acrylic acid) and polystyrene micropatterns, Soft Matter 8(32) (2012) 8429.
[25] K.A. Kilian, B. Bugarija, B.T. Lahn, M. Mrksich, Geometric cues for directing the differentiation of mesenchymal stem cells, Proceedings of the National Academy of Sciences of the United States of America 107(11) (2010) 4872-7.
[26] W. Song, H. Lu, N. Kawazoe, G. Chen, Adipogenic differentiation of individual mesenchymal stem cell on different geometric micropatterns, Langmuir : the ACS journal of surfaces and colloids 27(10) (2011) 6155-62.
[27] I. Lilge, S. Jiang, D. Wesner, H. Schonherr, The Effect of Size and Geometry of Poly(acrylamide) Brush-Based Micropatterns on the Behavior of Cells, ACS applied materials & interfaces 8(36) (2016) 23591-603.
[28] M. Thery, V. Racine, M. Piel, A. Pepin, A. Dimitrov, Y. Chen, J.B. Sibarita, M. Bornens, Anisotropy of cell adhesive microenvironment governs cell internal organization and orientation of polarity, Proceedings of the National Academy of Sciences of the United States of America 103(52) (2006) 19771-6.
[29] D. Lehnert, B. Wehrle-Haller, C. David, U. Weiland, C. Ballestrem, B.A. Imhof, M. Bastmeyer, Cell behaviour on micropatterned substrata: limits of extracellular matrix geometry for spreading and adhesion, Journal of cell

science 117(Pt 1) (2004) 41-52.
[30] A.T. Nguyen, S.R. Sathe, E.K. Yim, From nano to micro: topographical scale and its impact on cell adhesion, morphology and contact guidance, Journal of physics. Condensed matter : an Institute of Physics journal 28(18) (2016) 183001.
[31] C.W. Kuo, D.Y. Chueh, P. Chen, Investigation of size-dependent cell adhesion on nanostructured interfaces, Journal of nanobiotechnology 12 (2014) 54.
[32] S. Fujita, M. Ohshima, H. Iwata, Time-lapse observation of cell alignment on nanogrooved patterns, Journal of the Royal Society, Interface 6 Suppl 3 (2009) S269-77.
[33] P. Uttayarat, G.K. Toworfe, F. Dietrich, P.I. Lelkes, R.J. Composto, Topographic guidance of endothelial cells on silicone surfaces with micro- to nanogrooves: orientation of actin filaments and focal adhesions, Journal of biomedical materials research. Part A 75(3) (2005) 668-80.
[34] X. Wang, X. Hu, J. Li, A.C. Russe, N. Kawazoe, Y. Yang, G. Chen, Influence of cell size on cellular uptake of gold nanoparticles, Biomaterials science 4(6) (2016) 970-8.
[35] J. Li, J. Zhang, Y. Chen, N. Kawazoe, G. Chen, TEMPO-Conjugated Gold Nanoparticles for Reactive Oxygen Species Scavenging and Regulation of Stem Cell Differentiation, ACS applied materials & interfaces 9(41) (2017) 35683-35692.
[36] J. Li, Y. Chen, N. Kawazoe, G. Chen, Ligand density-dependent influence of arginine–glycine–aspartate functionalized gold nanoparticles on osteogenic and adipogenic differentiation of mesenchymal stem cells, Nano Research 11(3) (2018) 1247-1261.
[37] J.M. Dang, K.W. Leong, Myogenic Induction of Aligned Mesenchymal Stem Cell Sheets by Culture on Thermally Responsive Electrospun Nanofibers, Advanced materials 19(19) (2007) 2775-2779.
[38] P.Y. Wang, W.T. Li, J. Yu, W.B. Tsai, Modulation of osteogenic, adipogenic and myogenic differentiation of mesenchymal stem cells by submicron grooved topography, Journal of materials science. Materials in medicine 23(12) (2012) 3015-28.
[39] J. Fu, Y.K. Wang, M.T. Yang, R.A. Desai, X. Yu, Z. Liu, C.S. Chen, Mechanical regulation of cell function with geometrically modulated elastomeric substrates, Nature methods 7(9) (2010) 733-6.
[40] P.L. Kuo, H. Lee, M.A. Bray, N.A. Geisse, Y.T. Huang, W.J. Adams, S.P. Sheehy, K.K. Parker, Myocyte shape regulates lateral registry of sarcomeres and contractility, The American journal of pathology 181(6) (2012) 2030-7.
[41] M.S. Kim, A.Y. Kim, K.J. Jang, J.H. Kim, J.B. Kim, K.Y. Suh, Effect of nanogroove geometry on adipogenic differentiation, Nanotechnology 22(49) (2011) 494017.
[42] G. Abagnale, M. Steger, V.H. Nguyen, N. Hersch, A. Sechi, S. Joussen, B. Denecke, R. Merkel, B. Hoffmann, A. Dreser, U. Schnakenberg, A. Gillner, W. Wagner, Surface topography enhances differentiation of mesenchymal stem cells towards osteogenic and adipogenic lineages, Biomaterials 61 (2015) 316-26.
[43] K. Burridge, C. Guilluy, Focal adhesions, stress fibers and mechanical tension, Experimental cell research 343(1) (2016) 14-20.
[44] X. Wang, W. Song, N. Kawazoe, G. Chen, Influence of cell protrusion and spreading on adipogenic differentiation of mesenchymal stem cells on micropatterned surfaces, Soft Matter 9(16) (2013) 4160.

Chapter 5

Concluding remarks and future prospects

5.1 Concluding remarks

This dissertation describes the influence of cell morphology on the regulation of MSC functions and behavior by using nano- and micro-structured surfaces. Various kinds of micro-patterned and nano-micro hybrid pattern surfaces were prepared through photolithography and nanoimprinting method. The cell morphology including cell size, aspect ratio and alignment was controlled by the different kind of patterned surfaces. Furthermore, their functions in the regulation of MSCs differentiation, differentiated phenotype maintenance and gene transfection efficiency were investigated.

Chapter 1 introduces the multipotency, self-renewability, migratory capacity and immunomodulatory capacity of MSCs and their applications in tissue engineering and cell-based gene therapy. The different factors including biochemical factors, biophysical factors and cell morphology in the regulation of MSC functions and behavior are also introduced. The conventional nano- and micro-patterning techniques to control cell morphology are summarized and reviewed. In order to elicit the motivation of this study, some important issues issues in cell morphology regulated MSCs differentiation, differentiated phenotype maintenance and gene transfection are emphasized.

In chapter 2, the influence of cell size or spreading area on the regulation of MSCs osteogenic commitment and differentiated phenotype or stemness maintenance was investigated. The cell size was precisely controlled by the micro-patterned surfaces containing micro-dots having different size. The results of stemness marker expression, ALP activity and calcium deposition indicated that the larger cell size had the positive effects on stimulation of MSCs osteogenesis with biochemical stimuli and maintenance of osteogenic differentiated phenotype without biochemical induction factors was observed. In contrast, the smaller cells inhibited the osteogenesis while beneficial for the maintenance of stemness.

In chapter 3, the influence of cell size and aspect ratio on the regulation of MSCs transfection was investigate. The MSCs were cultured on micro-patterned surfaces and transfected by GFP encoded exogeneous gene. The results indicated that the MSCs with a larger spreading area and higher aspect ratio were related to higher transfection efficiency. To explore the possible mechanism of this result, the cellular uptake capacity of cationic complexes, DNA synthesis activity and cytoskeleton structure of MSCs with different morphology were also investigated. The highly spread or elongated MSCs with well-organized actin filaments improved the capacity of cellular uptake and

accelerated DNA synthesis. Therefore, the higher transfection efficiency of well spread and elongated MSCs was related with improved cellular uptake capacity and facilitated DNA synthesis.

In chapter 4, micro-nano hybrid pattern surfaces were prepared and applied to investigate the different role of cell alignment and elongation in the regulation of MSCs myogenesis, osteogenesis and adipogenesis. By changing the orientation of PS nano-grooves and spacing of PVA micro-stripes, the cell alignment and aspect ratio of MSCs were well controlled simultaneously. The myogenesis of MSCs was predominantly regulated by cell alignment. The osteogenesis of MSCs relied only on the cell elongation. The adipogenesis of MSCs was independent from cell alignment and elongation while related to the structure of FA.

In summary, micro-patterned and nano-micro hybrid pattern surfaces were successfully prepared through photolithography and nano-imprinting method. These structured surfaces were designed and prepared to control cell size, aspect ratio and alignment. The significant influence of the factors on the regulation of MSCs differentiation, differentiated phenotype maintenance and transfections revealed the critical role of cell morphology manipulation in the application of MSCs in tissue engineering and cell-based gene therapy. The results of this study will provide useful information in the design and development of biomaterials for the regulation of stem cells functions and behavior in tissue engineering and cell-based gene therapy.

5.2 Future prospects

In this study, the photo-reactive AzPhPVA was synthesized and applied to prepare micro-patterns on TCPS or nanogrooved PS surfaces. The importance of cell morphology in regulation MSC functions and behavior was systematically investigated. In spite of the interesting and useful results obtained in this study, some further researches are needed to completely mimic the *in vivo* microenvironment for practical applications. Because of the limitations of using the rigid substrate, the micropatterned surfaces are difficult to be applied *in vivo* experiments. Additionally, the nano- and microstructured surfaces regulated only the 2D topography of cell adhesion, 3D structure of cells has yet been manipulated.

Preparation of *in vivo* implantable nano- and micro-structured surfaces: Transplantation of the micropatterned surfaces *in vivo* may be considered to further demonstrate the functions of cell morphology on cell functions and tissue regeneration at *in vivo* microenvironment. The non-toxic, flexible and cell adhesive materials (hydrogels, electrospun nanofibers, immobilized ECM, and etc.) can be applied as the substrates. The thin layer of AzPhPVA can be coated on the substrate and UV irradiated through micropatterned photomask. After removal of unreacted AzPhPVA, cells are seeded on the micro-patterned surfaces *in vitro* firstly or directly transplant the micropatterned surfaces *in vivo*.

Preparation of 3D micro-patterned surfaces: Cells are surrounded by the 3D structures *in vivo* microenvironment, and precise control of 3D cell structure is meaningful for investigation of the mechanism of cell responding to the surrounding stimuli by changing of 3D structure. To do this, the pre-prepared micro-structured silicon template can be applied to prepare 3D concave structures on cell adhesive substrate. On the other hand, a thin layer of AzPhPVA can be coated on a transparent glass. Then, the 3D structured substrate can be contacted with the AzPhPVA thin layer and irradiated with UV to graft the photoreactive AzPhPVA on the contacted parts of cell adhesive substrate to prevent cell adhesion. Finally, after being cultured on the structured substrate, cells are only seeded within the 3D microstructured parts. The prepared 3D micro-structured substrates can provide an approach to investigate the influence of cell 3D structure on their functions and behavior.

List of publications and awards

Publications:

1. Yingjun Yang, Xinlong Wang, Tsung-Chun Huang, Xiaohong Hu, Naoki Kawazoe, Wei-Bor Tsai, Yingnan Yang, Guoping Chen. Regulation of mesenchymal stem cell functions by micro–nano hybrid patterned surfaces. Journal of Materials Chemistry B, 6(34) (2018) 5424-5434.

2. Yingjun Yang, Xinlong Wang, Xiaohong Hu, Naoki Kawazoe, Yingnan Yang, Guoping Chen. Influence of cell morphology in mesenchymal stem cell transfection. ACS Applied Materials & Interfaces, 2019, *11 (2), pp 1932–1941*

3. Yingjun Yang, Xinlong Wang, Yongtao Wang, Xiaohong Hu, Naoki Kawazoe, Yingnan Yang, Guoping Chen. Influence of cell size in osteogenic commitment and phenotype maintenance of mesenchymal stem cells. Submitted.

4. Xinlong Wang, Yingjun Yang, Xiaohong Hu, Naoki Kawazoe, Yingnan Yang, Guoping Chen. Morphological and Mechanical Properties of Osteosarcoma Microenvironment Cells Explored by Atomic Force Microscopy. Analytical Science 32(11) (2016) 1177-1182.

5. Jianmin Yang, Yingjun Yang, Naoki Kawazoe, Guoping Chen. Encapsulation of individual living cells with enzyme responsive polymer nanoshell. Biomaterials 197 (2019) 317-326.

6. Jingchao Li, Ying Chen, Yingjun Yang, Naoki Kawazoe, Guoping Chen. Sub-10 nm gold nanoparticles promote adipogenesis and inhibit osteogenesis of mesenchymal stem cells. Journal of Materials Chemistry B 5(7) (2017) 1353-1362.

7. Jianmin Yang, Jingchao Li, Xiaomeng Li, Xinlong Wang, Yingjun Yang, Naoki Kawazoe, Guoping Chen, Nanoencapsulation of individual mammalian cells with cytoprotective polymer shell. Biomaterials 133 (2017) 253-262.

Awards:

1. **Excellent poster award**, Tsukuba Global Science Week (TGSW) 2017, Tsukuba, Japan, 2017

2. **Best oral presentation**, 3rd Asian University Symposium for Biomedical Engineering, Seoul, Korea, 2018

Acknowledgements

This PhD dissertation was accomplished under guidance of Professor Guoping Chen. Within this 3-year, Professor Chen always keep patience and enthusiasm for guiding me in scientific researches. He is always scrupulous in designing the research topic and revising manuscripts. Even he is very busy in management of our group, he could always squeeze the time for discussion and providing many constructive suggestions for me. Without his help, I cannot graduate smoothly. In addition, Professor Chen is not only concerned on the researches but also care about our daily life in Japan. It is the great honor for me to stay in Professor Chen's group and get PhD degree under his supervision. Therefore, I want to use this opportunity to express my great appreciate for his help in this 3 year.

A lot of thanks are also needing to be expressed to Dr. Naoki Kawazoe. He always does a lot of things in obscurity. He also uses his professional knowledges to help us and giving many useful suggestions on our researches. With his kind help, we could fully focus on our researches and he will solve any problems for us.

I am also really appreciated for the valuable suggestions and accompany from Dr. Xinlong Wang, Prof. Gang Wu, Prof. Shujun Dong, Dr. Jianmin Yang, Dr. Jingchao Li, Dr. Jing Zhang, Dr. Ying Chen, Dr. Xiaomeng Li, Ms. Xiuhui Wang, Mr. Yazhou Chen, Mr. Kyubae Lee, Mr. Tsung-Chun Huang, Mrs. Hidaka, Mrs. Akiyama.

Additionally, I would also like to show my sincere appreciate to the professors in dissertation supervisory committee, Prof. Yukio Nagasaki, Prof. Kohsaku Kawakami, Prof. Tetsushi Taguchi. I got a wealth of knowledge from their meaningful suggestions and encouragement during my PhD defense, NIMS student seminars and various academic conferences. I also like to show my most sincere appreciates to my family and all of my friends for their help within this 3 year.

This research work was processed at Tissue Regeneration Materials Group of Research Center for Functional Materials (RCFM) in National Institute for Materials Science (NIMS) and supported by Graduate School of Pure and Applied Science of University of Tsukuba. I would also like to thank the finical support from NIMS Junior Research Assistantship.